KM3NeT

Conceptual Design Report for a Deep-Sea

Research Infrastructure in the

Mediterranean Sea Incorporating a

Very Large Volume Neutrino Telescope

KM3NeT

KM3NeT

Conceptual Design Report for a Deep-Sea

Research Infrastructure in the

Mediterranean Sea Incorporating a

Very Large Volume Neutrino Telescope

April 2008

The wrecks dissolve above us; their dust drops down from afar –
Down to the dark, to the utter dark, where the blind white sea-snakes are.
There is no sound, no echo of sound, in the deserts of the deep,
Or the great gray level plains of ooze where the shell-burred cables creep.

From: The Deep-Sea Cables by Rudyard Kipling

P. Bagley, A. Holford, A. Jamieson, M. Priede
University of Aberdeen, United Kingdom

M. Ageron, J.-J. Aubert, V. Bertin, S. Beurthey, M. Billault, A. Brown, J. Brunner, J. Busto, L. Caillat, A. Calzas, J. Carr, A. Cosquer, P. Coyle, C. Curtil, D. Dornic, S. Escoffier, F. Gensolen, C. Gojak, G. Hallewell, P. Keller, P. Lagier, P. Payre, C. Reed
University of Aix-Marseille II and Centre de Physique de Particules de Marseille/IN2P3/CNRS, Marseille, France

R. Bruijn, J. Koopstra, G. Lim, E. de Wolf
University of Amsterdam, the Netherlands

J. Aublin, B. Baret, C. Donzaud, A. Kouchner, V. Van Elewyck
APC–AstroParticule et Cosmologie–UMR 7164 (CNRS, Université Paris 7, CEA, Observatoire de Paris), Paris, France

E.G. Anassontzis, L.K. Resvanis
University of Athens, Greece

S. Anvar, J. Ballet, F. Chateau, E. Delagnes, F. Druillole, D. Durand, I. Grenier, F. Guilloux, P. Kestener, P. Lamare, H. Le Provost, S. Loucatos, F. Louis, G. Maurin, L. Moscoso, C. Naumann, J.-P. Schuller, T. Stolarczyk, B. Vallage, P. Vernin
CEA, IRFU, Centre de Saclay, 91191 Gif-sur-Yvette, France

C. Rabouille
CEA-CNRS-UVSQ , LSCE/IPSL, 91198 Gif-sur-Yvette, France

D. Baccila, M. Borghini, M. Fassin, G. Gasparini, K. Schroeder, S. Sparnocchia, P. Traverso
CNR–ISMAR, Ancona, Italy

J.A. Aguilar, J. Bernabeu-Verdu, J.J. Hernandez-Rey, D. Real, F. Salesa, S. Toscano, J.D. Zornoza
CSIC, Valencia, Spain

P. Razis
University of Cyprus

F. Aharonian, S. Delaney, L. Drury, S. Gabici, A. Hooper, D. Malishev, A. Taylor
Dublin Institute For Advanced Studies, Ireland

G. Anton, R. Auer, T. Eberl, F. Fehr, U. Fritsch, K. Graf, B. Herold, J. Hößl, O. Kalekin, A. Kappes, U.F. Katz, R. Klein, C. Kopper, S. Kuch, R. Lahmann, M. Millinger, H. Motz, M. Neff, F. Schöck, R. Shanidze
University of Erlangen, Germany

A. Albert, F. Cohen, J-P. Ernenwein, D. Stubert-Drouhin
Université de Haut Alsace-GRPHE, Mulhouse, France

G. Chronis, I. Georgiadou, H. Kontoyiannis, V. Lykousis, E. Papadopoulos
Hellenic Centre for Marine Research (HCMR), Greece

G. Bourlis, P.E. Christopoulou, N. Fragoulis, N. Gizani, A. Leisos, A. Tsirigotis, S. Tzamarias
Hellenic Open University, Patras, Greece

R. Bellotti, M. Circella, R. Megna, G. De Ruvo, M. Ruppi
INFN Sezione Bari and University of Bari, Italy

M. Bazzotti, S. Biagi, G. Carminati, S. Cecchini, T. Chiarusi, G. Giacomelli, A. Margiotta, G. Pilone, M. Spurio
INFN Sezione Bologna and University of Bologna, Italy

S. Aiello, L. Caponetto, A. Grimaldi, E. Leonora, D. Lo Presti, N. Randazzo, S. Reito, G.V. Russo, D. Sciliberto, V. Sipala, S. Urso
INFN Sezione di Catania and University of Catania, Italy

M. Anghinolfi, A. Bersani, M.Battaglieri, M. Brunoldi, R. Cereseto, R.DeVita, H. Costantini, K. Fratini, S. Minutoli, P. Musico, M. Osipenko, D. Piombo, G. Ricco, M. Ripani, M. Taiuti, D. Torazza
INFN Sezione Genova and University of Genova, Italy

I. Amore, A. Anzalone, G. Cacopardo, R. Cocimano, R. Coniglione, A. D'Amico, C. Distefano, E. Migneco, M. Musumeci, A. Orlando, R. Papaleo, V. Pappalardo, P. Piattelli, G. Raia, G. Riccobene, A. Rovelli, P. Sapienza, M. Sedita
INFN Laboratori Nazionali del Sud, Catania, Italy

R. Habel, A. Martini, L. Trasatti
INFN Laboratori Nazionali di Frascati, Italy

G. Barbarino, G. De Rosa , S. Russo
INFN Sezione Napoli and University of Napoli, Italy

E. Castorina, V. Flaminio, R. Garaguso, D. Grasso, A. Marinelli, M. Morganti, C. Sollima
INFN Sezione Pisa and University of Pisa, Italy

F. Ameli, M. Bonori, A. Capone, G. De Bonis, F. Lucarelli, R. Masullo, F. Simeone, M. Vecchi
INFN Sezione Roma and University of Roma 1, Italy

B. Bigourdan, P. Bouquet, D. Choqueuse, G. Damy, J. Drogou, Z. Guédé, J. Marvaldi, J. Rolin, P. Valdy
IFREMER, France

G. Etiope, P. Favali, C. La Fratta, G. Marinaro
Istituto Nazionale di Vulcanologia, Italy

K. Lyons, T. Pradier, C. Racca
Institut pluridisciplinaire Hubert Curien Strasbourg, ULP, CNRS, IN2P3, Strasbourg, France

D. Felea, O. Maris, G. Pavalas, V. Popa, A. Radu, M. Rujoiu, D. Tonoiu
Institute of Space Sciences, Machurele-Bucharest, Romania

N. Bellou, F. Colijn, P. Koske, T. Staller
University of Kiel, Germany

N. Kalantar-Nayestanaki, H. Löhner
KVI and University of Groningen, the Netherlands

S. Bradbury, J. Rose, R.J. White
University of Leeds, United Kingdom

F. Jouvenot, C. Touramanis
University of Liverpool, United Kingdom

P. Katrivanos, D. Lenis, C. Markou, Y. Papazoglou, P. Rapidis, I. Siotis
National Center of Scientific Research "Demokritos", Athens, Greece

A. Assis Jesus, R. de Boer, H. Boer Rookhuizen, M. Bouwhuis, C. Colnard, P. Decowski,   E. Heine, M. van der Hoek, J. Hogenbirk, P. Jansweijer, M. de Jong, H. Kok, L. Kruijer, S. Mangano, S. Mos, D. Palioselitis, H. Peek, E. Presani, G. van der Steenhoven, J.Steijger, P. Timmer, P. Werneke, G. Wijnker
NIKHEF, Amsterdam, the Netherlands

H. van Haren, M. Smit
Koninklijk Nederlands Instituut voor Onderzoek der Zee (NIOZ), Texel, the Netherlands

T. Athanasopoulos, A. Ball, A. Belias, A. Fotiou, Y. Kiskiras, A. Kostoglou, S. Koutsoukos, M. Maniatis, E. Markopoulos, A. Psallidas, L.K. Resvanis, G. Stavropoulos, V. Tsagli, G. Vermisoglou, V. Zhukov
NOA / NESTOR, Pylos, Greece

J. Perkin, L. Thompson
University of Sheffield, United Kingdom

F. Gasparoni, S. Giacopelli
Tecnomare, Venice, Italy

P. Kooijman
University of Utrecht, the Netherlands

C. Bigongiari, J. Zúñiga
University of Valencia, Spain

J. Alba, M. Ardid, M. Bou-Cabo, F. Camarena, V. Espinosa, J. Martínez-Mora, J. Ramis, J. Redondo, V. Sánchez-Morcillo
Universidad Politécnica Valencia / IGIC, Spain

EXECUTIVE SUMMARY

The scientific case for a neutrino telescope of a cubic kilometre scale in the Mediterranean Sea is overwhelming. The infrastructure it requires can easily be shared by a host of other, associated sciences, using it for continuous long-term measurements in areas such as oceanography, climatology, geophysics, geotechnics and marine biological sciences. This combination of neutrino telescope and multidisciplinary undersea observatory, the KM3NeT research infrastructure, is the subject of this Conceptual Design Report, which summarises the goals for its design and the options for its technical implementation.

The interaction probability of neutrinos is small, which allows them to pass almost unhindered through the cosmos; however, this small interaction probability, makes them hard to detect on Earth. Detection proceeds through the Cherenkov light emitted by the interaction products in transparent media. The Mediterranean Sea provides the large target mass necessary to enhance the detection rate and the transparency of its water makes it ideal to house a large array of light sensors to detect this Cherenkov light. The geographic location is ideal since the region of the sky observed by the neutrino telescope includes the bulk of the Galaxy. The KM3NeT neutrino telescope will be the most sensitive in the world, observing the Universe with this novel messenger. The sensitivity to cosmic neutrino sources will be more than 50 times larger than that of other neutrino telescopes observing the same part of the sky and more than three times larger than that of the detectors at the South Pole, which observe a different sky region.

The Mediterranean deep sea is of prime interest also for investigations in the fields of marine and earth sciences. The associated-sciences infrastructure will be a world-leading observatory with enormous discovery potential. These experiments will form part of wider global environmental monitoring systems.

For more than a decade, the feasibility of neutrino astronomy with a detector in the deep sea has been investigated in three pilot projects. In each of these, different configurations and techniques have been explored. These three projects, ANTARES, NEMO and NESTOR, have reached maturity and have demonstrated the potential of the detection technique by reconstructing the tracks of muons, the possible reaction products of the sought after neutrinos. These projects have provided a wealth of information on the technologies required for a large deep-sea neutrino telescope from which KM3NeT will reap the benefits.

Each of the three sites situated in different regions of Mediterranean Sea are suitable for installation of the neutrino telescope. Extensive measurements of environmental properties, such as water transparency and background light conditions, have been performed at these sites and in addition embryonic cabled observatories for the associated sciences have been installed and tested. These activities are continuing in the framework of the KM3NeT project and will provide input for the process of selection of the site for KM3NeT.

A number of options for the technical implementation of the KM3NeT infrastructure are being investigated. For the light detection units of the neutrino telescope, designs consisting of varying numbers and sizes of photomultiplier tubes inside pressure resistant glass housings and containing the necessary electronics components are being studied. The data from these optical modules will be multiplexed using passive optical or active electronic systems and the resulting data stream will be transported from the detector to shore using optical fibres. The mechanics of the detection units follow the main ideas developed for the pilot projects with some adaptations to ease transport and deployment being investigated.

Power supply for the infrastructure, which is dominated by the needs of the neutrino telescope, requires of the order of 50 kW to be transported to

the deep-sea structures over up to 100 km; studies for the power system and the main cable have been made. The cable choice is likely to be dictated by the standards of the telecommunications industry, which may restrict the number of communication fibres and the maximum power load. Small-scale local generation, via wind or photo-voltaic systems, of the required power for the underwater system as well as the onshore facilities has been considered. Such generation is viable for a modest investment. The possibilities for such renewable energy production will be pursued further.

At the landfall of the deep-sea cable a shore station is required, where power and computing facilities for the data handling for both the neutrino telescope and the associated sciences infrastructure will be housed. Easy access to a harbour with adequate warehousing capabilities is required. Deployment of the deep-sea structures will necessitate the use of deployment ships or platforms. Submersibles will be required for the underwater connection of equipment.

The final design of the neutrino telescope will require decisions to be made on the various concepts described in this document. To do this, a risk analysis of the most promising system designs must be performed. Laboratory qualification tests, including tests in hyperbaric chambers, are necessary to provide input data for this process. At a later stage, larger scale prototypes will be needed for integrated system tests. Deployment in the deep sea will allow for longer term testing of these prototypes. Before the start of manufacturing, a quality management system must be in place. Outsourcing of the production of major parts of the infrastructure is being considered.

The KM3NeT design study process has brought together a strong science and engineering community preparing all elements necessary for the successful design, construction, management and operation of a unique research infrastructure.

1 INTRODUCTION

This Conceptual Design Report describes the scientific objectives, and the concepts behind the design, construction, and operation of a large deep sea research infrastructure in the Mediterranean Sea hosting a cubic kilometre scale neutrino telescope and facilities for associated marine and earth sciences.

The work described here is performed within the framework of the KM3NeT design study which is funded by the EU in the 6th Framework Programme[1].

1.1 Scientific Objectives of Neutrino Telescope

The major scientific objective of high-energy neutrino telescopes is the study of the Universe in the 'light' of neutrinos.

Amongst the important objectives are the discovery and study of sites of acceleration of high-energy particles in the Universe. Since their discovery a century ago the origins of high-energy charged cosmic rays arriving at the Earth are still unknown; neutrinos offer a unique possibility to trace their origins. Having no electric charge, neutrinos are unperturbed by magnetic fields, and by being weakly interacting they can pass through dense dust clouds which might surround their sources.

There are numerous candidate neutrino sources in the cosmos; among them are supernova remnants, pulsars and microquasars in the Galaxy. Possible extragalactic sources include active galactic nuclei and γ-ray burst emitters. For such processes the neutrino energy scale is 10^{12} to 10^{16} eV.

Another important objective of neutrino telescopes is the search for dark matter in the form of WIMPs (Weakly Interacting Massive Particles). As an example in the case of supersymmetric theories with R-parity conservation, the relic neutralinos

from the big-bang are predicted to concentrate in massive bodies such as the centres of the Earth, the Sun or the Galaxy. At these sites neutralino annihilations and the subsequent decays of the resulting particles may yield neutrinos with energies up to 10^{10} - 10^{12} eV.

Additionally the study of the diffuse neutrino flux, originating from sources that cannot be individually resolved or from interactions of cosmic rays with intergalactic matter or radiation, may yield important cosmological clues. Such measurements would be significant for neutrino energies in excess of 10^{15} eV.

To have adequate sensitivity for the expected fluxes of neutrinos in these processes, detectors with very large volumes of the order of a cubic kilometre are required.

1.2 Neutrino Detection Techniques

A number of possible techniques exists for detecting high-energy neutrinos from space. The most widely exploited method for the core energy range of interest (10^{11} to 10^{16} eV) is the detection of neutrinos in large volumes of water or ice, using the Cherenkov light from the muons and hadrons produced by neutrino interactions with matter around the detector.

Water Cherenkov detectors (e.g. IMB [1] and Kamiokande/Super-Kamiokande [2]) are the only detectors that have so far observed neutrinos produced beyond the solar system; these were neutrinos with energies up to several tens of MeV produced in supernova 1987a. These detectors are much smaller than the proposed KM3NeT neutrino telescope.

MACRO [3] was the largest detector using a different technique. It used liquid scintillator and streamer tubes to detect charged particles and operated underground in the Gran Sasso laboratory in Italy.

---

[1] Contract Number 011937.

Experiments are also being developed based on the detection of radio waves or sound produced in neutrino interactions. These techniques become viable for neutrinos with energies roughly above 10^{18} eV.

1.3 WATER/ICE NEUTRINO TELESCOPE PROJECTS

The original idea of a neutrino telescope based on the detection of the secondary particles produced in neutrino interactions is attributed to Markov [4] who invoked the concept in the 1950's. Given the need of a kilometre-scale detector, only designs incorporating large naturally occurring volumes of water or ice can be viable. A deep sea-water telescope has significant advantages over ice and lake-water experiments due to the better optical properties of the medium. However, serious technological challenges must be overcome to deploy and operate a detector in the deep sea.

The pioneering project, DUMAND [5], attempted to deploy a detector off the coast of Hawaii in the years between 1980 and 1995. At that time technology was not sufficiently advanced to overcome these challenges and the project was cancelled.

In contrast, AMANDA [6] and BAIKAL [7] where the equipment is deployed from the surface of the solid glacial ice or the frozen lake surface have developed workable detector systems. After the completion of their detector in 2002, the AMANDA collaboration proceeded with the construction of a much larger detector, IceCube. Completion of this detector is expected in 2010.

The advantages of sea-water neutrino telescopes are significantly better angular resolution – down to 0.1° (RMS) for sea water compared to approximately 1° for IceCube – as well as a more uniform efficiency due to the homogeneity of the medium. A disadvantage of sea water is the higher optical background due to radioactive decay of ^{40}K and bioluminescence (light emission from living organisms). These backgrounds can be mitigated in the design of the detector by having a high density of optical modules and high-bandwidth data readout.

The pioneering work of DUMAND to build a deep sea neutrino telescope is being continued in the Mediterranean Sea by ANTARES [8], NEMO [9] and NESTOR [10].
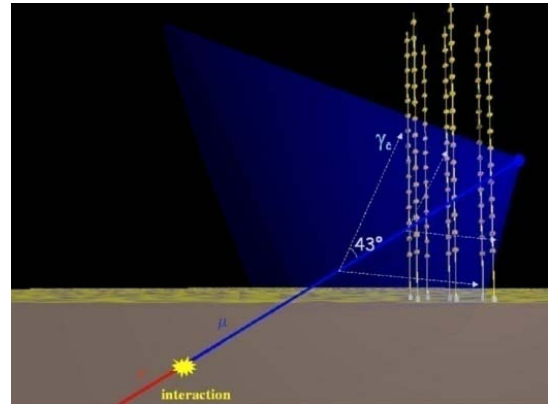
Figure 1-1: Principle of detection of high-energy neutrinos in an underwater neutrino telescope.

1.4 NEUTRINO INTERACTIONS AND EVENT SIGNATURES

There are three different flavours of neutrinos (called electron, muon and tau neutrinos, ν_e, ν_μ and ν_τ) which can undergo different reactions with the nuclei or electrons of the material surrounding the detector (water or rock). In addition, for each of the neutrinos, there is a corresponding antineutrino. Since the event signatures of neutrinos and antineutrinos of a given flavour are usually not distinguishable in neutrino telescopes, the term *neutrino* will be used to cover both neutrinos and antineutrinos in this document.

The relevant neutrino reactions and the different aspects of their detection in a neutrino telescope are summarised in Table 1-1. The muon channel, given its importance for point source searches and its increased sensitivity due to the long muon range in water or rock, is the primary signature for optimising the detector and estimating its sensitivity. Nevertheless, the other channels have also been studied and are considered where they add significantly to the physics potential of the KM3NeT neutrino telescope.

Reaction	charged current reactions			neutral current reactions, $x = e, \mu, \tau$
	$\nu_e + N \rightarrow e + X$	$\nu_\mu + N \rightarrow \mu + X$	$\nu_\tau + N \rightarrow \tau + X$	$\nu_x + N \rightarrow \nu_x + X$
Signature(s)	Electromagnetic + hadronic shower (superimposed).	Muon (+ hadronic shower if reaction inside detector).	(1) If $\tau \rightarrow \nu\bar{\nu}\mu$: Like $\nu_\mu N \rightarrow \mu X$ (2) If $\tau \rightarrow \nu\bar{\nu}e$: Like $\nu_e N \rightarrow e X$ (3) If $\tau \rightarrow \nu + $ hadrons: Hadronic shower For decays (2) and (3) and τ energies above some TeV the showers from primary reaction and τ decay are separated in space and may be resolved ("double-bang signature").	Hadronic shower.
Detectability	If reaction is inside detector light acceptance.	If muon crosses detector light acceptance.	If reaction is inside detector light acceptance, except for decay (1).	If reaction is inside detector light acceptance.
Measurement precision	Energy: good. Direction: fair (a few degrees at best).	Energy: fair (factor 2 at best at muon energies above 1 TeV). Direction: very good (0.1° at high muon energies).	Energy: fair (large fraction of the ν_τ energy goes to secondary neutrinos). Direction: Good for decay (1), fair otherwise.	Energy: poor (largest fraction of the ν_τ energy goes to secondary neutrino). Direction: Fair.
Remarks	Important for diffuse flux measurements and flavour studies. Not distinguishable from other shower signatures.	The golden channel for point source searches (neutrino astronomy). Muons of far-away events lose their energy before reaching the detector and may be of limited use for some analyses.	Like $\nu_e + N \rightarrow e + X$, except that energy measurement is less precise. Double-bang signatures might be very distinctive; otherwise not distinguishable from other shower signatures.	Like $\nu_e + N \rightarrow e + X$, except that energy measurement is much less precise. Not distinguishable from other shower signatures.

Table 1-1: The major neutrino reaction types and their signatures. For the reactions N denotes a proton or neutron in a nucleus and X stands for a system of hadronic particles. The charged leptons are symbolised by e, μ and τ. Showers, both hadronic and electromagnetic, are particle cascades with an overall range of less than 10 m that appear as "point-like", intense sources of Cherenkov light. Muons have a range above 1 km for energies exceeding 1 TeV and are extended line sources of Cherenkov light.

One further reaction channel that might be important is $\bar{\nu}_e e$ scattering, which for most of the energy range has a small cross section compared to the reactions in Table 1-1. However, at neutrino energies around 6.4 PeV the reaction proceeds through the resonant production of a W boson and has a large cross section, exceeding even the νN cross sections (Glashow resonance [**11**])

Detection Principles

The detection of high-energy muon neutrinos exploits:

- The emission of Cherenkov light by the muon and other charged secondary particles produced in a neutrino interaction;
- The directional correlation of the muon and parent neutrino trajectories to within 0.3° for E_ν >10 TeV;
- The fact that upward-going muons can only originate from local neutrino interactions since the Earth filters out all other particles;
- The long range of muons in water and rock in the energy range of interest. As a result muons may be generated far from the instrumented volume and still be detected.

The detection of electron and tau neutrinos is also possible in telescopes optimised for muon neutrino detection but the detection efficiency for these neutrino types is lower.

To detect the Cherenkov light, an array of light detectors, in the form of photomultipliers housed in glass spheres (optical modules), is deployed in the deep sea. The optical modules measure the time of arrival and the amount of the Cherenkov light. Figure 1-1 illustrates this principle of neutrino detection.

Measurement of the arrival times of the light and the knowledge of the position of the optical modules allow for the reconstruction of the muon direction with a precision of a few tenths of a degree. At high energies the muon direction is closely aligned with that of the neutrino. As shown in Figure 1-2, the average difference between the direction of the neutrino and the muon is small and at

energies above 100 TeV the neutrino direction can be determined with a precision better than 0.1° (RMS).

$$\Theta_{\nu-\mu} \approx \frac{0.7°}{(E_\nu(\mathrm{TeV}))^{0.6}}$$
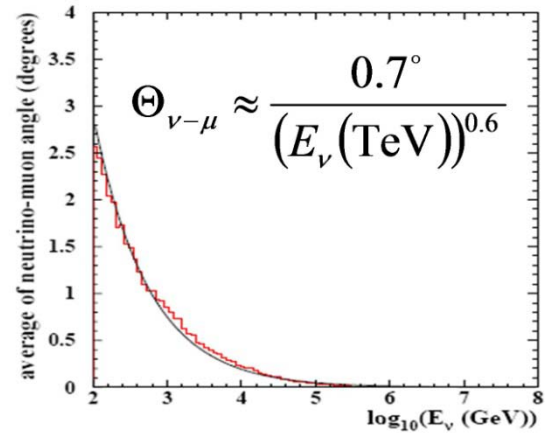
Figure 1-2: Average difference between the neutrino and muon directions from a simulation; the indicated functional form reproduces the observed energy dependence (solid curve).

The energy of a muon as it passes through the detector can be estimated from the measured intensity of the Cherenkov light, and can be used to set a lower limit of the neutrino energy.

The energy of electromagnetic or hadronic showers can be determined more accurately, provided that they are within the detector volume.

1.5 Backgrounds

Backgrounds in a neutrino telescope are caused either by random light, not associated with particles traversing the detector, or by muons or neutrinos generated in cosmic ray interactions in the terrestrial atmosphere. The muons ("atmospheric muons") can penetrate the water above the detector and give rise to a reducible background. The neutrinos ("atmospheric neutrinos"), on the other hand, are an irreducible background.

Random Backgrounds

Daylight does not penetrate at any detectable level to depths beyond a kilometre. Sea water however contains small amounts of the naturally occurring radioactive potassium isotope, ^{40}K. This isotope

decays mostly through β-decay releasing electrons that produce Cherenkov light and so create a steady, isotropic background of photons with rates of the order of 350 Hz per square centimetre. Although the induced number of photoelectrons per photomultiplier during the time it takes a muon to pass the detector (a few microseconds) is moderate, there is still a chance that these hits may mimic the signature of a muon or shower or, more importantly, contaminate the hit pattern of a neutrino induced event.

Many life forms that inhabit the deep sea emit light. This bioluminescence has two contributions, a continuous component usually attributed to bioluminescent bacteria, and a component of localised bursts of light with high rates probably connected to macroscopic organisms passing the detector.

These random backgrounds can be reduced by coincidence methods to an acceptable level.

Atmospheric Muons

Cosmic rays entering the atmosphere produce extensive air showers which contain high-energy muons. Although the sea water above the detector serves as a shield, many such muons reach the detector. This background is reduced by deploying a neutrino telescope at great depth (see Figure 1-3).

The remaining flux of atmospheric muons is still many orders of magnitude larger than any neutrino induced muon flux. Since the atmospheric muons come from above this can be exploited to eliminate them. However, multiple coincident atmospheric muons can produce a hit pattern that resembles that of an up-going muon. Therefore care must be taken in the detector design and the reconstruction algorithms to minimise the rate of these fake events.

Atmospheric Neutrinos

Large numbers of charged pions and kaons are produced in cosmic ray interactions in the atmosphere. Their subsequent decays produce neutrinos, resulting in a large flux of atmospheric high-energy

neutrinos. They are an irreducible background for the detection of neutrinos of cosmic origin.
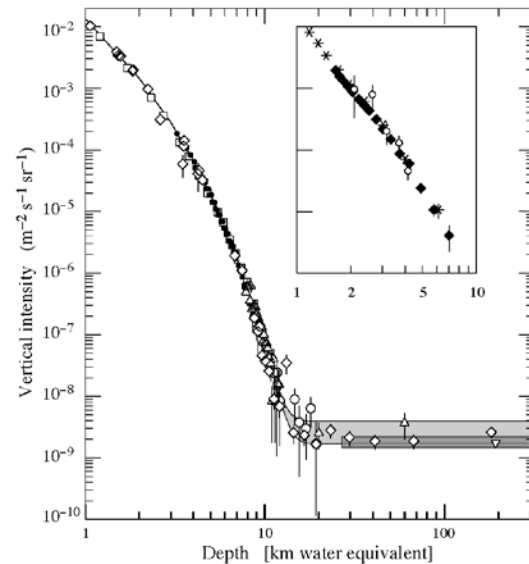
Figure 1-3: Vertical muon intensity versus depth (1 km water equivalent = 10^5 g cm^{-2} of standard rock). The experimental data are from: ♦: the compilations of Crouch [12], □: Baksan [13], ○: LVD [14], ●: MACRO [3], ■: Frejus [15], and △: SNO [16]. The shaded area at large depths represents neutrino-induced muons of energy above 2 GeV. The upper line is for horizontal neutrino-induced muons, the lower one for vertically upward muons.

To study neutrinos arriving from cosmic point sources, a small search cone, commensurate with the angular resolution, is used. This reduces the background from atmospheric neutrinos to a manageable level.

For the investigation of any diffuse neutrino flux of cosmic origin one relies on the fact that its expected energy spectrum is harder than the spectrum of atmospheric neutrinos. Thus it is possible to search for an excess of neutrinos of cosmic origin at higher energies. However this may be complicated by the presence of the so called 'prompt' atmospheric neutrino flux with a hard energy spectrum, arising from the decay of charm particles in atmospheric showers.
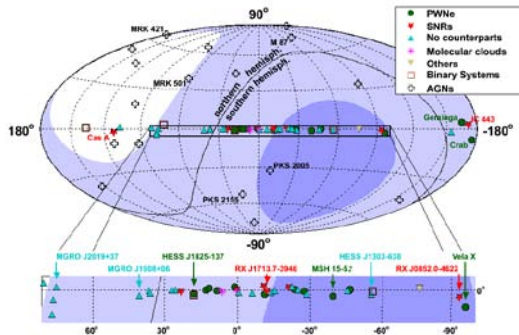
Figure 1-4: Sky coverage in Galactic coordinates for a detector located in the Mediterranean Sea and at the South Pole. The shading indicates the visibility for a detector in the Mediterranean with 2π downward coverage; dark (light) areas are visible at least 75% (25%) of the time. The locations of recently observed sources of high-energy γ-rays are also indicated.

1.6 Observable Sky

The KM3NeT neutrino telescope, situated in the Mediterranean Sea, at a latitude λ between 36° and 43° North, can observe upward-going neutrinos from most of the sky (about 3.5π sr), due to the rotation of the Earth. Declinations below $-90° + \lambda$ are always visible, while those above $+90° - \lambda$ are never visible. Declinations between these two values are visible for part of the sidereal day (Figure 1-4). Most of the Galactic plane, including the Galactic centre, is visible most of the sidereal day. Since the IceCube telescope at the South Pole is sensitive to positive declinations, the two detectors will have a reasonable common field of view for cross-checks (about 1.5π sr). At very large neutrino energies it may be possible for the KM3NeT telescope to reconstruct downward-going neutrinos and so extend its coverage further into the northern hemisphere. Together KM3NeT and IceCube provide full sky coverage for neutrino astronomy.

1.7 Associated Science Projects

The KM3NeT deep sea infrastructure serves also as a platform for a wide spectrum of marine and geological scientific research. For these "associated science" projects the permanent connection to the shore for powering and reading out instruments is of great value. Such permanent connections from the deep sea to the shore are rare. The only sites

cabled at present in Europe are those of the neutrino telescope pilot projects, which already feature extensive programmes in oceanography, biology, and geology. The ESONET-EMSO project is studying many sites for permanent undersea observatories including these neutrino telescope sites.

Associated science activities at the pilot project sites to date have included a series of measurements of environmental parameters and details are given in Chapter 5.

1.8 Structure of the Report

The broad range of discoveries in astroparticle physics, earth and marine sciences possible with the undersea observatory is described in Chapter 2.

In order to give numerical predictions, a specific detector geometry for the neutrino telescope has been adopted, even though it is not the final one since at this stage the design is not yet complete. This "reference detector" is described in Chapter 3. Figure 1-5 shows the effective neutrino area (defined below) of the reference detector together with an analytical approximation to the results of the detailed Monte Carlo simulation.

Other detector geometries tried so far have similar effective neutrino areas. The effective neutrino area, A, is defined by $N = \Phi A$, where N is the number of detected neutrino events, and Φ is the time integrated flux of incident neutrinos.

Chapter 3 also gives a summary of the detector concepts both for the neutrino telescope and for the infrastructure for the associated sciences.

The characteristics of a neutrino telescope required in order to achieve the goals summarised in the science case are listed in Chapter 4

Chapter 5 presents the progress of the existing "pilot" neutrino telescope projects in the Mediterranean Sea: ANTARES, NEMO and NESTOR with locations and depths as indicated in Figure 1-6. The most advanced project is that of the ANTARES collaboration which is operating a detector with 900 optical modules at a site off the south coast of
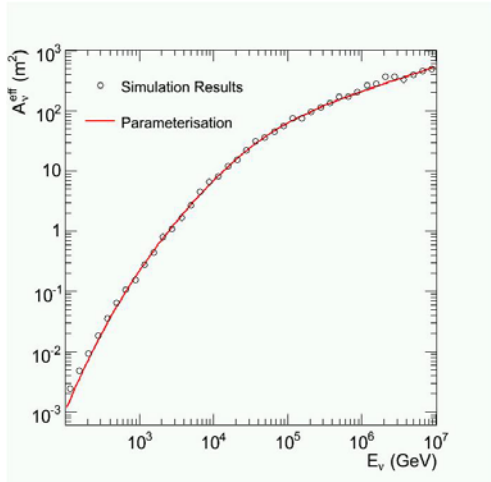
Figure 1-5: The effective neutrino area for the reference detector compared to an analytic parameterisation.

France near Toulon. The ANTARES detector is complete and is collecting data. The NEMO collaboration is exploring a site off Sicily (Capo Passero). The NEMO group is operating a test site in the bay of Catania to perform R&D for a future large detector. In 2007 prototype detector elements, a junction box and a "mini-tower", were deployed and operated on this site. A deep-sea station at Capo Passero is under construction. The NEMO collaboration is planning to deploy a full detection unit in 2008. The NESTOR collaboration intends to build a detector with 168 optical modules at a site near Pylos off the coast of Greece. During a period in 2003 a storey of the NESTOR structure was operated at the site at 3800 m. Plans include the deployment of a five storey tower in 2009.

The three projects have chosen different solutions for the technical implementation of the deep-sea neutrino telescope concept. The success of these projects demonstrates the feasibility of an under-sea neutrino telescope.
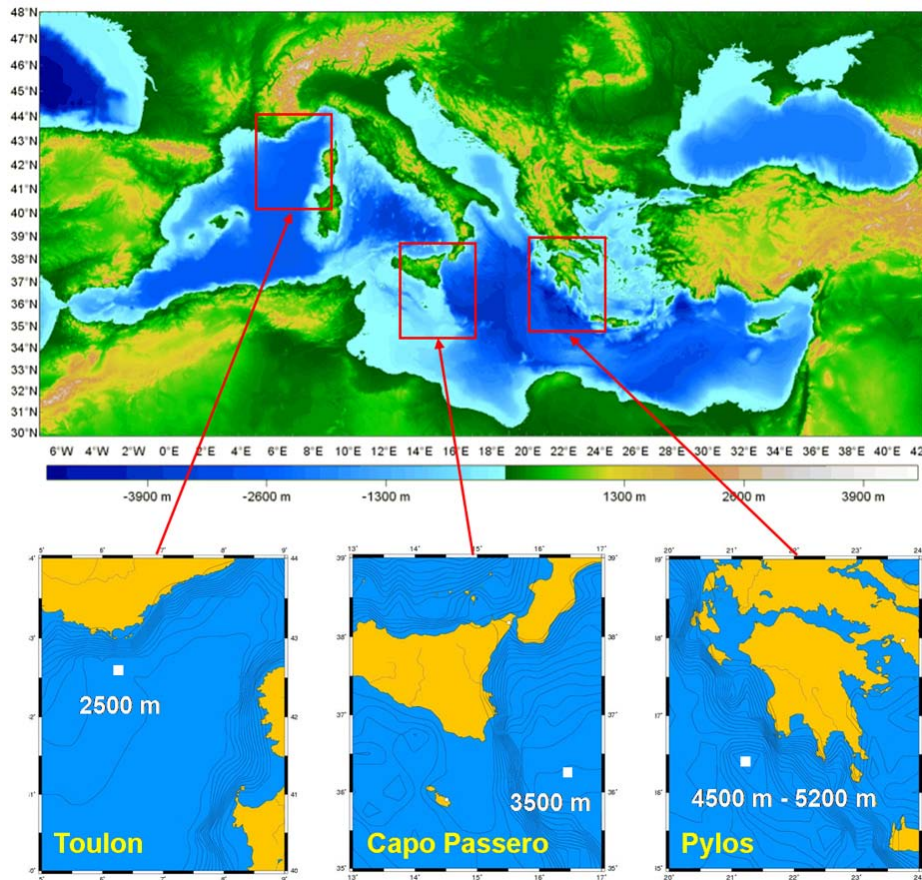
Figure 1-6: Locations of the sites of the three Mediterranean neutrino telescope projects.

Chapter 6 describes the investigations of the environmental conditions performed at the three sites.

The various design options for the technical implementation of the KM3NeT research infrastructure are described in Chapter 7. In particular issues relating to optical modules, electronics and data acquisition, mechanical structures, seafloor, sea surface, and sea shore infrastructure, calibration, and marine and Earth science nodes are addressed.

Chapter 8 provides a development plan towards the construction of KM3NeT, based on strict strategies for risk assessment and quality assurance. The project implementation is covered in Chapter 9.

The interaction probability of neutrinos is small, which allows them to pass unhindered through the cosmos. This small interaction probability, however, makes them hard to detect on Earth. Their interaction products do provide measurable signals through the Cherenkov effect in water. The Mediterranean Sea provides the large mass necessary to enhance the detection rate and the transparency of its water makes it ideal to house a large array of light sensors to detect the Cherenkov light. The location is ideal, as the observed region of the sky includes the centre of our Galaxy. The Mediterranean deep sea is also of prime interest for investigations in the fields of marine and earth sciences.

2 SCIENCE CASE

The undersea neutrino observatory will have enormous potential for spectacular discoveries in a wide range of scientific domains. The main thrust of the programme is in astroparticle physics where the neutrino telescope will be the largest and most precise instrument of its kind in the world. Here the unique properties of the neutrino as a messenger from distant confines of the cosmos may lead to breakthroughs in our understanding of the Universe.

Due to the deep-sea location of the detector and the permanent nature of the read-out, the observatory opens a great avenue for original discoveries in sea and Earth sciences with many potential applications.

2.1 ASTROPARTICLE AND PARTICLE PHYSICS

Neutrino astronomy is an essential element of multi-messenger and multi-wavelength astronomy which for the past 50 years has been extending our knowledge of objects and structures in the Universe. Optical astronomy explores sources emitting in the visible light. Multi-wavelength astronomy from radio wave to γ-rays has discovered a host of different sources emitting non-thermal radiation, ranging from extragalactic objects such as active galactic nuclei and γ-ray bursts to galactic objects such as supernova remnants and microquasars. Neutrino telescopes, together with ultra high-energy charged cosmic ray detectors and gravitational wave detectors, extend further the discovery capability of this new astronomy. Each different messenger probes the various sources in different ways and gives diverse possibilities for new observations. The unique neutrino property of weak interaction with matter means that neutrinos can escape from dense matter environments surrounding sources when all other messengers might be absorbed, leaving neutrino telescopes as the only devices capable of observing some astrophysical sources. Further, high-energy γ-rays and ultra high-energy charged cosmic rays are absorbed by the

inter-galactic radiation fields giving a limit to their possible viewing horizons. Charged cosmic rays are deflected by magnetic fields and so cannot be traced back to their origins except at extremely high energies [17]. In contrast, neutrinos propagate without significant absorption or deflection from the most distant objects in the Universe. Neutrinos will yield vital information on the nature of known sources. Another very exciting discovery would be of hitherto unknown astronomical sources where only neutrinos emerge.

Dark matter can be searched for by using the same unique properties of the neutrino. The existence of dark matter and its dominance over normal matter in the Universe is well established from many observations since the original hypothesis of Zwicky [18] in the 1930's to explain the stability of galaxy clusters; however the nature of dark matter is unknown. If dark matter is composed of WIMPs, there will be an enhanced density of such particles in massive celestial bodies such as the Sun, the Earth and the Galactic centre. It is this concentration of dark matter in precise locations in the Galaxy that would be detectable by neutrino telescopes in certain dark matter models. Such a discovery would be an immense advance in our understanding of nature.

Predictions of Neutrino Rates

The total flux of neutrinos fixes the required detector size and the energy spectra of the neutrinos constrain the layout of the detector elements. Given the novelty of neutrino astronomy, large uncertainties exist in the predictions of neutrino fluxes emitted from sources and hence in the event rates in a neutrino telescope.

Estimates of neutrino fluxes come from models of astrophysical particle accelerators and from measured fluxes of other species of particles, mainly γ-rays. Neutrinos are produced as secondary products of interactions of the accelerated charged cosmic rays in all models of cosmic sources of high-energy radiation. Typical neutrino production reac-

tions are $pp \rightarrow \pi + X$, with the decay of the charged pions, $\pi^{\pm} \rightarrow \mu\nu_{\mu}$. In the same reactions the neutral pions decay through $\pi^0 \rightarrow \gamma\gamma$, thereby linking the production of neutrinos and γ-rays. This allows for neutrino rates to be estimated from γ-ray rates, under the assumption that γ-ray production by electromagnetic mechanisms can be neglected. For sources with low matter fields surrounding the accelerating region, so that γ-rays cannot be absorbed, realistic estimates of neutrino fluxes can be made based on measured γ-ray fluxes and detailed simulations of the ratio of γ-rays to neutrinos in the production reactions. Predictions of neutrino rates from source modelling are much less reliable but are the only means available for many sources.

The following sections give numerical values for neutrino rates based on these methods. In the published literature vast ranges of estimates for neutrino fluxes are reported even when they are based on the same measured γ-ray fluxes. Therefore such estimates should only be taken as a first indication of possible rates. Only a flux measurement in a neutrino telescope will provide constraints on the underlying models.

Neutrino Source Characteristics

Following Waxman [**19**], it can be shown that the minimum apparent luminosity for neutrino detection is:

$$L_{\nu} \approx N \left(\frac{d}{4\,\mathrm{Gpc}}\right)^2 \left(\frac{AT}{1\,\mathrm{km^2yr}}\right)^{-1} \times 10^{46}\,\mathrm{erg/s,}$$

where d is the distance to the source, N is the number of detected neutrinos, A is the muon effective area[2] of the telescope and T the total observation time. For a telescope with a muon effective area $A \sim 1$ km^2 and for extragalactic distances $d \sim 4$ Gpc, the source luminosity must be $L_{\nu} \sim 10^{47}$ erg/s, which is more than 13 orders of magnitude higher than the solar luminosity, and such objects are rare in the Universe.

---

[2] The muon effective area is defined in analogous manner as the neutrino effective area (see section 1.8), but with the neutrino flux replaced by the muon flux induced by incident neutrinos.

At extragalactic distances the known sources with sufficient luminosity to be detected by a cubic kilometre scale neutrino telescope are Active Galactic Nuclei (AGN), with continuous luminosities of about 10^{48} erg/s, and Gamma Ray Bursts (GRBs), with instantaneous luminosities of around 10^{52} erg/s that last a few tens of seconds. Within the Galaxy the much smaller distances involved, kpc rather than Gpc, mean sources with luminosities lower by a factor of 10^{12} could be detected. Many examples of such sources with luminosities of 10^{34} erg/s exist in the Galaxy: Supernova Remnants (SNRs), Pulsar Wind Nebulae (PWN) and microquasars.

The effective detection area of a neutrino telescope increases dramatically with neutrino energy and allows for the study of neutrinos over a broad energy range starting from a few hundred GeV (see Figure 1-5). The expectation is that most neutrino sources mentioned above will have an energy spectrum proportional to $E^{-\alpha}$, with differential spectral index $\alpha \approx 2$ as resulting from the Fermi model of stochastic particle acceleration and the measurements from γ-ray telescopes. Given the effective neutrino area of the reference detector, for such a neutrino energy spectrum the bulk of the detected events will be in the energy range 1 to 100 TeV.

2.1.1 Point Sources

The sensitivity of the reference detector to point sources with angular size less than the average neutrino direction resolution of 0.1° is shown in Figure 2-1 as a function of the source declination. The plot compares the KM3NeT sensitivity with other experiments and in particular IceCube. The plot shows that KM3NeT will be more than 50 times more sensitive than ANTARES for the same region of the sky and more than 3 times more sensitive than IceCube in complementary regions of the sky. As mentioned already (see Figure 1-4), the sensitive region for KM3NeT contains the bulk of the Galaxy where proximity opens many possibilities for discoveries.

Active Galactic Nuclei

Active Galactic Nuclei have the luminosities necessary to be observed by neutrino telescopes of a cubic kilometre scale. They are believed to be super-massive black holes accreting matter from the nucleus of the host galaxy. They exhibit highly collimated jets of relativistic plasma with opening angles of a few degrees or less. AGN, that have their jet axis aligned close to the line of sight of the observer, blazars, give a significant flux enhancement through Doppler broadening, and neutrinos are expected to experience a higher degree of collimation than γ-rays (about 1° compared to 5°) [20]. Hence, blazars present the best chance of detecting AGNs as individual point sources of neutrinos.
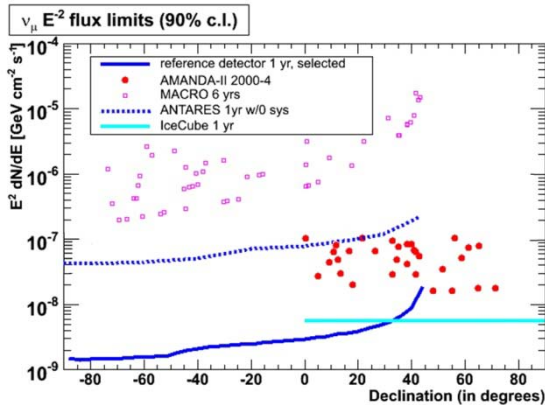
Figure 2-1: The sensitivity of the reference detector compared to existing limits from MACRO and AMANDA-II as well as expected limits from ANTARES and IceCube. The data points indicate limits for specific candidate sources.

Blazars exhibit continuum emission from radio to gamma energies, clearly non-thermal, and characterised by two broad bumps peaking at infrared and at X-ray/γ-ray frequencies. They are also highly variable, with fluxes varying by factors of around 10 over timescales from less than an hour to months. A total of 66 blazars have been detected as GeV γ-ray sources by EGRET and an increasing population of TeV blazars at higher redshifts is being detected by the latest generation of γ-ray Cherenkov telescopes. Currently around 18 blazars have been discovered at TeV energies over a range of redshifts from 0.03 to beyond 0.2. Since

the high-energy neutrinos are produced together with the high-energy photons in pion photo-production, the presence of high-energy photons in the spectrum of a given source may indicate an associated neutrino flux. The southern-hemisphere GeV blazars detected by EGRET and the TeV blazars detected by H.E.S.S. [21], such as PKS2155, PKS2005, H2356, 1ES1101, 1ES0229, 1ES0347 and PG1553, are therefore all potential targets for large neutrino telescopes.

In hadronic blazar models, the TeV radiation is produced by hadronic interactions of the highly relativistic baryonic outflow with the ambient medium or by interactions of protons of extreme energy with synchrotron photons produced by electrons spiralling in the jet's magnetic field, or both. Because of the observed variability blazars can only become bright neutrino sources if a dense photon radiation field is present. The density of soft photons in the core must be high enough for protons to interact at least once with the background photons while they traverse the core. The observed γ-ray spectrum from extragalactic sources is steepened due to absorption by the extra-galactic background light (EBL). The spectral energy distribution of neutrinos, however, is unaffected by the EBL and is related to the intrinsic spectrum of the emitted γ-rays. In the case of a distant blazar, such as 1ES1101 at $z = 0.186$, the observed spectral index of 3 corresponds to an intrinsic spectral index as hard as 1.5 [22]. This hardening results in a higher event rate in KM3NeT, as shown in Figure 2-2. Even the most distant TeV-bright blazars will produce muon-neutrino fluxes exceeding the atmospheric neutrino background [23].

The H.E.S.S. collaboration recently reported highly variable emission from the blazar PKS2155 [24]. A flux increase by two orders of magnitude, reaching about 10 Crab Units (CU: $E^2 \frac{dF}{dE} \approx 10^{-11}$ TeV cm^{-2} s^{-1}) was observed during a one hour period. Such flaring episodes are interesting targets of opportunity for neutrino telescopes. A typical TeV blazar with a quiescent flux of 0.02 CU and observed spectral index of 2.5 at a redshift of $z > 0.1$ could (depending on the amount of EBL

absorption) have an intrinsic spectral index as hard as 1.5. Assuming that half of the γ-rays are accompanied by the production of neutrinos, a flare of 10 CU lasting around 2.5 days would result in a neutrino detection at the significance level of 3 sigma.
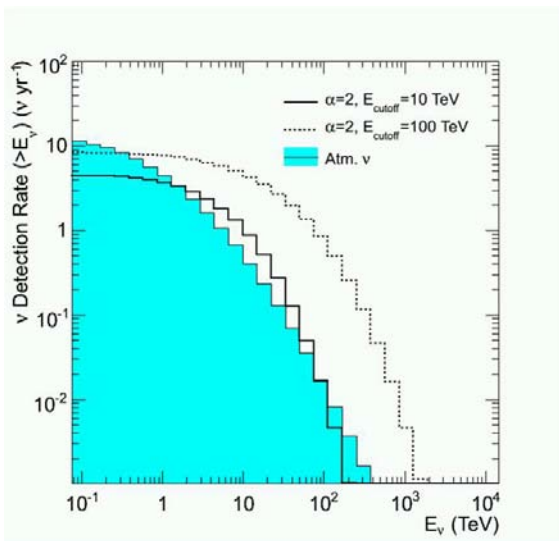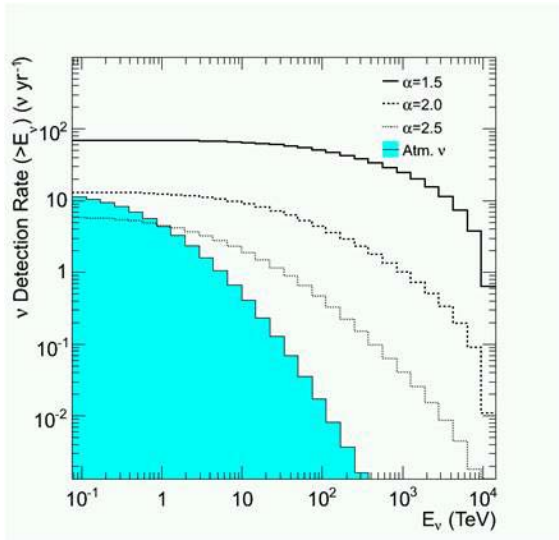
Figure 2-2: The total neutrino event rates above each energy detected by KM3NeT for the spectral indices α=1.5, 2, 2.5 and no energy cut-off (upper), and for a spectral index of α=2 and different cut-off energies E_0 = 10,100 TeV (lower).

Supernova Remnants

A major objective for neutrino astronomy is to solve the enigma of the origin of cosmic rays. Based on the approximate equality of the total energy in cosmic rays and the average power emitted by supernovae in the Galaxy, young supernova remnants have been considered for many years to be the best candidates for the acceleration of galactic cosmic rays.

The particle acceleration in SNRs is accompanied by the production of γ-rays and neutrinos due to interactions of accelerated protons and nuclei with the ambient medium. The very high-energy protons that generate multi TeV γ-rays and neutrinos can be accelerated only during a relatively short period of the evolution of the SNR, namely at the end of the free expansion phase and the beginning of the Sedov phase, when the shock velocity is high enough to provide a sufficient acceleration rate. When the supernova enters the Sedov phase, the shock gradually slows down and correspondingly the maximum energy of the particles that can be confined within the remnant decreases. This causes the most energetic particles to escape from the SNR, and the emission of γ-rays and neutrinos is suppressed. However, multi-TeV γ-rays and neutrinos can still be generated by the cosmic rays that escape the remnant, provided that they encounter an effective target such as a molecular cloud [25]. The duration of the emission in this case is determined by the time of propagation of cosmic rays from the SNR to the cloud and not by the (shorter) dynamical time of the remnant, so that the neutrino and γ-ray emission of the cloud lasts much longer than the emission of the SNR itself.

Recently, observations of some young SNRs have been made in TeV γ-rays with fluxes quite close to the early theoretical predictions. However this γ-ray data alone does not provide a clear and direct evidence of proton acceleration in SNRs; the competing inverse Compton scattering of directly accelerated electrons may significantly contribute to the observed γ-ray fluxes, provided that the magnetic field in the acceleration region does not exceed 10 μG. However, if the γ-rays come from π^0 decays and are thus accompanied by neutrinos, neutrino detection would provide an unambiguous evidence for proton acceleration in SNRs [26,27].
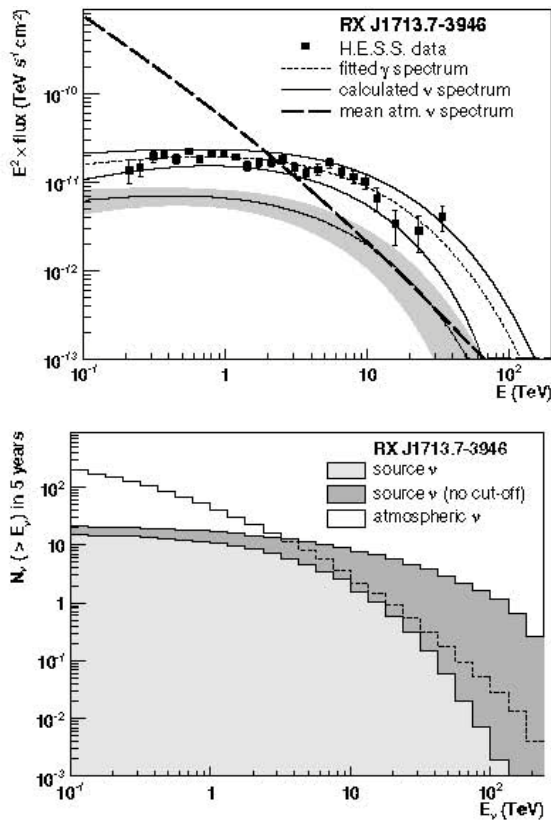
For RXJ1713.7-3946, the brightest TeV γ-ray SNR, an estimate of the neutrino flux can be obtained by assuming that the observed γ-ray TeV radiation is of hadronic origin. Figure 2-3 shows the measured γ-ray spectrum from this source and a prediction of neutrino rates based on this data. Since this supernova remnant is extended and larger than the angular resolution of the detector, the sensitivity limits in Figure 2-1 do not apply. This source has a source extension of 1.3° and is below the horizon 75% of time.

A study, with full reconstruction and quality cuts to ensure well measured events and an energy cut of 5 TeV, indicates that in 5 years of observation of this source 4.6 signal events would be observed with a background from atmospheric neutrinos of 8.2 events [28]. An improvement in sensitivity is

possible by reducing the search cone to focus just on the observed hot spot of γ-rays.

It has been shown in [25] that if a cloud with mass equal to 10^5 solar masses is located within 50-100 pc from a SNR that was active in the past as a cosmic ray accelerator, then a neutrino flux from the cloud can be expected up to roughly the level of one CU, which is within the capabilities of a cubic kilometre detector.

The close associations of some of the extended TeV galactic sources discovered by H.E.S.S. with several well established synchrotron X-ray nebulae (MSH 15-52, PSR J1826-1334, Vela X, etc.) confirm the early theoretical predictions [29] on TeV γ-ray visibility of young PWN with a spin-down "flux" ($L_0/4\pi d^2$) exceeding 10^{34} erg kpc^{-2}s^{-1}. The broadband spectral energy distributions of these sources are readily explained by the standard PWN model which assumes acceleration of ultra-relativistic electrons by the pulsar wind termination shock. Yet, in some of these systems particle acceleration could be driven by ions present in the relativistic pulsar wind. These ions are expected to produce γ-rays and neutrinos via inelastic interactions with the ambient medium. In this regard, the extended TeV source associated with the pulsar PSR B0833-45 (Vela X) is a possible candidate for such a "hadronic plerion". Indeed, although the observed γ-ray emission can be interpreted as inverse Compton emission of non thermal electrons [21], some strong (non-trivial) assumptions are needed in order to explain the rather unusual spectrum of this source with a photon spectral index of 1.5 and an exponential cut-off around 14 TeV. The steady-state electron distribution constrained by γ-ray data requires an E^{-2} type power-law spectrum with a sharp cut off around 70 TeV. Such a spectrum of electrons can only be understood if the magnetic field is negligible (a few micro-Gauss or less). Moreover, the total energy in relativistic electrons and in the magnetic field, which is required to match the observed X-ray and γ-ray fluxes, is only a negligible fraction ($\sim$0.1%) of the pulsar spin-down energy released over the pulsar's life-time of 11000 years. This begs the question as to where the remaining energy has gone. Interest-

ingly, if a large fraction of the spin-down luminosity of the pulsar is assumed to be carried away by relativistic protons and nuclei, both the absolute flux and the spectrum of TeV γ-rays of this unusual source can be satisfactorily explained. The TeV neutrino flux expected within this scenario should be detectable by KM3NeT [28], making Vela X one of the best candidates for the first detected astronomical TeV neutrino source.

Microquasars

Microquasars are stellar-mass black holes or neutron stars ejecting jets by accreting matter from their environment, i.e. they are a scaled-down version of an AGN. If the energy content of the jets in these transient sources is dominated by electron− proton plasma, a several hour outburst of 1 to 100 TeV neutrinos and high-energy photons produced by photo-production of pions should precede the radio flares associated with major ejection events.

Recently TeV γ-rays have been detected from two binary systems tentatively called microquasars, LS 5039 by H.E.S.S. [21] and LSI 61 303 by MAGIC [30], clearly demonstrating that such Galactic binary systems containing a luminous optical star and a compact object are sites of effective acceleration of particles to multi-TeV energies. As for other sources the key question is whether the γ-rays are of hadronic or leptonic origin; for which the answer is not straightforward. The critical analysis of conditions of particle acceleration and radiation in these sources, based on the temporal and spectral behaviour of TeV γ-ray emission, in particular on the modulation of the TeV flux of LS 5039 with a period of 3.9 days, and the extension of its energy spectrum to 10 TeV and beyond, reduces the possible interpretations to a few options. One of these gives a preference to the hadronic origin of TeV photons, especially if they are produced within the binary system. The maximum energy is determined by its size and magnetic field and is estimated to be $E_p \leq 10^{15}$ eV. These protons can trigger photo-meson processes on X-ray photons in the accretion disk or interact with the ambient plasma in the accretion disk, in the stellar wind or in the jet. These interactions may lead to copious production of high-energy neutrinos, γ-rays and electrons. While neutrinos escape the source without significant suppression, the electromagnetic fraction of the energy is effectively reprocessed, and escapes the source mainly in the form of hard X-rays and low energy γ-rays. If so, the detected γ-rays should be accompanied by a flux of high-energy neutrinos emerging from the decays of $\pi^{\pm}$ mesons produced by the pp or $p\gamma$ interactions. The neutrino fluxes, which can be estimated on the basis of the detected TeV γ-ray fluxes, taking into account the severe internal $\gamma \rightarrow e^+ e^-$ absorption, depend significantly on the location of the γ-ray production region(s). The minimum neutrino flux above 1 TeV is expected to be at the level of 10^{-12} cm^{-2}s^{-1}; however, it could be higher by a factor of 10, or even more. The detectability of the TeV neutrino signals significantly depends on the high-energy cut-off in the spectrum of parent protons. If the spectrum of accelerated protons continues to 10 TeV and beyond, the predicted neutrino fluxes of LS 5039 can be detected with the KM3NeT telescope.

Monte Carlo simulations have been used to evaluate the sensitivity of a cubic kilometre scale telescope to neutrinos from known Galactic microquasars [31]. The detector sensitivity was calculated for each microquasar, optimising the event selection to reject the atmospheric muon and neutrino backgrounds. An average sensitivity for 5×10^{-11} erg cm^{-2} s^{-1} was found, with some dependence on the source declination. This analysis shows that some transient microquasars could be identified in a few outburst events. Among persistent microquasars, about 70 events are expected in one year from SS433 and GX339-4. Despite the uncertainties affecting the flux predictions and the neutrino oscillations (that roughly halve the number of expected muon neutrinos), a cubic kilometre telescope could identify these microquasars in a few years of data taking. Otherwise the telescope would be able to strongly constrain the neutrino production models and the source parameters.

Gamma Ray Bursters

Gamma Ray Bursts are observed as extremely luminous flashes of MeV γ-ray radiation lasting from

seconds to tens of seconds. The nature of the progenitors of these objects is unclear, though many models consider the energy to originate from a gravitationally collapsing massive star. From timing measurements, a bimodal population has been revealed, with "short" GRBs (< 2 s) and "long" GRBs. These objects are found to be randomly distributed in the sky, located at cosmological distances, with measured redshifts extending beyond $z = 4$. The γ-ray spectrum was found to be approximately parameterised by a broken power law [**32**] of the form $dN/dE = E^{-\alpha}$ with $\alpha \approx 1$ below E_{break} and $\alpha \approx 2$ above, where typical values of E_{break} are around 1 MeV.

Since their discovery in the 1960s, GRBs have been considered promising candidates for high-energy cosmic ray acceleration. The energy output of each GRB in γ-rays amounts to 10^{52} erg, if isotropic, and they occur roughly once every million years per galaxy. The power density output into photons is thus 3×10^{44} erg Mpc^{-3}yr^{-1}. This is comparable to the power required to sustain the high-energy cosmic ray population [**33**].

With large photon densities anticipated in GRB shock regions, some degree of $p\gamma$ interactions can be expected to occur before the high-energy protons and nuclei have escaped from the accelerating region. The neutrino flux generated in the prompt emission from a single GRB may be calculated with the Waxman-Bahcall assumption that protons only leave the acceleration site once they have changed to neutrons, through $p\gamma$ interactions, such that they are no longer magnetically confined.

The search for neutrinos from GRBs is easier than for those from steady point sources, due to the time stamp available from the satellite observation of the γ-rays which are coincident with the neutrino production. In the Waxman-Bahcall model the neutrinos are expected to arrive within 10 seconds of the γ-rays and so events can be searched for in a narrow time window, making the GRB searches almost background-free. For 300 GRBs at cosmological distance the Waxman-Bahcall model predicts about 3 events on an atmospheric neutrino background of 0.006 for a cubic kilometre

scale detector. The chance probability of 3 or more events with this background is about 3.6×10^{-8}.

Models which unify GRB and supernova (SN) events lead to the possibility that at least a class of SN also produce high-energy neutrino fluxes [**34**]. The connection between these objects is motivated by the observation of correlated local GRBs and SN such as GRB 980425 and SN 1998bw (at a distance of about 40 Mpc). In such unifying models, SN observations in which the line of sight lies along the relativistic jet are classed as GRB events. Such a connection leads to the expectation that SN with mildly relativistic jets also exist. These jets, however, fail to burrow through the stellar envelope material, leading to a large fraction of the jet's energy being dumped into GeV-TeV neutrinos primarily through $p\gamma$ interactions in the dense radiation fields present within the stellar body.

A neutrino fluence can be derived by making assumptions about the jet luminosity and its Lorentz factor. The dominant part of the fluence produced through pion decay is:

$$F_\nu = 10^{-2} \left(\frac{E_{tot}}{10^{51.5}[\text{erg}]} \right) \left(\frac{\Gamma}{10^{0.5}} \right)^2 \times$$
$$\left(\frac{20\,Mpc}{D} \right)^2 \left(\frac{0.1}{\epsilon_B} \right) \left(\frac{E_\nu}{0.3\,[\text{TeV}]} \right)^{-4} \text{TeV}^{-1}\,\text{cm}^{-2}$$

where E_{tot} is the total kinetic energy of the jet and Γ is the jet's Lorentz factor. This fluence yields for a cubic kilometre sized detector the expectation of roughly one detected ν in the energy range of 0.3 to 300 TeV per GRB at a distance of 20 Mpc. With a small time window for these events, the atmospheric neutrino background contamination of the signal is insignificant.

Relativistic shocks are predicted by many authors to be the acceleration sites of high-energy (extragalactic) cosmic rays. Large energy gains are obtainable at these shocks for protons crossing the shock front; however a common problem of such models is the large decrease in the energy gain after the first crossing, due to the difficulty of providing a method of randomizing the proton's direction in the upstream region before the shock catches up and returns it across the shock.
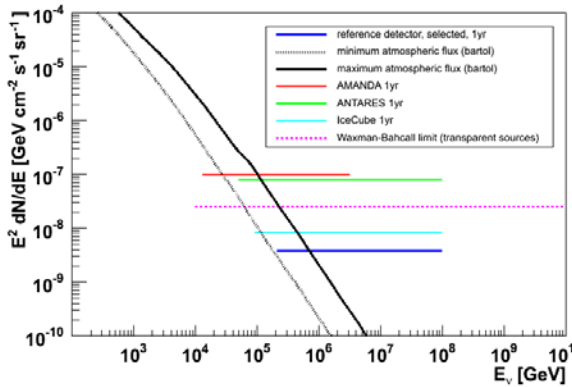
The convertor mechanism [**40**] provides a possible solution to this problem, by the proton changing into a neutron through $p\gamma$ interactions. In the neutral state, the particle may run far ahead of the shock and be given sufficient time to decay back to a proton and becomes isotropic before the shock catches up with it. As a by-product of this mechanism, high-energy neutrinos are produced at each $p\gamma$ interaction, leading to the possibility of large neutrino fluxes.

Hidden Sources

It is possible that sources exist from which no other messengers except for neutrinos can escape; such sources are referred to as "hidden sources". Given the lack of any other knowledge about these sources, an estimation of the neutrino fluxes arising from them is impossible. However, one should bear in mind the unanticipated discoveries with the advent of other fields such as X-ray astronomy in the 70's and γ-ray astronomy in the 90's, when it was found how rich the sky was in these wavelengths. Similarly, hidden neutrino sources may have to await the turning on of cubic kilometre scale neutrino detectors for their discovery.

2.1.2 Diffuse Neutrino Flux

The unique penetrating nature of the neutrino means that signals from a multitude of very distant objects will not be resolved as coming from point sources but will build up an isotropic diffuse flux.

Another contribution to the diffuse flux, of a different nature, is that which comes from interactions of charged cosmic rays with radiation and matter fields in the Universe. Extremely high-energy cosmic rays interact with photons from Cosmic Microwave Background and infrared radiation fields (the "GZK" effect) with interactions such as $p\gamma \rightarrow n/\Delta + X$, with subsequent n or Δ decays producing neutrinos with a significant fraction of the initial proton energy. This is referred to as the "cosmogenic" neutrino flux. Interaction of cosmic rays with matter in the local galaxy such as molecular and dust clouds give another diffuse neutrino flux which maps the target matter distribution.

Upper limits have been published [**38**] for the diffuse neutrino energy flux using arguments based on the measured charged cosmic ray flux.

These calculations require as input: the power output of the cosmic ray sources; the fraction of total power output going into neutrinos and the time for which such sources have been active. Assuming the observed flux of ultra-high-energy cosmic rays is the result of cosmologically distributed sources, the energy injection rate is inferred to be $5 \times 10^{44} \, \mathrm{erg \, Mpc^{-3} \, yr^{-1}}$ [**33**]. The energy density of neutrinos produced through pion photo-production from cosmic rays can be directly related to this injection rate. Assuming maximum energy transfer from the cosmic rays to the neutrinos one obtains the "Waxman-Bahcall limit" [**38**] on a diffuse neutrino flux of this origin.

Figure 2-4 shows the sensitivity of the reference detector for a diffuse flux of neutrinos (sum of ν_μ and anti-ν_μ), calculated assuming an E^{-2} spectrum as expected for sources such as AGN. Effective areas for upward-going neutrinos were used for the calculation of event rates.

The expected diffuse flux limit, after one year of operation, is $3.8 \times 10^{-9} E^2 \, \mathrm{GeV \, cm^{-2} \, s^{-1} \, sr^{-1}}$ for the reference detector. This can be compared to the limit of $8.1 \times 10^{-9} E^2 \, \mathrm{GeV \, cm^{-2} s^{-1} sr^{-1}}$ from IceCube. It should be noted that the IceCube limit includes full energy reconstruction, not yet implemented in the KM3NeT analysis.

Neutrino Flux from Multiple Point Sources

The diffuse flux of neutrinos originating from all GRBs and AGN in the Universe can be calculated based on the flux of cosmic rays, under the assumption that the sources are optically thin. Using the spatial distribution of GRBs and AGN as a function of redshift, the total diffuse neutrino emission produced by such sources is obtained (see Figure 2-5).
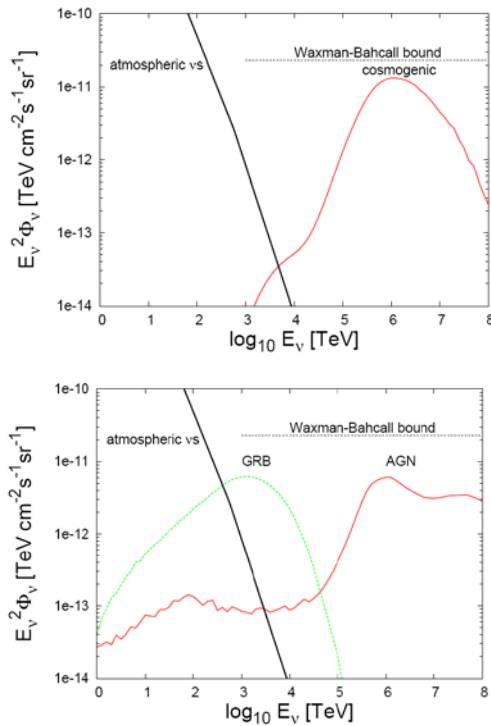
Figure 2-5: Diffuse extragalactic neutrino fluxes: the cosmogenic flux is shown in the upper panel and the flux due to the entire population of GRBs and AGNs over their complete cosmic history [41] in the lower panel.

Cosmogenic Neutrino Flux

The transition from Galactic to extragalactic origin in the arriving cosmic ray spectrum is thought to occur at energies of 10^{17}-10^{18} eV. This result is inferred indirectly from the composition information obtained from cosmic ray shower measurements. The cosmic ray protons propagating through the relic microwave radiation lose energy predominantly through pion photo-production for energies greater than $10^{19.5}$ eV. These pions generate the cosmogenic neutrino flux (see Figure 2-5). Simi-

larly, cosmic ray interactions within the source region may generate another component of the diffuse flux of high-energy neutrinos.

Extragalactic neutrino flux calculations are not as strongly constrained by high-energy γ-ray observations compared to the constraints placed on the galactic neutrino fluxes. This is due to the attenuation of high-energy photons from π^0 decays through pair production interactions with the cosmic radio, microwave, and infrared background radiation fields. This mechanism makes the high-energy neutrino flux, which is sensitive to the entire history of cosmic ray pion photo-production, independent from the flux of high-energy photons, which can only propagate about 10 Mpc in distance.

Galactic Neutrino Flux

The Galaxy contains interstellar thermal gas, magnetic fields and cosmic rays. Measurements of these three components indicate that they are roughly in energy equipartition, suggesting a strong coupling between them. Cosmic ray protons and nuclei are diffusively confined within the Galaxy by the inhomogeneous magnetic field and they interact with the interstellar material producing a diffuse flux of γ-rays and neutrinos. Originating from the same processes, the fluxes of γ-rays and neutrinos are expected to be equal within roughly a factor of two [42]. Thus, by assuming that all observed γ-ray emission comes from hadronic processes, it is possible to obtain an upper limit on the diffuse neutrino flux.

If, as a first approximation, one assumes that the cosmic ray spectrum everywhere in the Galaxy is the same as that observed on Earth, the hadronic γ-ray and neutrino emission is simply proportional to the gas column density in the Galaxy and the largest neutrino emission is expected from directions along which the line of sight intersects most matter. Several estimates of the diffuse neutrino flux from the galactic plane have been published. Recently, the MILAGRO collaboration has reported the detection of extended multi-TeV emission from the Cygnus region [43]. The γ-ray emission correlates very well with the gas density, strongly fa-
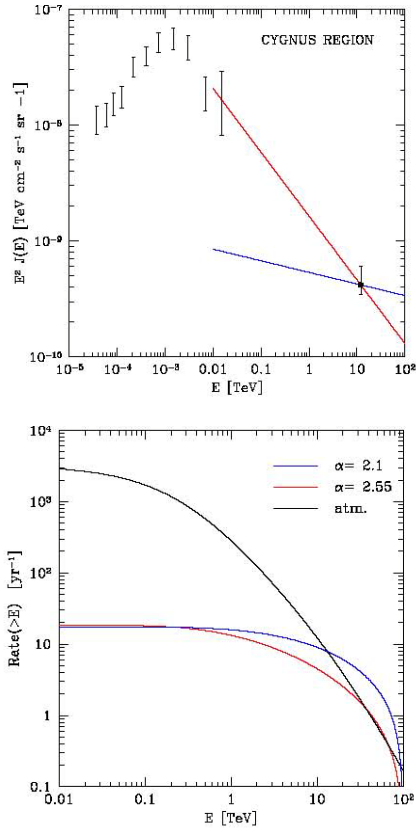
Figure 2-6: The upper panel shows the γ-ray emission from the Cygnus region; the two spectra adopted in the calculation are shown. The bottom panel shows the integrated detection rate for the inner Galaxy. The black line refers to the atmospheric neutrino background, the red and blue lines represent the predicted rates for the assumed soft and hard γ-ray spectrum from the inner Galaxy.

vouring a hadronic origin of the radiation. Moreover, the MILAGRO observations are inconsistent with an extrapolation of the EGRET flux measured at energies of tens of GeV [44] to the TeV region. This suggests that in some areas of the galactic disk the cosmic ray spectrum might be significantly harder than the local one. An estimate has been made of the diffuse neutrino flux from the inner Galaxy, which is in the field of view of a neutrino telescope located in the Mediterranean Sea. This estimate is based on the assumption that the γ-ray emission from the inner Galaxy is equal to that observed from the direction of the Cygnus region and that all of the γ-ray emission comes from hadronic interactions. The upper panel in Figure 2-6 shows the measured diffuse flux of γ-rays from the Cygnus region with the lines representing energy

spectra with indices $\alpha = 2.55$ (soft) and 2.1 (hard) which are used to estimate the neutrino fluxes shown in the bottom panel of this figure.

The detection of diffuse neutrinos from the inner Galaxy seems feasible with KM3NeT after about 1 year for neutrino energies above 10 TeV. The expected signal rate is 4 and 9 events per year for the soft and hard spectrum respectively, with an atmospheric neutrino background of about 12 events per year.

2.1.3 Dark Matter

The presence of dark matter in the Universe is well established. Results from analysis of the Cosmic Microwave Background from WMAP [45], when combined with data on high-redshift type Ia supernovae [46], indicate a flat Universe which comprises 27% matter (dominated by cold dark matter) and 73% dark energy. The nature of the dark matter is unknown. A particle-based description is that dark matter consists of stable weakly interacting light or massive particles, which may exist in one or more of several forms including axions, supersymmetric (SUSY) dark matter and super-heavy dark matter such as cryptons and wimpzillas that are relics from the early Universe. The model with the widest acceptance assumes the existence of WIMPs, which are heavy weakly interacting particles, and are referred to as Cold Dark Matter (CDM). The WMAP experiment has measured today's relic density of CDM to be $0.094 < \Omega_h < 0.129$.

The assumption of a thermal origin of the CDM in a primordial Universe without matter/antimatter asymmetry leads to expected annihilation processes today with rates scaling as the square of the dark matter density. Astrophysical regions with very high CDM densities are natural sites of WIMP annihilation. Potential sites include the centre of the Sun, the centre of the Earth, regions around the black holes such as the one located at the centre of the Galaxy and perhaps intermediate mass ones located throughout the Galaxy. For neutrino telescopes, the most promising source is the Sun, since it is expected to be an efficient and nearby gravitational trap for dark matter, for which the
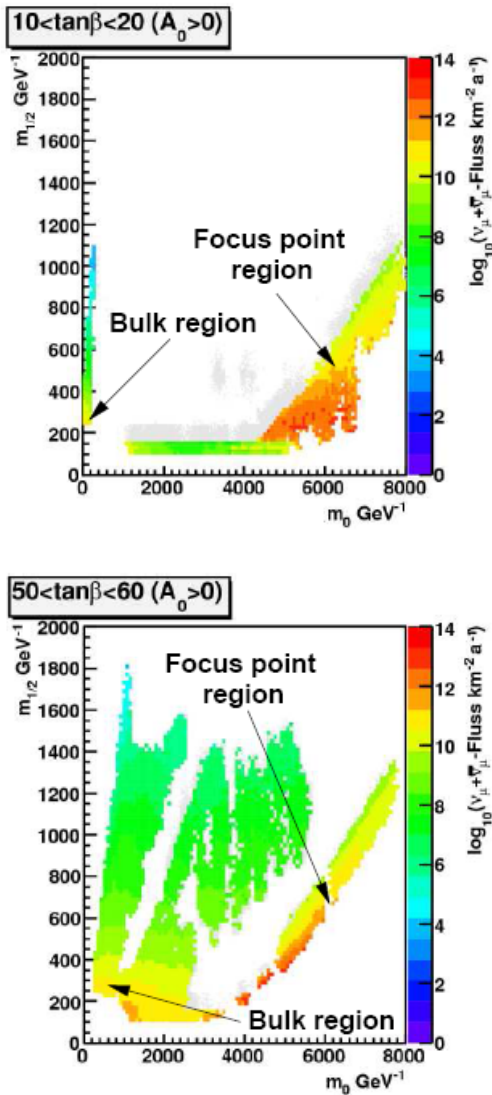
Figure 2-7: Neutrino flux on the Earth as a function of mSUGRA parameters.

expected rate of neutrino production can be reliably predicted. In universal extra-dimensional theories [**47,48**] neutrinos can be produced directly in the annihilation of two WIMPs, while in supersymmetric [**49**] scenarios they only result from the fragmentation or decay of various heavy particles created in the annihilation. Among these, heavy quarks as well as massive gauge bosons and tau leptons produce high-energy neutrinos before losing energy through interaction with the ambient matter. Within the framework of gravity mediated Supersymmetry (mSugra [**50**]) with unification at the grand unification scale, the number of free parameters is reduced to only five (m_0, the com-
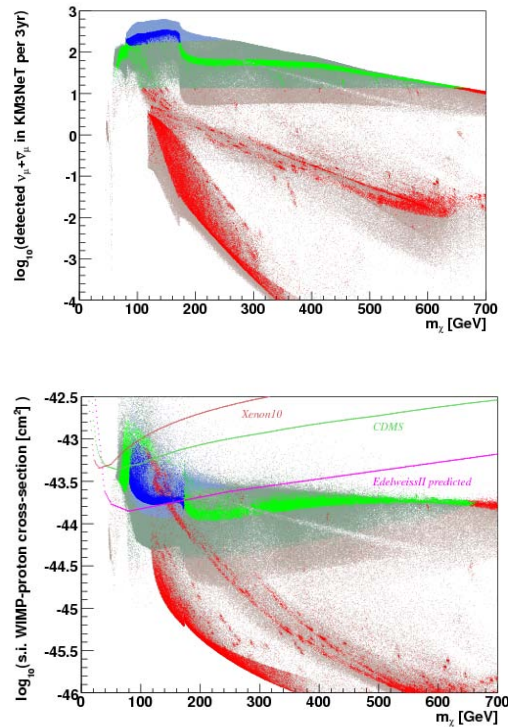
Figure 2-8: Neutrino detection rates in the reference KM3NeT detector from a scan of the mSugra parameter space based on DarkSUSY [51] (upper panel) and the spin-independent cross section from the same scan (lower Panel). Limits from direct search experiments are also indicated. Green points can be excluded at 90% confidence level with KM3NeT. Red points are not excludable by KM3NeT.

mon scalar mass scale; $m_{1/2}$, the gaugino mass; A_0, the common trilinear term; $\tan\beta$, the ratio of the vacuum expectation values of the two Higgs fields and $\text{sign}(\mu)$, the sign of the Higgs mass parameter).

Assuming R-parity conservation, the lightest supersymmetric particle, the neutralino, is stable and provides a compelling candidate for the WIMP. In such models the neutralino is a mixed state of gauginos and higgsinos. In Figure 2-7, the neutrino flux observed at the Earth due to neutralino annihilations in the Sun is shown as a function of mSugra parameters. Two regions are highlighted, the so

called bulk region where fluxes are relatively low and the focus point region, where the flux reaches its maximum. The latter region features a higgsino-dominated neutralino which annihilates into heavy gauge bosons, leading to a hard neutrino spectrum favourable for neutrino detection. In Figure 2-8 the calculated neutrino detection rates in the reference detector are shown as a function of the neutralino mass for a scan of the mSugra parameters. The dark blue and green points are those points in the Focus Point Region favoured by the WMAP relic density measurement. This region is almost completely accessible to the KM3NeT detector. As also shown in Figure 2-8, the sensitivity of KM3NeT will be better than that of current or near-future direct detection experiments. Since the capture rate in the Sun is determined by the elastic cross section of WIMPs off nuclei (dominantly spin independent coupling), the neutrino indirect detection provides complementary information on the true nature of the dark matter in contrast to direct searches that focus on energy deposits on deep-underground targets.

2.1.4 Exotic Particles

Magnetic Monopoles

In 1931 Dirac introduced magnetic monopoles in order to explain the quantisation of the electric charge [52]. Grand Unified Theories (GUT) predict the existence of super-massive monopoles with masses of 10^{17} GeV [53,54]. They could be present in the penetrating cosmic radiation travelling with low velocities, $10^{-4}c$ to $10^{-2}c$, though in the presence of strong magnetic fields, they may reach higher velocities. Possible intermediate mass magnetic monopoles ($m < 10^{15}$ GeV) could achieve relativistic velocities.

A magnetic monopole with unit magnetic Dirac charge $g_D = 137e/2$ and a velocity close to c would emit Cherenkov radiation along its path, exceeding that of a bare relativistic muon by a factor of 8300 for $\beta \approx 1$. Due to the production of δ-electrons, a magnetic monopole can produce photons even below its Cherenkov threshold.

Another detection mechanism is the possible catalysis of nucleon decay induced by a GUT monopole. According to [55,56] this process takes place with a cross section of the order of 10^{-26} to 10^{-24} cm^2, transforming the passage of a GUT monopole into a succession of light flashes, spaced by distances ranging from some metres to several hundred metres.

The reference sensitivity level for a significant magnetic monopole search is the Parker bound, the maximum monopole flux compatible with the survival of the Galactic magnetic field. This limit is 10^{-15} cm^{-2}s^{-1}sr^{-1}, but it could be reduced by almost an order of magnitude when considering the survival of a small Galactic magnetic field seed [57]. Figure 2-9 shows the sensitivity of the KM3NeT detector compared to existing limits, which are below the Parker bound. A cubic kilometre detector could improve the sensitivity of this search by about two orders of magnitude compared to the present AMANDA limit. As mentioned above, the search could be extended down to velocities $\beta = 0.5$ by detecting the electrons generated along the monopole's path. The contribution due to nucleon decay catalysis depends on the cross section for the catalysis process.

Nuclearites

Strange quark matter could be the ground state of quantum chromodynamics [58]. Nuggets of strange quark matter, with masses ranging from those of heavy nuclei to macroscopic values, could be present in cosmic rays and are referred to as "nuclearites" [59]. Nuclearites with masses larger than a few 10^{13} GeV, travelling with typical galactic speeds (about 300 km/s), could reach the depth of an underwater neutrino telescope from above. The main energy loss mechanism for such exotic objects is through elastic collisions with the atoms in the traversed media; a fraction of this energy is expected to be emitted as visible black-body radiation along the over-heated path of the nuclearite.

A cubic kilometre scale neutrino telescope could reach sensitivities of the order of 10^{-18} cm^{-2}s^{-1}sr^{-1} in about one year of data tak-
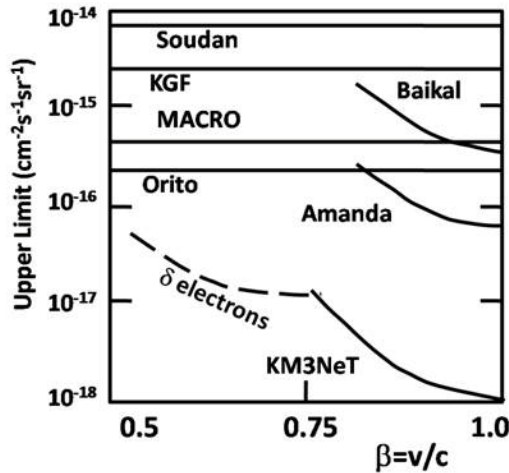
Figure 2-9: Limits on the flux of relativistic monopoles achievable with KM3NeT compared to existing limits.

ing, which is two orders of magnitude better than the present best flux limit reported by MACRO [**3**].

2.1.5 Atmospheric Muons and Neutrinos

Atmospheric muons and neutrinos, even though they are the main background for any neutrino signal, are in themselves interesting objects to be studied. They are produced in the extended air showers induced by the interactions of primary cosmic ray particles in the upper atmosphere. Muons and neutrinos are the most penetrating particles in such air showers. Whereas the muons reach the detector from above, neutrinos arrive from all directions.

It is expected that more than 10^8 atmospheric muon events can be detected per year in a water Cherenkov detector of a cubic kilometre size. The precise number will depend on the installation depth and details of the detector layout. Apart from being an excellent calibration source this data sample will provide information about the primary cosmic rays at energies of 10 TeV to 10 PeV. By measuring the zenith angle distribution of the muon bundles, their energies, multiplicities and lateral distributions, it will be possible to investigate the primary cosmic ray spectrum and its composition. This will be complementary to the measurements provided by air shower arrays and balloon experiments. The heavy quark component present in the air showers can also be probed.

Mesons which contain charm or beauty decay before interacting and lead to an enhanced production of energetic muons ("prompt muons").

The KM3NeT telescope will measure more than 100,000 upward-going atmospheric neutrinos per year, independent of its installation depth. Together with the corresponding IceCube data sample, this will be the world's largest data set of TeV neutrinos. Their angular and energy distribution can be studied as well as their flavour composition. Above 1 TeV the effect of neutrino oscillation is negligible for atmospheric neutrinos; therefore mainly muon neutrinos from pion decays are expected. At energies above about 50 TeV prompt neutrinos from the decays of heavy mesons will start to contribute, at a level that is essentially unknown today. It can be derived from a change of the spectral index and from an enhancement of non-muonic flavours.

Another interesting topic is the tomography of the internal structure of the Earth [**60**]. For a 25 TeV neutrino the diameter of the Earth represents approximately one absorption length. By analyzing the angular distribution of atmospheric neutrinos with energies higher than 10 TeV one can determine the presence (or absence) of strong density changes in the Earth's interior such as the transition between the mantle and the core. Such a measurement is complementary to the conventional seismological methods.

2.1.6 Neutrino Cross Sections

Measurements of the ratio of fluxes of the various neutrino flavours and of the neutrino-nucleon cross section enable the study of elementary particle physics in a high-energy regime.

Since neutrinos are produced and detected through their flavour eigenstates, flavour carries information about the process in which the neutrino was originally produced. The flavour ratio at the source of high-energy neutrinos and antineutrinos, originating from pion photo-production is $\phi_{\nu_e} : \phi_{\nu_\mu} : \phi_{\nu_\tau} = 1 : 2 : 0$. At distances much larger than the oscillation lengths between neutrino flavours, the flavour ratio becomes $1 : 1 : 1$.

Exploiting the various event signatures described in Table 1-1, neutrinos of different flavours can be separated, even though not perfectly, and the flavour ratio of the arriving high-energy neutrinos may be determined [61]. Using the flavour ratio of the high-energy neutrinos, the production mechanism, such as π or K decay from pp interactions or π decay from $p\gamma$ interactions, may therefore be tested [62]. Beyond this, with a good understanding of the neutrino production processes occurring in the source, the possibility to probe new particle physics arises. Neutrino decay during propagation [63], neutrino oscillations to sterile states, CPT and Lorentz invariance violation [64] may all, to some extent, be tested through observations of the high-energy neutrino flavour ratios. It was through an analogous comparison of the calculated versus measured solar neutrino flux, for the different neutrino flavours, that it was discovered that neutrinos have mass and that they oscillate between flavour states [65].

The centre of mass energies for neutrino nucleon interactions studied by neutrino telescopes are many orders of magnitude above those achievable at accelerators. The neutrino nucleon cross section at centre of mass energies above 300 GeV has not been measured, though theoretical calculations of the cross sections exist for neutrino energies up to and beyond 10^{20} eV [66]. A measurement of the number of neutrino induced events observed by a neutrino telescope is effectively a determination of the product of the neutrino scattering cross section (with nucleons or, in the case of the Glashow resonance, with electrons) and the incoming neutrino flux. Since the high-energy neutrino spectrum is not a priori known, the event rate alone cannot be used to determine the neutrino scattering cross section. However, the fact that the Earth is opaque to particles with a scattering cross section with nucleons larger than roughly 2×10^{-7} mb can be exploited. This cross section corresponds to the Standard Model prediction for neutrinos with energy of about 100 TeV. At energies above this value, the flux of neutrinos that penetrates through the Earth becomes increasingly suppressed. Neutrino detectors can compare the rate of neutrinos observed from the direction of the Earth (or slightly skimming the Earth in the case of ultra-high-energy neutrinos) to the rate of neutrinos observed from other directions. In this way, an effective neutrino-nucleon cross section measurement can be attained. Deviations from the Standard Model predictions would indicate the onset of new phenomena, e.g. due to microscopic black whole production or electroweak instanton induced interactions.

2.2 ASSOCIATED SCIENCE

Undersea observatories will greatly expand our knowledge of the deep-sea environment. In general, observations in the deep sea have until now been made by autonomous measuring systems, deployed in the sea for up to one year, which must be recovered in order to retrieve data for analysis. Data storage and battery energy capacity have limited data sampling rates in such systems to once every 10 minutes or every hour and there are inevitable breaks in data collection.

The proposed sub-sea infrastructure, permanently cabled to the shore, will enable continuous data to be collected without interruption over long periods. Data capture rates will be orders of magnitude faster than used hitherto and will allow new phenomena to be investigated with sampling rates of the order of 1 Hz. For example, using sensors distributed throughout the telescope array it will be possible for the first time to investigate phenomena such as internal waves and short time-base oscillations in the water column. Real-time tracking of bioacoustic emissions or vertical migrations of organisms will be possible. Both the spatial and temporal scale of measurements will be transformed and real-time availability will revolutionise data applications. The system will also provide continuous vigilance in the face of transitory hazardous events such as earthquakes, slope failures and tsunamis.

Sensors placed on the seafloor and in the water column will ensure efficient tracking of environmental change on daily, annual and decadal time scales. The associated science infrastructure within KM3NeT will form the basis for the Mediterranean

section of the EU plan for long-term monitoring of the ocean margin environment around Europe. It is part of GMES (Global Monitoring for Environment and Security) which has capabilities in geophysics, geotechnics, chemistry, bio-chemistry, oceanography, biology and fisheries. It will complement oceanographic networks such as GOOS (Global Ocean Observing System), EuroGOOS and DEOS (Dynamics of Earth and Ocean Systems), and will be multidisciplinary, with stations monitoring the rocks, sediments, bottom water, biology and events in the water column.

The KM3NeT infrastructure will incorporate reconfigurable junctions boxes to which new associate sciences instruments can be connected; for example it will be feasible to connect elements of the new Ocean Tracking Network that will be capable of tracking fishes and other animals equipped with implanted transmitters [67].

The Mediterranean Sea contains numerous natural phenomena amenable to study by an observatory system. Such investigations will be of utmost importance for understanding the historical and future geological development of the Mediterranean, to assess the impact of potential geological events and to understand the biosphere Mediterranean Sea, also with respect to anthropogenic changes.

Geologically the Mediterranean Sea is at a pivotal point between the African and Eurasian tectonic plates and some authors have argued that it contains some of the oldest ocean floor on the planet, recognisable as remnants of the Tethys Sea that was an embayment of the single proto-continent, Pangaea. The present-day Mediterranean area remains tectonically active with 23 active volcanoes in Italy and six in Greece associated with subduction of the African plate beneath Eurasia. Vesuvius on the mainland and Etna on the island of Sicily are the best known in Italy and the island of Santorini in Greek waters erupted most recently in 1950. Hydrothermal activity is also seen around volcanic islands. Earthquakes occur regularly in this region, particularly in the eastern basin despite relatively slow motion of the tectonic plates. Im-

portant seafloor features associated with subduction and accretion are the Hellenic trench and the parallel Mediterranean ridge which extends across the Ionian Sea to Cyprus. Deep sea mud volcanoes occur on the Mediterranean Ridge with emissions of methane from the seafloor. Slope failures have been detected capable of generating turbidite flows and tsunamis.

The Mediterranean Sea is the most recently colonised of the world's oceans, with limited time for evolution of new species but very special conditions and partial isolation of basins that give opportunities for endemic species to appear. Colonisation and re-colonisation have been from the Atlantic Ocean; 50.2% of species are of Atlantic origin, 16.8% Atlantico-Pacific and 4.4% of Indo-Pacific origin [68]. Of species in the Mediterranean 28.6% are endemic or unique to this area. Owing to the direction of colonisation and stagnation events in the east there is a general impoverishment of fauna from west to east. It is estimated that the Mediterranean Sea contains about 8500 species [69] of which only half are generally represented in the Eastern Basin. The east is therefore impoverished not only in productivity but also in biodiversity. Despite apparent sparseness of life in the Mediterranean it contains between 4 and 18% of world marine species in 0.32% of the world ocean volume. Numbers of species decrease rapidly with depth so that at 1000m there is 8% of the shallow water number and only 3% at 2000m.

The Mediterranean supports a wide range of fishing activity including pelagic (near surface) such as tuna, sardine and anchovy, demersal species (bottom living), crustacean and molluscs. Generally the Mediterranean is less productive than other seas reflecting its oligotrophic status. However there is evidence that production of fish has increased. The Western Basin has moved from below the world average to above average production in sea shelf fishery production. This increase may be attributable to fertilisation by run-off from human activity on land. The main increase has been due to small inshore pelagic fishes whereas bottom living fishes have declined. So whilst

catches have increased, the quantity of big valuable fish has decreased.

Nineteen species of cetaceans have been recorded in the Mediterranean Sea of which eight are considered of common occurrence. There is only one species of pinniped, the Mediterranean Monk Seal (*Monachus monachus*) which is listed as endangered. Colonies are now confined to the Alboran and Aegean Seas. Public interest in cetaceans of the Mediterranean Sea is great and there is support for research activity. Recently a Cuvier's beaked whale, *Ziphius cavirostris* [**70**] was recorded to a depth of 1900 m during a dive lasting 85 minutes in the Ligurian Sea. This is the world record for deep diving in mammals.

The KM3NeT deep-sea research infrastructure hosting a cubic kilometre neutrino telescope and permanent installations for marine and earth science measurements promises major original discoveries in a wide range of scientific domains. The neutrino telescope will be the most sensitive in the world, observing the Universe with this novel messenger. The sensitivity for discovering neutrino sources will be more than 50 times larger than other neutrino telescopes observing the same part of the sky and more than 3 times larger than the detectors at the South Pole which observe a different sky region. The associated sciences infrastructure will provide a world leading observatory for long-term, continuous deep-sea measurements in the fields of marine biology, oceanography, geology and geophysics.

3 THE KM3NET CONCEPT

The KM3NeT research infrastructure will consist of the neutrino telescope and an associated sciences infrastructure supporting one or several science nodes.

Neutrino Detection Principle

Only one feasible solution is currently known to realise neutrino telescopes beyond a target size of some 10 megatons for neutrinos of energies beyond about 100 GeV: Use the Cherenkov light emitted by secondary charged particles created through a neutrino interaction in an optically transparent medium, such as water or ice. The detection of the Cherenkov light must proceed on a single-photon level, where a precise measurement of place and time of arrival of the photons associated with a neutrino event is the basis for identifying neutrino reactions and reconstructing the neutrino direction and energy. This basic principle is adopted for the KM3NeT neutrino telescope; the target material will be the water in the Mediterranean deep sea.

Generic Structure of the KM3NeT Neutrino Telescope

The basic task is to instrument at least a cubic-kilometre of deep-sea water with suitable photo-sensors. Even though a variety of solutions is conceivable for the types of photo-sensor, for their exact geometrical arrangement, for the mechanical structures and so on, all solutions pursued or envisaged so far are variants of a common generic concept that will also underlie the design of the KM3NeT neutrino telescope and is summarised in the following.

The neutrino telescope is composed of a number of vertical structures (the "Detection Units"), which are anchored to the seabed and usually kept vertical by one or several buoys at their top. Each detection unit carries photo-sensors and possibly further devices for calibration and environmental measurements on "Storeys", i.e. mechanical structures supporting the necessary sensors, interfaces

to power supply and data lines and electronic components where applicable. The basic photosensor unit is an "Optical Module (OM)" housing one or several photomultiplier tubes, their high-voltage bases and their interfaces to an acquisition system of the nanosecond-precision data. In each detection unit, the data and power flow proceeds vertically and is connected via the anchor to a deep-sea "Cable Network". This network typically contains one or more junction boxes and one or several electro-optical cables to shore, through which the OM data are transferred to shore. It also provides power and slow-control communication to the detector. On shore, a "Shore Station" equipped with substantial computing power is required for collecting the data, applying online filter algorithms and transmitting the data to mass storage devices. The overall setup is schematically depicted in Figure 3-1. A more specific description of the options that are considered for the implementation of this scheme is given below.
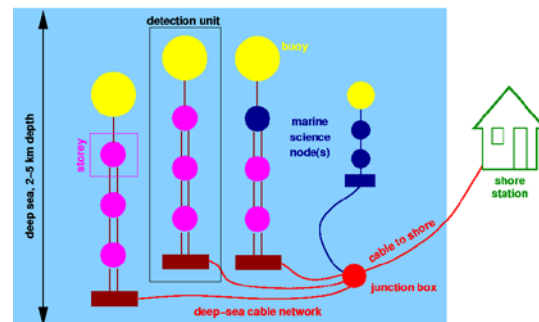
Figure 3-1: Schematic view of the major components of the KM3NeT neutrino telescope. Note that the drawing is not to scale and that the number of components indicated is much smaller than in reality. An associated-science node is also shown.

Associated-Sciences Infrastructure

It is intended to connect associated-science nodes to the neutrino telescope cable infrastructure thus providing electrical power and data links to a series of sensors. These may be positioned under the
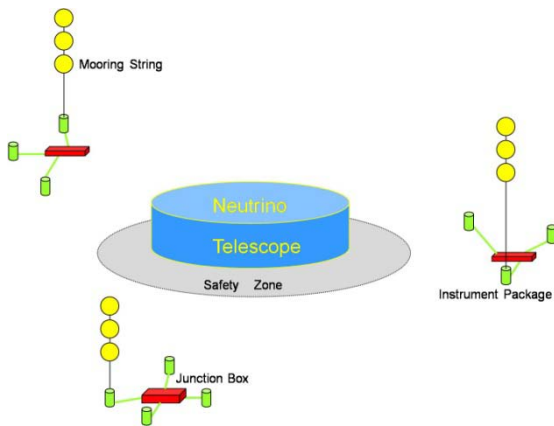
Figure 3-2: Schematic concept of complementing the KM3NeT neutrino telescope with marine science instrumentation.

seafloor, on the seafloor and reaching up through the water column to the mixed layer below the sea surface (see Figure 3-2).

These nodes are to be positioned at optimal places around the detector to provide environmental data relevant to the neutrino telescope and also allow the associated science communities to perform continuous long-term monitoring experiments and implement earthquake and tsunami early warning systems. A safety zone around the neutrino telescope will ensure independent deployment, operation and maintenance of both installations.

The associated science infrastructure will be designed taking into account the concepts currently being implemented in the MARS and NEPTUNE experiments in the USA and Canada and in the neutrino telescope pilot projects.

Each node will be connected to the deep sea infrastructure via a junction box. Typically the junction box will have connections to one or two mooring strings with profilers or fixed sensors, and a suite of seafloor sensors, cameras and acoustic instruments. The data will be transmitted to shore in real-time, for processing and dissemination. Instruments may be controlled via commands transmitted from the shore station.

The associated science infrastructure will be continually evolving and as such needs to be designed in a flexible manner so that adding or removing components can be achieved in a simple and cost-effective manner.

Installation Concepts

The first step in the installation of KM3NeT is the construction of the deep-sea infrastructure comprising the cable network and possibly auxiliary tools needed for the deployment.

Once the detection units and associated science instruments have been assembled ("Integration"), they must be installed on site ("Deployment"). In addition, the shore station and related infrastructure need to be built.

In view of the large number of detection units expected for the neutrino telescope, and the correspondingly vast effort for component assembly and integration, a detailed plan for the installation phase including logistics and resource allocation is required.

Detection Unit Concepts

Several possibilities to implement mechanically the generic structure described above have been pursued by the pilot projects or have been introduced during the design study. Four of these concepts are further pursued (see Section 7.3).

Extended tower structure: In this option the storeys are rigid, star-like structures with 6 arms, extending 50 to 60 m from the centre. Eight to twelve of these storeys are deployed one by one and suspended vertically with 50 to 60 m spacing to form a tower-like detection unit. Optical modules are placed at the apices of the stars and optionally along the arms. Power and readout lines proceed from the OMs to the centres of the storeys and from there, via a central cable, to a connection at the foot of the tower.

Compact tower structure: The detection units are composed of relatively compact, transportable horizontal bars (length ≤ 12 m) that are connected to each other by mechanical cables and thus form a flexible tower. The cabling for power and data transport is separated from the mechanical cabling. Optical modules are attached to the ends of the bars. After production, the full detection unit will be easy to transport. Deployment is performed in a compact state, and the detection unit unfurls

in the water, using the inherent buoyancy once it has reached the seabed.

String structure: The storeys in this solution are very compact without specific electronics containers. The full detection unit is "rolled up" inside a ready-to-deploy container. At deployment it can be winched to the seabed or left to freefall, after which it is positioned with a submersible. The unit is unfolded on the seabed by raising the container while leaving the anchor on the seabed.

Cable-based concept: In this concept, each storey carries a single OM with very large total photocathode area. An oil-filled cable system (hose) is used, with breakouts of fibre optic and electrical connections terminated by connectors to the corresponding OMs. The OMs are mechanically connected to the cable via a minimal structure. The mechanical part of the cable structure is continuous. Deployment will be similar to that of the previous concept.

Configuration Studies for the Neutrino Telescope

Different possible detector configurations for the neutrino telescope have been investigated in detailed simulation studies using a modified version of the ANTARES software [**39**]. The conclusions were confirmed by studies using independent simulation and reconstruction software [**71**,**72**]. A flux of muon neutrinos with an energy spectrum proportional to E_ν^{-2} was considered in the energy range 10^{10} to 10^{16} eV, covering the characteristic energy ranges for dark matter searches, neutrino point sources and the measurement of the diffuse neutrino flux. Only the muon emerging from charged-current reactions $\nu_\mu + N \rightarrow \mu + X$ has been simulated and reconstructed. The random light background from potassium decays was included in the simulation at a rate of 100 Hz per cm^2 of photocathode area.

Two benchmark parameters have been considered for the comparison of simulated detector configurations: (i) the neutrino effective area, which defines the event rates in a neutrino telescope, and (ii) the angular resolution of the reconstructed

muon, which defines the size of the search window for neutrino point sources and is crucial for the background rejection capabilities.

In order to "normalise" the different detector configurations to a common standard, the total photocathode area was kept constant, and the instrumented volume was in all cases chosen to be one cubic kilometre. Three main detector configurations have been investigated:

- homogeneously instrumented configurations (cuboid geometries);
- cluster configurations, densely instrumented sub-volumes, separated by larger inter-cluster distances; note that such configurations would automatically result from tower structures;
- ring-type configurations, combining dense instrumentation inside the ring with a large instrumented volume.

Example layouts of these three configuration types are shown in Figure 3-3. To specify a detector configuration, one needs to define the light detection capability of each storey in terms of photocathode area, quantum efficiency and angular sensitivity. Two basic types of photomultiplier tubes have been investigated: (i) large 10 inch photomultipliers, and (ii) small 3 inch photomultipliers. Several OM and storey configurations composed of these photomultipliers have been investigated. For given photocathode area per storey and fixed quantum efficiency the results for different configurations are rather similar. In Figure 3-4 one of these options is shown, which is also incorporated in the reference detector (see below). Muons from 10^9 muon-neutrino interactions have been simulated for each detector configuration; the simulation included the generation of the neutrino-nucleon interactions, the transport of the muons, the generation and transport of the Cherenkov light and finally the generation of the detector hits. These hits were reconstructed with a modified ANTARES reconstruction programme (not yet optimised for cubic kilometre scale configurations), using local coincidence requirements to suppress the potassium light background. For each detector configuration, the muon neutrino effective area and the
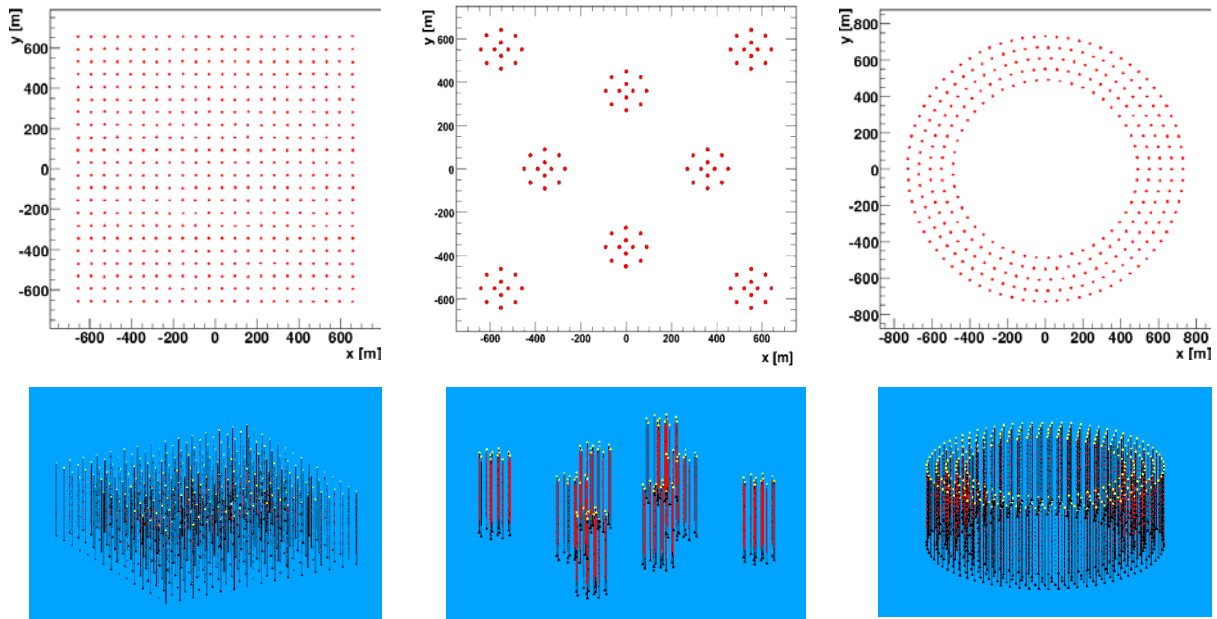
Figure 3-3: Seafloor layouts (top) and 3-dimensionl visualisations (bottom) of example neutrino telescope configurations of the types "homogeneous", "cluster" and "ring" (left to right). In the top panel, each red point indicates a vertical arrangement of OMs or storeys; in the bottom panel each red point represents a storey. Note that for the cluster-type configuration, each cluster might be implemented as one detection unit.

muon angular resolution have been calculated as benchmark parameters.
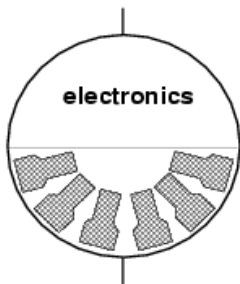
Figure 3-4: One of the storey types considered in the detector configuration studies, with 21 3-inch photomultipliers covering the lower hemisphere of the outer glass sphere.

It is found that none of the configurations is superior over the full energy range. It will therefore be crucial to define the physics priorities of the KM3NeT neutrino telescope before concluding on a final detector layout. Basically, configurations with densely instrumented regions (cluster and ring) are preferable for low neutrino energies, whereas homogeneous solutions yield the best efficiency for an intermediate energy range (1 to 100 TeV), characteristic for point source searches. Ring geometries may have advantages at very high neutrino energies; however, like cluster structures, they suffer from a rather inhomogeneous angular acceptance.

From these studies, a homogeneous configuration with 225 (15x15) detection units, each carrying 37 storeys with one OM of the type shown in Figure 3-4, has been selected as a "reference detector" for further studies. The distance between detection units is 95 m and vertically between adjacent storeys 15.5 m. The investigations of the physics sensitivity of the KM3NeT neutrino telescope reported in this document have been obtained assuming this reference detector; note that this does not imply any decision or pre-decision on the final detector configuration which is still under study.

The neutrino telescope concept requires an array of light detectors distributed over a volume of at least one cubic kilometre of sea water. Various configurations are possible and are being investigated in order to arrive at the optimal detector. To allow estimates of counting rates to be made, a reference detector has been defined for simulation purposes. The results from these simulations have given confidence in the feasibility of the project.

The neutrino detector infrastructure is readily expanded to provide long-term monitoring of climatic, oceanographic and geophysical processes.

4 NEUTRINO TELESCOPE DESIGN GOALS

This chapter deals with the design goals for the neutrino telescope, from which implementation goals for the hardware of the experiment follow. These requirements are summarised in Table 4-1.

Lifetime

The neutrino telescope is planned as a long term observatory. A data taking period of at least 10 years is required between major maintenance operations. A maximum period of four years is anticipated for the construction and deployment of the detector, taking into account logistics and availability of components.

Environmental Impact

The KM3NeT research infrastructure will be designed to survive a time of at least a decade in the deep sea, under high pressure and in the chemically aggressive salt water environment. The environmental impact will be carefully assessed making use of the expertise of the marine science groups in the KM3NeT consortium. The design goal is that neither installation nor operation of the KM3NeT research infrastructure will adversely affect the deep-sea biosphere.

Energy Range

Neutrino telescopes have effective areas which increase with energy due to the physics of the neutrino interactions and the detection technique, while the energy spectra of most relevant neutrino fluxes are expected to fall with energy. This combination typically gives most of the detectable events in the energy range of 1 TeV to 1 PeV. Optimising the sensitivity in this range will also provide access to lower energies for searches for low-mass dark matter candidates and to higher energies for the investigation of cosmogenic neutrino fluxes.

Zenith Angular Acceptance

To avoid background from atmospheric muons, large scale neutrino telescopes focus on neutrino candidates that originate from below the horizon. The shielding by the deep sea water (see Fig. 1-3)

provides an effective mechanism for reducing this background and allows for the observation of neutrinos above the horizon. Figure 1-4 showing the detector sky coverage in the Mediterranean Sea and at the South Pole is made assuming this 2π acceptance of the detector. Because of the better angular resolution (see below), a sea-water telescope can extend the angular coverage above the horizontal. The objective for KM3NeT is to have full acceptance for neutrinos originating from directions up to at least 10° above the horizontal. For neutrinos with energies above about 100 TeV, for which the background from atmospheric muons is manageable and the light intensity of the produced Cherenkov radiation is high, angular acceptance will be limited only by the absorption in the Earth.

Time resolution (for a single photon, photomultiplier + electronics)	< 2 ns (RMS)
Position resolution	< 40 cm (RMS)
Charge dynamic range	≈ 100 pe /25 ns
Two-hit time separation	< 25 ns
Coincidence acceptance	> 50 %
False coincidences	Dominated by random coincidences from marine background photons
Dark noise rate	< 20 % of the ^{40}K rate
Failure rate of optical modules	< 10 % over 10 years without major maintenance

Table 4-1: Technical requirements for the KM3NeT neutrino telescope.

Angular Resolution of Detector

Due to the largely reduced light scattering in sea water as compared to ice, a major advantage of a sea water neutrino telescope is the obtainable an-

gular resolution in reconstructing muons. To take full advantage of this, the contribution to the resolution from detector effects should not dominate the contribution from the kinematics of the neutrino interaction over most of the energy range. At a neutrino energy of about 30 TeV, the latter is 0.1° and is larger for lower energies. For a $1/E^2$ energy spectrum the bulk of the detected events will be below this energy and so the goal for the muon angular resolution[3] of the telescope is set to 0.1°. The systematic uncertainty in the direction reconstruction of muons must also be kept below this value.

Time and Position Resolution

The time and position resolution of the detector impacts on the angular resolution. The angular resolution of a muon track is determined by the number of photons used in the track fit, the resolution for the arrival time of each photon, the resolution of position of the photon detector and the length of the lever arm over which the photons are detected. The fundamental limit to the time resolution of a single photon is given by a combination of the chromatic dispersion and scattering in the sea water. In Table 4-2, the results of a Monte Carlo study of the angular resolution of muons in the reference detector, as a function of the single photon arrival time resolution are presented. A total instrumental time resolution of 3 ns from the photon detection then follows from the goal of an angular resolution for muon reconstruction of better than 0.1°. This effective time resolution has a contribution from the time measurement as well as the position measurement. To some extent a trade-off between position and time resolution will be possible. Assuming equal contributions and no correlation between position measurements, the photomultiplier and electronics time resolution should be better than 2 ns and the precision in position should be better than 40 cm.

Time Resolution (ns)	Angular Resolution (degrees)
1.5	0.08
3	0.11
6	0.22
12	0.36

Table 4-2: Effect of time resolution on the median angular resolution for muon tracks with energy of 100 TeV in the reference detector.

Charge Dynamic Range

Muons passing through the detector typically do not produce large photon fluxes on the optical modules, except through high-energy Bremsstrahlung. The dynamic range of the optical module is therefore determined by shower reconstruction. Simulations indicate that a 1 PeV shower will, at 100 m from the shower, produce a flux of photons of 6 cm^{-2} within 100 ns in the forward direction of the shower. In the rear direction the fluxes are reduced to 1 cm^{-2} in 150 ns. Such an event is typically registered by hundreds of optical modules at hundreds of metres from the shower. For determining the design goal for the dynamic range it is important to specify the (energy-dependent) resolution, with which the energy of the shower must be measured. At low energy, two-photon recognition, which will be discussed later, is important. At high energies a resolution of the order of 0.3 in $\log(E)$ is appropriate. A shower above 1 PeV at a distance of 100 m would give around 600 photoelectrons in 100 ns for a photocathode area of 500 cm^2 with a quantum efficiency of 20%. Although a corresponding dynamic range is achievable for photomultipliers, simulations must be performed in order to see if this can be reduced, while still maintaining the resolution. Until these simulations are completed, a dynamic range of 100 photoelectrons/25ns is assumed (see Table 4-1).

Two-hit Time Separation

The two-hit time separation of the front-end electronics determines the ability of the detector to

---

[3] All resolution requirements are shown as RMS deviations.

identify photons close in time, and is for example important for recognising background induced by multi-muon cosmic ray showers. The better the two-hit separation the better this background can be recognised. A natural limit is given by the width of a typical photomultiplier pulse, 20-25 ns. The design goal is therefore that the system downstream of the photomultiplier will not increase this.

Coincidences

For pattern recognition it is imperative to suppress the noise from the sea environment. In general the noise consists of single photons in the typical integration windows of the readout (25 ns). Passing muons produce signal fluxes on an OM that can be larger, and so measurement of coincident photons allows for a fraction of the muon signal to be identified with a high degree of certainty. There is therefore a premium on recognising coincident photons with high efficiency and purity. The requirement is thus that the rate of fake two-photon signals is at the level of that caused by the accidental coincidence of background photons from the marine environment. Furthermore, when two photoelectrons are produced locally (inside about 3 m) within 25 ns, they are required to be recognised as such 50% or more of the time.

Dark Noise Rate

The sea water is a relatively noisy environment due to the presence of radioactive ^{40}K decays and bioluminescence. Simulations and measurements indicate that singles rates of $100\,\mathrm{Hz\,cm^{-2}}$ are expected for a threshold of 30% of the average one-photoelectron signal. For the muon trigger, this level of noise is readily eliminated by the use of local coincidences. The photomultiplier dark count should not significantly increase this rate. The photomultiplier dark noise rate is therefore required to be less than 20% of the expected ^{40}K rate.

Failure Rate of Optical Modules

Monte Carlo studies have shown that the main effect of random permanent optical module failures is to reduce the detector sensitivity at low energies. For example, a 10% failure rate results in

the loss at the trigger level of 40% of muons with energies between 400-500 GeV, but only 10% for muons of 1 TeV. Above 30 TeV there is almost no effect. The effect on the angular resolution is small. For 10% failure, a 3% degradation in the angular resolution is observed for muon tracks. As a result, a permanent optical module failure rate of less than 10% is required over a 10-year period without major maintenance.

To optimise the physics potential of the neutrino telescope, design goals have been quantified for the technical implementations.

5 PILOT PROJECTS

5.1 ANTARES

The geometrical layout and readout architecture of the ANTARES detector have been optimised using four criteria: total detection efficiency; neutrino direction precision; background rejection and cost. The background reduction requires optical modules spaced closely enough to be able to recognise tracks by timing associations within the distribution of random hits due to the light backgrounds in the sea water from radioactive decays and bioluminescence.

An artist's impression of the layout of the neutrino telescope is shown in Figure 5-1. The detector consists of 12 lines, each with a total height of about 450 m, which are weighted to the seabed and held nearly vertical by syntactic-foam buoys at the top. Figure 5-2 illustrates the components within a typical line. Each line carries a total of 75 photomultipliers housed in glass spheres, referred to as optical modules (OM) [**73**], designed to detect Cherenkov light from charged particles in the sea water. The seabed at the site is at a depth of 2475 m and the OMs are positioned at depths between about 2400 m and 2000 m.
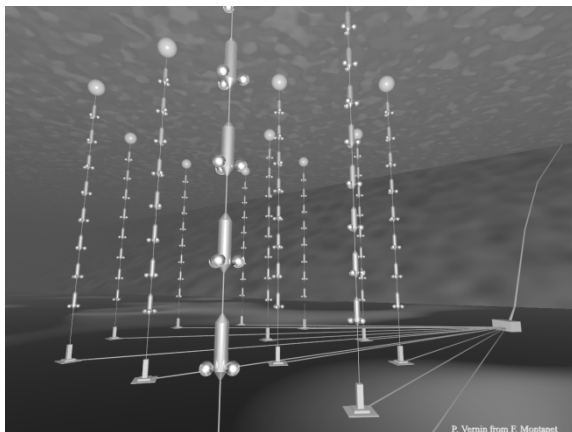
Figure 5-1: Artist's impression of the ANTARES neutrino telescope on the seafloor, showing the detector lines, the seabed interlinks cables, the junction box and the cable to the shore. For clarity, in this illustration the number of storeys per line is reduced and items are not drawn to scale.

The lines are flexible and so move with the sea current, with displacements being a few metres at the top for a typical sea current of 5 cm/s. The positions of the OMs are measured with a system of acoustic transponders and receivers on the lines and on the seabed, together with tilt meters and compasses. The positioning system gives a real-time measurement, typically once every few minutes, of the position of every OM with a precision better than 10 cm in space.

The default readout mode of ANTARES is the transmission of the time and amplitude of any photomultiplier signal above a threshold corresponding to 1/3 of a photoelectron signal for each optical module. Time measurements are referenced to a master clock signal sent from shore. All photomultiplier signals are digitised and sent to shore where they are processed in a computer farm to find hit patterns corresponding to muon tracks or other physics events producing light in the water. The grouping of three optical modules in a storey allows local coincidences to be used for this pattern finding. In addition the front end electronics allows for sampling the full waveform of the signal with 128 samples separated by 2 ns.

The readout architecture of the detector has several levels of multiplexing. The first level is in the local control module in each storey, where the analogue electrical photomultiplier signals are digitised in a custom built ASIC chip, the analogue ring sampler. A data acquisition card, containing an FPGA and microprocessor, outputs the multiplexed signals of the three local optical modules on an Ethernet optical link. The links from 5 storeys, forming a sector, are combined in an Ethernet switch at every fifth storey and the combined output is sent on a particular wavelength to a dense wavelength division multiplexing system in an electronics container at the bottom of each line, the string control module. In this control module the data from the line are multiplexed on to one pair of optical fibres. These fibres are connected to a

junction box on the seabed via interlink cables. In the junction box the outputs from the lines are gathered onto a 48-fibre electro-optical submarine cable and sent 45 km to the shore station at La Seyne-sur-Mer. The optical links between the sectors and the shore station are implemented using only passive components.
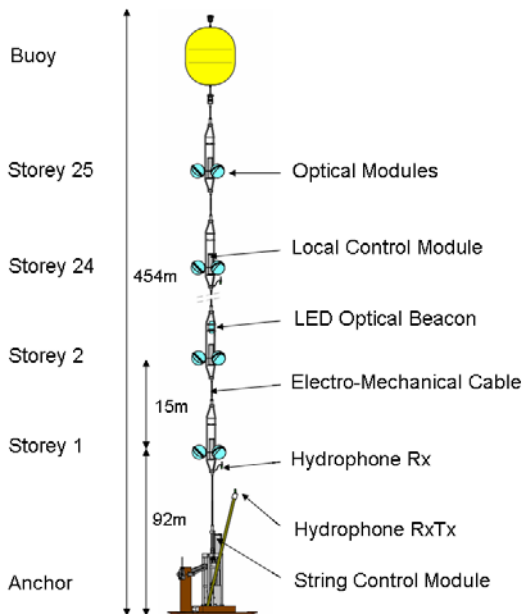
Figure 5-2: Schematic view of an ANTARES detector line. For clarity, only 4 of the 25 storeys are shown and the cable lengths are not drawn to scale.

The electrical supply system has an architecture similar to the readout system. The submarine cable supplies about 4.4 kV, 10 A alternating current to a transformer in the junction box. The independent secondary outputs from the transformer provide 500 V, 4 A to the lines via the interlink cables. At the base of each line a power supply, sharing the same container as the String Control Module, distributes 400 V DC to the Local Control Modules. Each of these contains a local power box that provides the various low voltages required by the electronics cards.

The shore station houses the computer farm for the on-shore event filtering. After selection the data are sent via a data link to be recorded at a computer centre in Lyon.

Early ANTARES Activities and Test Lines

The R&D activities towards the construction of the neutrino telescope started in 1996 with the deployment and recovery of autonomous mooring lines used to measure the environmental properties at the ANTARES site. In these campaigns [74,75], comprising more than 60 line deployments, extensive measurements were made of bio-deposition, sedimentation, light attenuation and light background from bioluminescence.

The earliest test line connected to a readout system on shore was deployed in November 1999 and used an old, existing, undersea cable donated by France Telecom to connect the line to a recording station in Marseille. Located at a site near Marseille at a depth of 1200 m, the line was operated for a few months and was used to verify various concepts of the ANTARES design, in particular the acoustic positioning system. Atmospheric muons were reconstructed with the seven optical modules of this line [76].

In 2001 the construction of the actual detector started with the deployment of the cable between the ANTARES site and the shore station in La Seyne-sur-Mer. This cable was initially deployed with only a loop-back container at the sea end. A year later the end of the cable was brought to the surface, connected to the junction box and redeployed. Since then the battery operated slow control in the junction box has sent to shore measurements of various parameters demonstrating perfect operation of the cable and junction box system for more than five years.

Two prototype lines were deployed and connected between November 2002 and March 2003: the "MIL", an instrumentation line and the "PSL", a short detector line with 15 optical modules. These lines were operated in situ until May and July 2003, respectively. Again the validity of various aspects of the design was verified but certain problems with loss of optical transmission in the line cables and leaks in the cables and containers were discovered. Nevertheless, it was possible to measure the counting rates in the optical modules of the
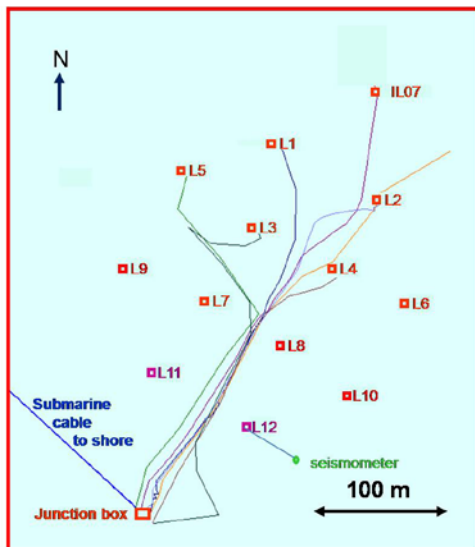
Figure 5-3: Seabed layout of the ANTARES detector. The lines indicated in red were in place and connected as of January 2008; meanwhile, all lines are operational.

PSL, in particular the rates of bioluminescence, over a period of about 4 months.

After the experiences with MIL and PSL, some significant changes were made to the detector design and a line incorporating these changes, the "MILOM" was deployed in March 2005 and connected, using the ROV Victor, in April 2005. This line has been operated successfully for several months in 2005 [**8**].
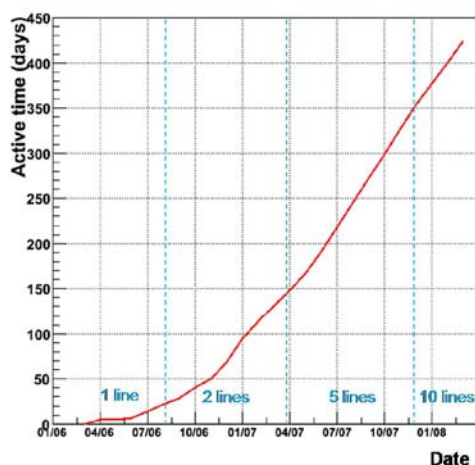
Figure 5-4: Active days of data taking as a function of date since the connection of the first complete line.
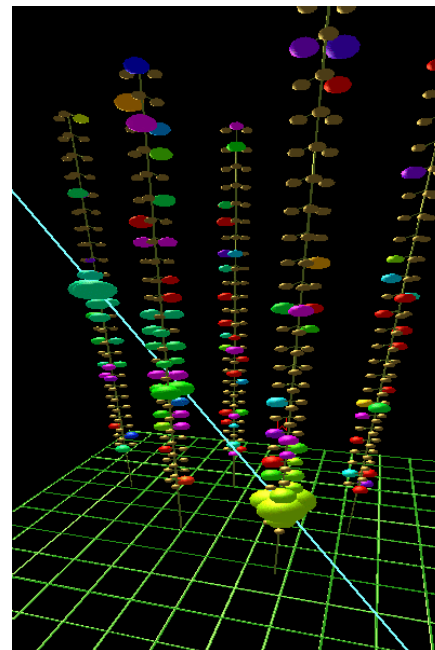
Figure 5-5: The first candidate neutrino event seen with the detector with five lines.

Current Status of ANTARES

Since May 2008, all 12 ANTARES lines are operational. Figure 5-3 indicates the seabed layout of the detector lines. The lines have been deployed at various dates since February 2006; the seabed connections have been made using the submersibles Nautile or Victor of IFREMER.

First Results

The ANTARES detector has been increasing in size as lines have been connected. Figure 5-4 shows the number of active days of data taking and the periods of one, two, five and ten line operation. The slope of the graph indicates an overall data taking efficiency of about 70% since spring 2007.

At present a number of algorithms for event reconstruction are being developed within the collaboration. One of these algorithms was developed using Monte Carlo simulations performed before the operation of the detector [**77**]. This algorithm is applied to the data with exactly the same cuts as developed on the simulations. Figure 5-5 shows an event reconstructed using this algorithm, while Figure 5-6 shows the zenith angle distribution from the first months of five line operation.
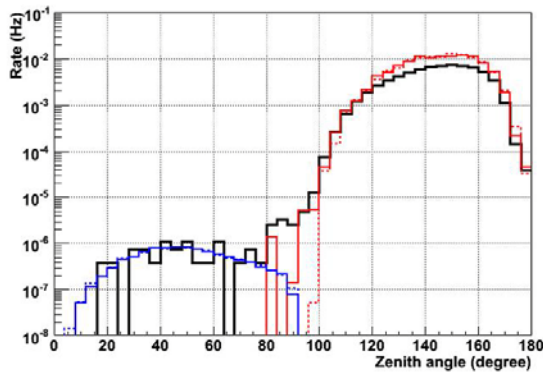
Figure 5-6: Zenith angle distribution for tracks reconstructed from data taken for 37 active days with the five line configuration. Black histogram is reconstructed data and red and blue curves are simulated expectations from atmospheric muons and atmospheric neutrinos, respectively.

The reconstruction algorithm is preliminary and uses nominal detector geometry. The zenith angular distribution of Figure 5-6 illustrates clearly the separation between upward- and downward-going tracks. Simulations indicate that the majority of the tracks that are reconstructed as upward-going are due to neutrino interactions.

5.2 NEMO

Starting from 1998 the NEMO collaboration has carried out R&D activities aimed at developing and validating key technologies for a cubic-kilometre scale underwater neutrino telescope [**78**]. A first phase focussed on site investigation and characterisation studies as well as the development of a suitable detector concept.

The NEMO detector concept is based on semi-rigid vertical structures (towers) composed of a sequence of 12 m long horizontal structures in marine grade aluminium (bars), see Figure 5-7. Each of these has two optical modules at either end, one looking vertically downwards and the other horizontally outwards, and contains instrumentation for positioning and monitoring of environmental parameters. A tower, which consists of 16 such structures interlinked by a system of ropes, is anchored to the seabed and kept vertical by appropriate buoyancy on the top. The spacing be-

tween storeys is 40 m, while an additional spacing of 150 m is added between the anchor and the lowermost storey. The structure is designed to be assembled and deployed in a compact configuration, and unfurled on the sea bottom under the pull provided by the buoy. Once unfurled the bars assume an orthogonal orientation with respect to their vertical neighbours.

The power and readout is provided by a lightweight electro-optical cable that is kept separated from the system of tensioning ropes in order to reduce interference with the mechanical structure. Fibre-optic technology is used for data transfer. The towers are connected through a network of undersea cables and junction boxes and a single main electro-optical cable to shore. The towers are connected to the junction boxes through underwater wet-mateable electro-optical connectors operated by a remotely operated vehicle (ROV).

The R&D activities of the NEMO collaboration are organised in two successive phases. During Phase-1 a demonstrator tower was installed at a test site close to Catania at a depth of 2000 m. The Phase-2 project, which is currently under construction, aims at installing an infrastructure, comprising a 100 km electro-optical cable, a shore station and a full-scale tower, at the Capo Passero site at a depth of 3500 m.

NEMO Phase-1

The Phase-1 project started in 2002 and was completed in December 2006 with the deployment and connection of two components: the junction box and a prototype NEMO tower [**79**]. All key components of an underwater neutrino detector are included: optical and environmental sensors; power supply; front-end electronics and data acquisition; time and position calibration; slow control systems; on-shore data processing.

The junction box (Figure 5-8) provides connection between the main electro-optical cable and the tower. It has been designed following an innovative concept to withstand pressure and corrosion. These two issues have been decoupled by placing the electronics inside a pressure-resistant steel
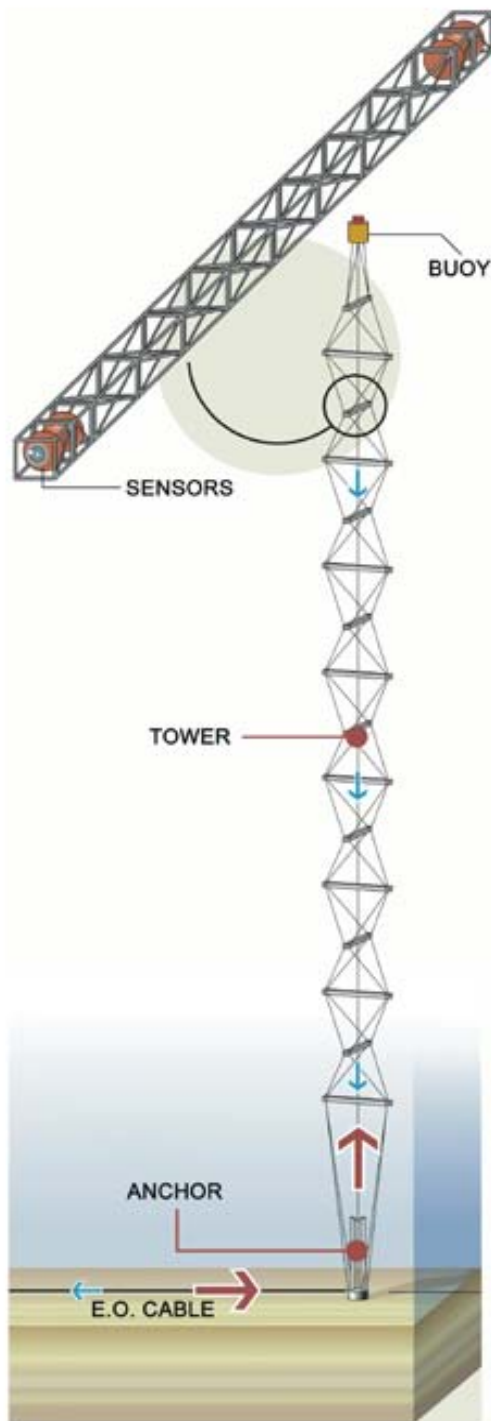
Figure 5-7: The NEMO tower structure.

Figure 5-8: The junction box of the NEMO Phase-1 project.

placed directly in the oil bath. The double containment technology has the further advantage of preventing water ingress in case of failure of an internal connector or penetrator.

The prototype tower has four bars. A schematic of the prototype tower is shown in Figure 5-9. In addition to the 16 optical modules the instrumentation includes several sensors for calibration and environmental monitoring. In particular two hydrophones are mounted on the tower base and at the ends of each bar. These, together with an acoustic beacon placed on the tower base and other beacons installed on the seabed, are used for precise determination of the tower position. The other environmental probes are: a Conductivity-Temperature-Depth (CTD) probe used for monitoring water temperature and salinity; a light attenuation probe (C*) and an Acoustic Doppler Current Profiler (ADCP) that provides continuous monitoring of the deep-sea currents along the whole tower height.

The NEMO Phase-1 apparatus was successfully operated for several months after the installation. The installation operation allowed for full validation of the underwater connection concept and the "unfurling" technique. The power supply, data transmission and time and position calibration procedures were also validated.

vessel housed inside a fibreglass container filled with silicone oil, that is pressure compensated. Moreover, all electronics components proven to withstand pressure in laboratory tests have been
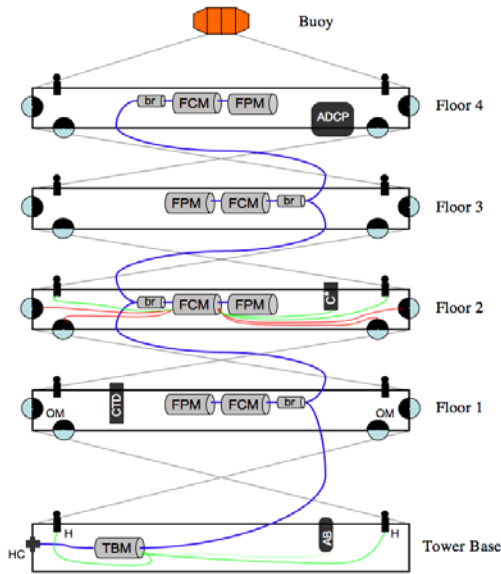
Figure 5-9: Schematic of the prototype tower of the NEMO Phase-1 project with the backbone cabling (blue), the Tower Base Module (TBM), the floor breakouts (br), the Floor Control Modules (FCM) and the Floor Power Modules (FPM). Connection to the Junction Box is provided through a wet mateable hybrid connector (HC) on the tower base. For clarity the layout of the floor internal cabling is drawn only for floor 2, with electro-optical connections as red lines and electric connections as green lines.

Figure 5-10: Reconstruction of a down-going atmospheric muon track with the NEMO Phase-1 prototype tower.

Power is distributed by means of a three-phase AC system to each Floor Power Module, where a conversion to DC is made. The system has been designed to have most of its components working under pressure inside an oil bath [80].

Data transmission is based on a synchronous communication protocol, which embeds data and synchronisation and clock signals in the same serial bit stream [81]. The technology relies on Wavelength Division Multiplexing techniques, using only passive components with the exception of the electro-optical transceivers. The architecture of the data transmission system is based on a Floor Control Module located at the centre of each bar, which collects data and streams them to shore. In the opposite direction, the Floor Control Module receives slow control data, commands and auxiliary information, as well as the clock and synchronisation signals needed for timing.

Time calibration is performed by measuring time delays from shore to each Floor Control Module from the propagation times of signals that are distributed via a network of optical fibres [82]. This system was demonstrated to provide an accuracy of 1 ns.

Since the tower structure can flex under the influence of sea currents, a determination of sensor positions is necessary. This is achieved by means of acoustic triangulation measurements using acoustic beacons placed on the seafloor and a couple of hydrophones on each bar. In addition the inclination and orientation of each bar is measured by a tilt-meter and a compass. A positioning accuracy of 10 cm was obtained.

Using the NEMO Phase-1 installation, down-going muon tracks have been reconstructed; an example is shown in Figure 5-10.

NEMO Phase-2

In the NEMO Phase-2 project an underwater infrastructure at the Capo Passero site and a complete tower structure with 16 storeys will be constructed at a depth of 3500 m.

The NEMO Phase-2 deep-sea infrastructure includes a 100 km long electro-optical cable, laid in July 2007, which links a shore station, located in the harbour area of Portopalo di Capo Passero to an underwater infrastructure needed to connect detector prototypes. The shore station, hosting power supply and data acquisition systems, will also include integration and test facilities for detector structures.

A DC power system with sea return was chosen. The main electro-optical cable, manufactured by Alcatel, carries a single electrical conductor, that can be operated at 10 kV DC allowing for a power load of more than 50 kW, as well as 20 single-mode optical fibres for data transmission. The Phase-2 infrastructure will include a cable termination assembly with a 10 kW DC/DC converter to 400 V [**83**]. This system will be deployed at the end of 2008.

The experience gained with the Phase-1 tower has led to a revision of the design aimed at simplifying the tower integration and reducing construction costs. The major changes concern: the electro-optical backbone, with a new segmented structure that allows for easier integration; the integration of all the electronics, power systems and fibre breakouts in a single pressure vessel; a revision of the time calibration system to eliminate fibres along the storey. The power system has also been modified to comply with the new DC design.

The completion of Phase-2 at the end of 2008 will allow for a full validation of the deployment and connection techniques and of the functionality of the system at a depth of 3500 m. At the same time it will permit a continuous long term monitoring of the site properties.

Associated Science Activities
On the NEMO test site in the bay of Catania a geo-seismic station has been deployed and connected to the electro-optical cable of the NEMO underwater infrastructure by the Istituto Nazionale di Geofisica e Vulcanologia in January 2005 and has operated ever since. This station, which includes a seismometer, a magnetometer and several water

environmental probes, is the first working node of the ESONET network.

On the same site a set of hydrophones has been installed to test the feasibility of acoustic detection of high-energy neutrinos. It was operated from January 2005 to December 2006 and provided a large set of deep-sea acoustic data. Analysis of the acoustic data allowed for the detection of sperm-whales at a distance of more than 40 km, revealing a population larger than previously estimated.

5.3 NESTOR
The acronym NESTOR stands for Neutrino Extended Submarine Telescope with Oceanographic Research. NESTOR is a deep-sea neutrino telescope under construction in the southern Ionian Sea off the coast of Greece, at depths exceeding 3500 m (see Figure 5-11).

Deep-Sea Station
The NESTOR collaboration has developed an approach to operating a deep-sea station, permanently connected to shore by an in-situ bi-directional cable, for multi-disciplinary scientific research.

Construction and deployment of such a multidisciplinary deep-sea station, at a depth of 4100 m was achieved in January 2002 [**84**]. This deep-sea station, developed in the project LAERTIS [**85**], also serves the purpose of being the bottom platform for a deep-sea neutrino telescope. It was operated with power from and data transfer to shore in real-time via an electro-optical cable. Recovery and redeployment operations with payload exchange were performed. Data from temperature and pressure sensors, a compass, a light attenuation meter, a water current meter and an ocean bottom seismometer were transmitted to shore.

An important feature of the deployment and recovery procedure developed by NESTOR lies in allowing the instrument package, once deployed at the seafloor, to be recovered, modified or serviced at the surface and be deployed again, without recourse to manned submersibles or remotely operated vehicles. The feasibility of this procedure has been demonstrated in repeated redeployments.
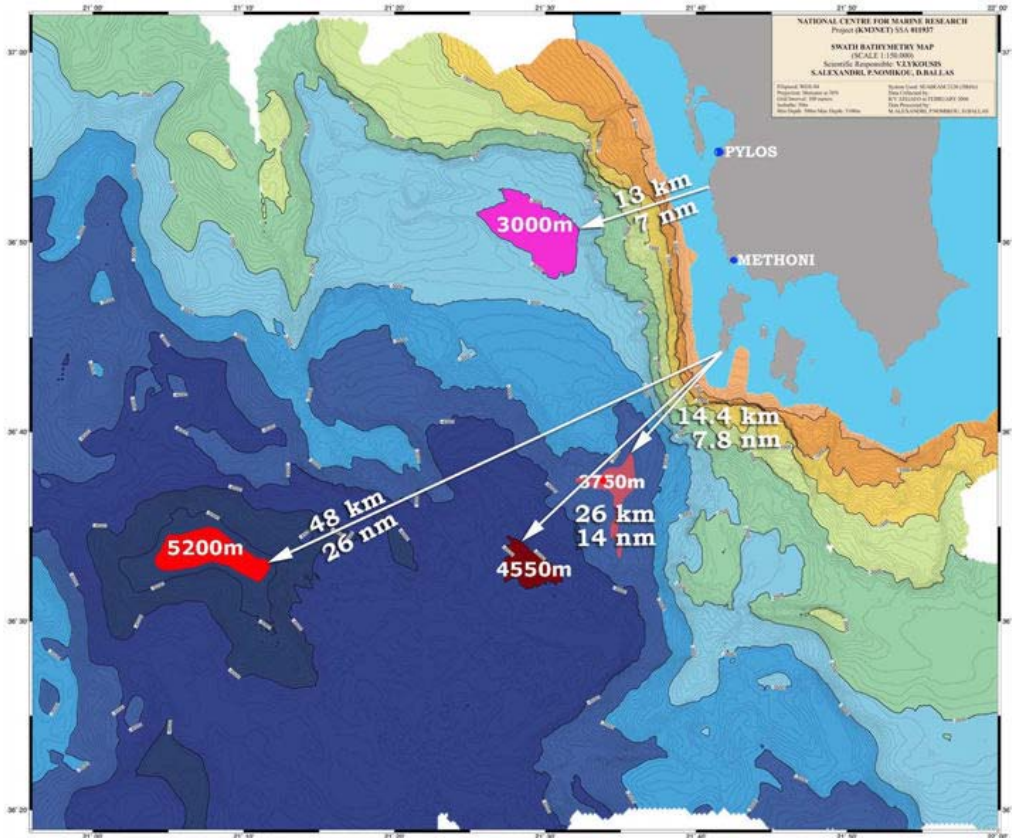
Figure 5-11: Bathymetry of the sea at the NESTOR site, distances to nearest landfall are in kilometres and nautical miles (nm). In 2003 the deployment took place to the 3750 m plateau.

Performance of the Test Detector

In March 2003, the NESTOR collaboration successfully deployed a test floor of the detector tower, fully equipped with 12 optical modules, final electronics and associated environmental sensors [**86**]. In this operation, the electro-optical cable and the deep-sea station, previously deployed at 3850 m, were brought to the surface, the floor was attached and cabled and redeployed to 3800 m.

The basic element of the NESTOR detector is a hexagonal star-shaped floor. Six arms, built from titanium tubes to form a lightweight lattice girder, are attached to a central casing. Two optical modules are attached at the end of each of the arms, one facing upwards and the other downwards. The electronics for the floor is housed in a 1 m diameter titanium sphere within the central casing. The diameter of the floor deployed in 2003 was 12 m.

The optical module [**86**] consists of a 15 inch diameter photomultiplier tube enclosed in a spherical glass housing which can withstand the hydro-

static pressure up to 630 bar. To reduce the effect of the terrestrial magnetic field, the photomultiplier is surrounded by a high-magnetic-permeability cage. Its optical coupling to the glass sphere is made with glycerine, sealed by a transparent silicone gel gasket.

Other modules, above and below each floor, house LED flasher units that are used for calibration of the detector and are controlled and triggered from the floor electronics.

The detector was continuously operated for more than a month and over 5 million events were accumulated, investigating different trigger modes, coincidence levels and photomultiplier thresholds. In addition, several million calibration triggers were taken at various photomultiplier high-voltage settings.

The readout and DAQ chain performed well and with practically zero dead-time. The monitored experimental parameters, operational and envi-

ronmental, remained stable within acceptable tolerances.

The photomultiplier pulse height distributions, the trigger rates and the total number of photoelectrons inside the trigger window as functions of the signal thresholds and coincidence level settings, as well as the arrival time distribution of the photoelectrons, agree very well with Monte Carlo predictions based on the atmospheric muon flux parameterisation of Okada [87], the natural [40]K radioactivity in the sea water, and the photomultiplier dark currents and afterpulses.

Several studies have been made to ensure that the event selection trigger was unbiased and that the signals from the photomultipliers can be attributed to the expected sources. In addition, calibration in the sea using the LED flasher units mounted above and below the detector floor provided a rigorous test on the time stability of the detector as well as a measurement of the resolution of the arrival time of the signals.

For about 1.1% of the total experimental time bioluminescent activity has been observed around the detector. This caused about 1% dead time and is consistent with previous measurements at the same site performed with autonomous devices [88]. Events collected during such periods of activity were easily identified and rejected.

Measurement of the Cosmic Ray Muon Flux

The prolonged period of running under stable operating conditions made it possible to measure the cosmic ray muon flux as a function of the zenith angle θ [10,89].

For this measurement only events with six or more photomultiplier pulses coincident inside a time window of 60 ns were used to reconstruct tracks, employing first the information on the arrival time and then the amplitude of the digitised pulses.

A Monte Carlo package [86,89] has been developed to simulate the detector response to atmospheric muons arriving at the detector depth, using the energy and angular distributions taken from the Okada parameterisation. Simulated muons are

propagated through water, taking into account energy loss, secondary particle production and multiple scattering. A detailed simulation of the Cherenkov light detection, [40]K background contribution, trigger selection and photomultiplier waveform digitisation was included.

The vertical intensity and the zenith angle distribution of cosmic ray muons at the detector depth have been measured and are consistent with previous underwater measurements [90,91] and with phenomenological predictions.

The measured muon intensity parameterised as $I = I_0 \cos^\alpha(\theta)$, at a depth of 3800 m water equivalent, is found to be

$$\alpha = 4.7 \pm 0.5 \ (stat) \pm 0.2 \ (syst)$$

$$I_0 = (9.0 \pm 0.7 \ (stat) \pm 0.4 \ (syst))$$
$$\times 10^{-9} \ \mathrm{cm}^{-2}\mathrm{s}^{-1}\mathrm{sr}^{-1}$$
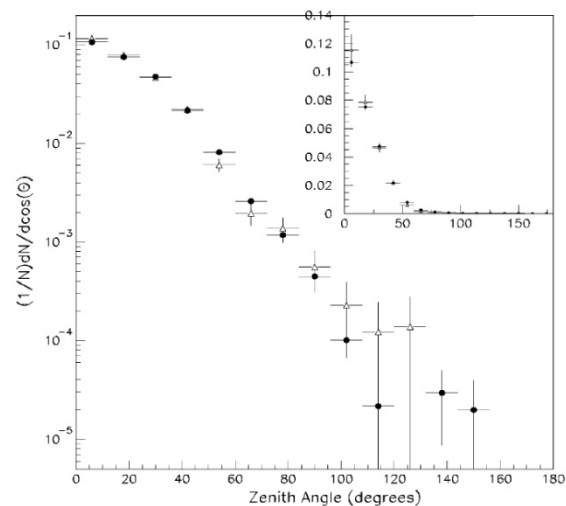
Figure 5-12: Distribution of the zenith angle of reconstructed tracks for the data (open triangles) and Monte Carlo (solid points) event samples. The insert shows the same distributions on a linear scale. Figure taken from [86].

For more than a decade, the feasibility of neutrino astronomy with a detector in the deep sea has been investigated in three pilot projects. In each of these, different configurations and techniques have been explored. These three projects ANTARES, NEMO and NESTOR have reached maturity and have demonstrated the potential of the detection technique by reconstructing the tracks of muons. These projects have provided a wealth of information on the technologies required for a large deep-sea neutrino telescope. KM3NeT will reap the benefits.

6 SITE INVESTIGATIONS

The Mediterranean Sea offers optimal conditions, on a worldwide scale, to host an underwater neutrino telescope. Several suitable sites have been identified.

Many criteria can drive the site choice, the most relevant of which are:

- Proximity to the coast to ease deployment and reduce the expense of the power and signal cable connections to shore;
- A sufficient depth to reduce background from atmospheric muons, in particular from those that are mis-reconstructed as up-going;
- Good optical properties of the water, i.e. absorption and scattering lengths close to the ones of optically pure sea water for light in the wavelength range of 350 nm to 550 nm;
- Low level of bioluminescence;
- Low rates of biofouling (bacterial film deposition and marine life accretion) on optical surfaces;
- Low rates of sedimentation;
- Stable low sea current velocities.

Careful studies of candidate sites have been carried out in order to identify the most suitable one. The ANTARES, NEMO and NESTOR Collaborations have started dedicated research programmes to characterise the candidate sites, which are currently pursued within the context of the KM3NeT project. The locations of the three candidate regions, shown in Figure 1-6, are:

Toulon - Ligurian Sea (ANTARES):
- 42°48' N 06°10' E, depth: 2475 m.

Capo Passero - West Ionian Sea (NEMO):
- 36°16'N 16°06' E, depth: 3500 m.

Pylos - East Ionian Sea (NESTOR):
- 36° 33'N 21°08'E, depth: 5200 m or
- 36° 33'N 21°29'E, depth: 4500 m or
- 36° 38'N 21°35'E, depth: 3750 m.

Deep-sea water optical properties (absorption and diffusion) and environmental properties (water temperature, salinity, biological activity, optical background, water currents and sedimentation) have been studied.

Given the large amount of data collected to date and the ongoing character of these investigations the data presented below are typical examples of the overall sample. The complete set of data will be used to aid in the site selection.

6.1 WATER OPTICAL PROPERTIES

6.1.1 Light Transmission

The study of the deep-sea water optical properties will be performed through a long-term programme carried out spanning all the seasons. Sea water absorbs and scatters light depending on the water temperature, salinity, as well as the characteristics and concentration of the suspended particulate. These parameters are different at different marine sites and may vary as a function of time.

In order to properly describe the transparency of natural waters, as a function of wavelength, it is necessary to measure the inherent optical properties of the water, such as the absorption length $L_a(\lambda)$, scattering length $L_b(\lambda)$ and attenuation length $1/L_c(\lambda) = 1/L_a(\lambda) + 1/L_b(\lambda)$ [92,8]. Each of these lengths represents the path after which a beam of initial intensity I_0 and wavelength λ is reduced in intensity by a factor of 1/e through absorption, scattering or both according to:

$$I_{a,b,c}(x) = I_0 e^{(-x/L_{a,b,c})},$$

where x is the optical path traversed by the beam. In the literature the coefficients of absorption, $a = 1/L_a$, and scattering, $b = 1/L_b$, are also used to characterise the light transmission through matter. The sum of scattering and absorption coefficients is called attenuation coefficient c.

Scattering is only taken into account for processes in which the direction of the light is changed with-

out any other alteration. Scattering phenomena in which the photon wavelength changes (e.g. Raman effect) happen less frequently. Scattering can take place either on molecules (Rayleigh scattering) or on particulate matter (Mie scattering). Other parameters commonly used in the literature are the effective scattering length

$$L_b^{eff} = \frac{L_b(\lambda)}{1 - \langle \cos \vartheta \rangle} = \frac{1}{b^{eff}}$$

and the effective attenuation length

$$L_c^{eff} = \frac{1}{c^{eff}} = \frac{1}{a + b^{eff}},$$

where $\langle \cos \vartheta \rangle$ is the average cosine of the scattering angle. The estimation of the latter parameter is difficult since it needs the knowledge of another inherent optical property, the volume scattering function $b(\lambda, \vartheta)$, that must be measured with appropriate devices.

Light Transmission Measurements

The Toulon site has been studied for many years with dedicated setups designed to characterise water optical properties. Early measurements [93] taken between 1997 and 2000 were made for blue (473 nm, with 10 nm of FWHM) and UV (375 nm, with 10 nm of FWHM) light. The results for the absorption, scattering, and effective attenuation lengths are summarised in Table 6-1 and Table 6-2.

The Capo Passero site has been investigated [94] using a setup including a commercial instrument (the AC9 by WETLABS) capable of measuring, in a well collimated geometry, the absorption and the attenuation coefficients for nine wavelengths ranging from 410 nm to 715 nm. The values of the absorption and attenuation lengths have been determined for each measurement by averaging the data for depths greater than 2850 m. The results [95] of four sets of measurements taken in different seasons are shown in Figure 6-1 and Figure 6-2. For comparison light absorption and attenuation data for optically pure sea water are also shown. At all wavelengths, deep waters at that location have an absorption length compatible with that of pure sea water. There is no evidence of a seasonal dependence of the optical parameters.

Date	Effective attenuation length (m)	Absorption length (m)	Effective scattering length (m)
July 1998	60.6±0.4± 5	68.6±1.3±5	265±4±28
Mar. 1999	51.9±0.7±1	61.2±0.7±1	228±11±24
June 2000	46.4±1.9±2	49.3±0.3±2	301±3±27

Table 6-1: Summary of results obtained at the Toulon site using blue light. The first error is statistical and the second one is systematic.

Date	Effective attenuation length (m)	Absorption length (m)	Effective scattering length (m)
July 1999	21.9±0.8±2	23.5±0.1±2	119±2±10
Sept.1999	22.8±0.3±2	25.6±0.2±2	113±3±10
June 2000	26.0±0.5±1	28.9±0.1±1	133±3±12

Table 6-2: Summary of results at the Toulon site using UV light. The first error is statistical and the second one is systematic.
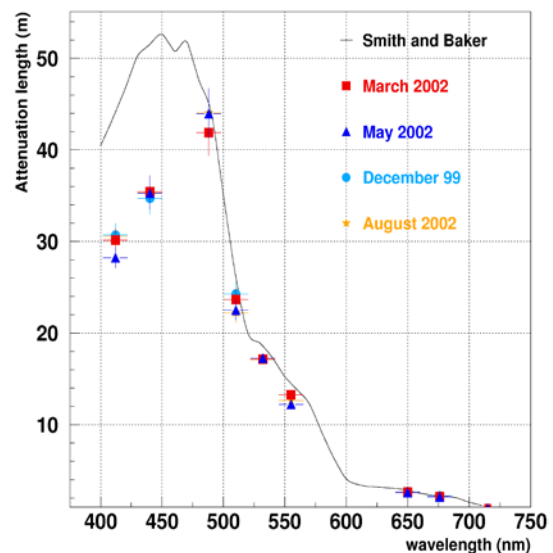
Figure 6-1: Average attenuation length as a function of wavelength, for four seasons at the Capo Passero site.

Light absorption has also been measured at different locations in the Pylos area with an open geometry photometry using a non-collimated light source at a wavelength of 460 nm. Measurements were made at various depths and for distances between light source and sensor ranging from 7.44 m to 40.37 m. Figure 6-3 shows the results of the measurements. A transmission length of 55±10 m describes the data satisfactorily [96].

6.1.2 Optical Background

The background counting rate in the optical modules of an undersea neutrino detector has two main natural contributions, from the decay of radioactive elements in the water, and from the luminescence produced by organisms (bioluminescence).

Of all the radioactive isotopes present in natural sea water ^{40}K is by far the dominant one. Both ^{40}K decay channels

$$^{40}K \rightarrow \ ^{40}Ca + e^- + \bar{v}_e \quad (BR = 89.3\%)$$
$$^{40}K + e^- \rightarrow \ ^{40}Ar + v_e + \gamma \quad (BR = 10.7\%)$$
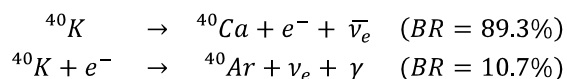
contribute to the production of optical noise. A large fraction of electrons produced in the first reaction is above the threshold for Cherenkov light production. The photon originating in the second reaction has an energy of 1.46 MeV and therefore,
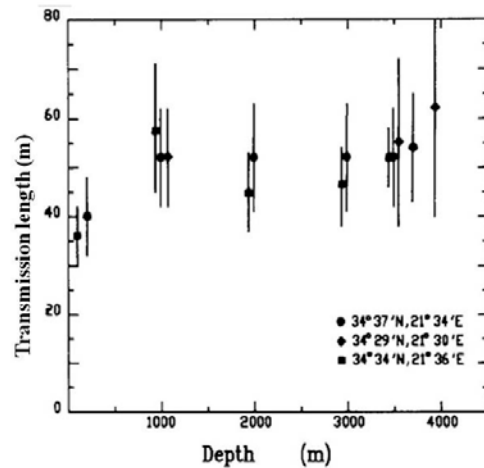
Figure 6-3: Transmission (1/e) length versus depth at 460 nm wavelength in the Pylos area.

through Compton scattering, produces electrons to electrons above the threshold for the Cherenkov effect. The intensity of Cherenkov light from ^{40}K radioactive decays depends mostly on the ^{40}K concentration in sea water. Since the salinity in the Mediterranean Sea has small geographical variation, this Cherenkov light intensity is largely independent of the site.

Bioluminescence is ubiquitous in the oceans and in the deep sea there are two sources, the steady glow of bacteria and flashes produced by animals. These can give rise to an optical background several orders of magnitude more intense than the one due to ^{40}K. Relatively little is known about bioluminescence at great depth. The typical spectrum of bioluminescence light is centred around 470-480 nm [97,98], the wavelength of maximal transparency of water, which is of greatest interest for undersea neutrino telescopes. The distribution of luminescent organisms in the deep-sea varies with location, depth and time but there is a general pattern of decrease in abundance with depth. The Istituto Sperimentale Talassografico di Messina (CNR), has cultured bacteria from samples of water taken from near the Capo Passero site in 2000 and has detected no luminescent bacteria cultivable at atmospheric pressure from samples taken deeper than 2500 m (see Figure 6-4) [99].

Scientists from the University of Aberdeen have counted the number of bioluminescent animals *in situ* (see Figure 6-5) and found a decrease with
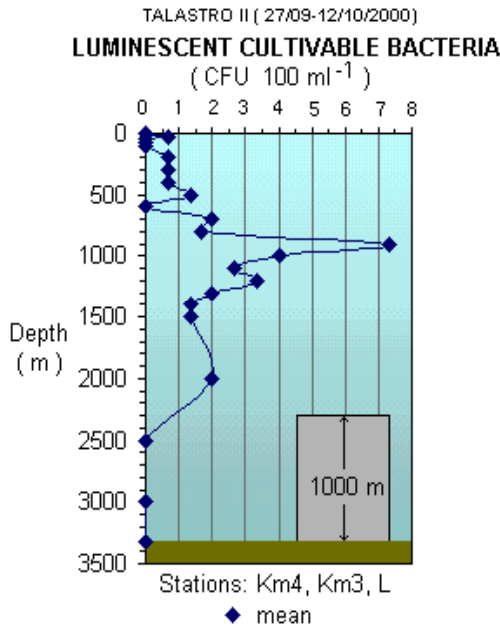
Figure 6-4: Amount of luminescent cultivable bacteria as a function of depth, measured at the Capo Passero site.

depth and an abundance which is significantly lower than that in the Atlantic Ocean at similar depths [**100**,**101**].

Optical Background Measurements

Before detector construction, the ANTARES Collaboration performed a series of in situ measurements of the background light in the Toulon site using 8 inch photomultiplier tubes on autonomous device systems [**74**]. Two contributions to the optical background were observed: a continuous base rate ("baseline") of a few tens of kHz, varying slowly on time scales of a few hours, and sharp peaks lasting a few seconds and rising to tens of MHz ("bursts").

A typical time stream of data, acquired in April 2005 [**8**], is shown in Figure 6-6. Counting rates were acquired with a threshold of 0.3 photoelectrons. The two components of optical background described above are clearly visible. Bursts observed in the counting rates are probably due to the passage of light emitting animals close to the detector.

The baseline component is neither correlated with the sea current, nor with the burst frequency; however, long-term variations of the baseline were

observed with the ANTARES detector. Periods of high burst activity are not correlated with variations of the baseline component, suggesting that each of the two contributions is caused by a different population. Moreover, a strong correlation is observed between burst activity and the current velocity [**102**], as shown in Figure 6-7.
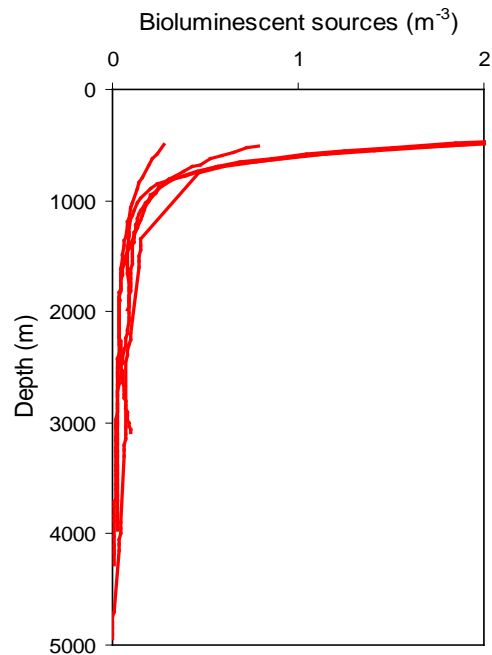
Figure 6-5: Abundance of bioluminescent animals per cubic meter of sea water as a function of depth off Pylos.
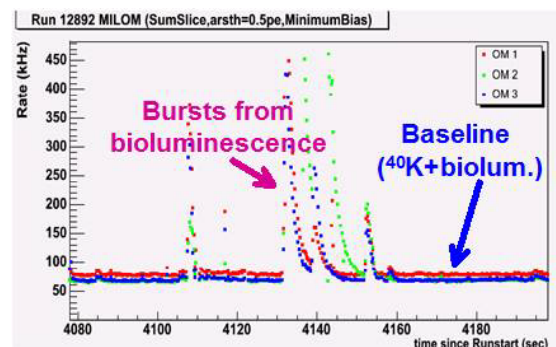
Figure 6-6: Photomultiplier counting rates, as function of time, with a threshold of 0.3 photoelectrons.
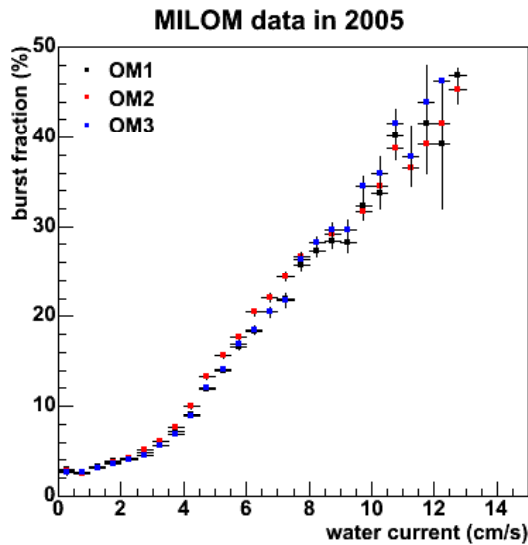
Figure 6-7: Correlation between the burst fraction and the sea water current velocity. The burst fraction is the fraction of time with count rates exceeding 120% of the baseline rate.
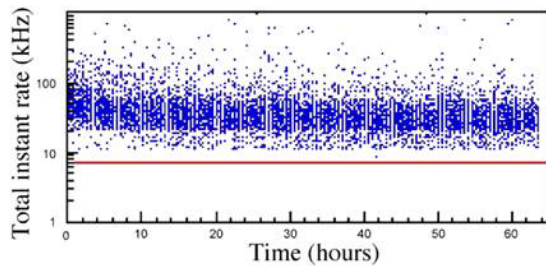
Figure 6-8: Photomultiplier count rate, as function of time, for data collected at the Capo Passero site. The red line indicates the dark current count rate.

Data in Capo Passero were collected by means of two different setups. One, built by the NEMO Collaboration, consisted of two 8 inch photomultipliers and the associated electronics, the second, built by the ANTARES Collaboration, used an optical module containing a 10 inch photomultiplier. The two devices have been used to collect data separately, but also together in order to assess systematic uncertainties. Figure 6-8 shows the photomultiplier rate as a function of time, as obtained with the NEMO setup [**99**] using a threshold equivalent to 0.33 photoelectrons.

After subtracting the dark count rate of 7 kHz a counting rate of 28.4 ± 2.5 kHz is obtained. This background is rather constant and shows only rare

bioluminescence bursts. From this rate, taking into account the properties of the optical module and the photomultiplier, an isotropic photon flux of $360 \pm 40 \ \mathrm{cm}^{-2}\mathrm{s}^{-1}$ in the wavelength range of sensitivity of a bi-alkali photocathode is found. This flux is consistent with the expectation from just the $^{40}\mathrm{K}$ decays.
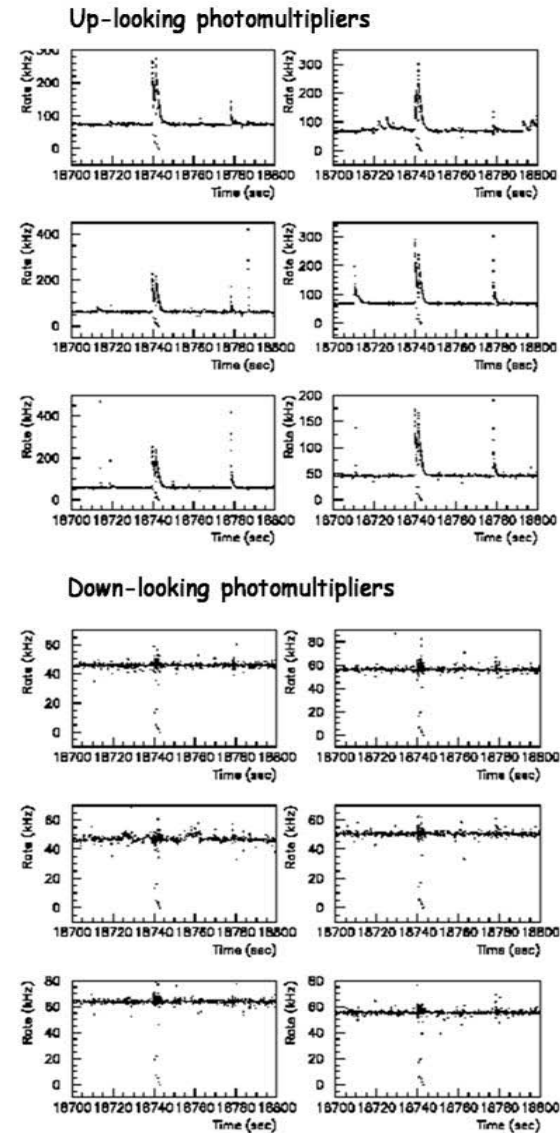
Figure 6-9: Count rates of the 12 photomultipliers of the NESTOR floor; bioluminescence bursts are clearly seen.

Also in the Pylos area the optical noise has been measured on several occasions and with different devices. A number of free-drop experiments have been performed since 1996, at a depth of 4000 m,

with an apparatus composed of two optical modules. The NESTOR floor deployed in 2003 and described in Section 5.3 was also used to study the optical background [89]. A data sample of 100 s duration is shown in Figure 6-9 [103]. From the analysis of the full data sample it is concluded that bioluminescence occurs during 1.1% ± 0.1% of the time.

6.2 Deep-Sea Currents

Deep sea currents were monitored at the three sites for long time periods.

At the Toulon site measurements were performed during the exploratory phase using autonomous mooring lines. Since the deployment and the connection to the shore of the instrumentation line (2005), the measurements are continuously performed in real-time.

As an example the plot in Figure 6-10 illustrates the time dependence of the current velocity and direction during August 2006.

Measurements of deep-sea currents in the region of Capo Passero have been performed with current-meter moorings. Current intensity and direction have been monitored almost continuously since 1998, in a range up to 500 meters above the seabed.

A complete analysis of the current meter data for the period July 1998 – December 1999 has been reported [104]. This analysis shows no significant depth dependence of the deep sea currents. Measured currents were stable both in direction

and intensity with an average value of about 3 cm/s and peaks not exceeding 12 cm/s. These results were confirmed by the analysis of data from the period August 1999 – August 2002.
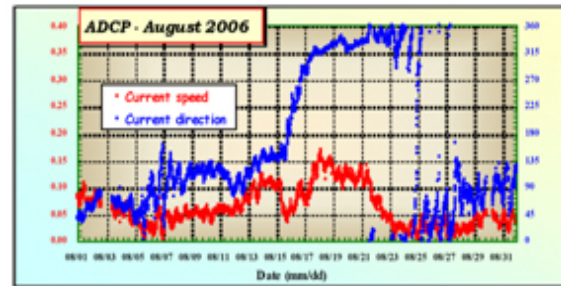
Figure 6-10: Current velocity and direction measured with an acoustic Doppler current profiler at the Toulon site.

At the Pylos site the deep-sea currents have been monitored since 1989 with different moorings and current-meters [105,85].The deep currents have low velocities that rarely exceed 6 cm s^{-1}. In general, as shown in Figure 6-11, the flow at the Pylos site of 4500 m depth is northward and 90% of the time is below 4 cm s^{-1}, and at the 5200 m deep site is southward but substantially weaker, with 95% of the time the current speed being below the measurement threshold.

6.3 Sedimentation

The rate of sedimentation at three areas has been obtained from sediment traps deployed at the sites in different years. The highest mass flux during the
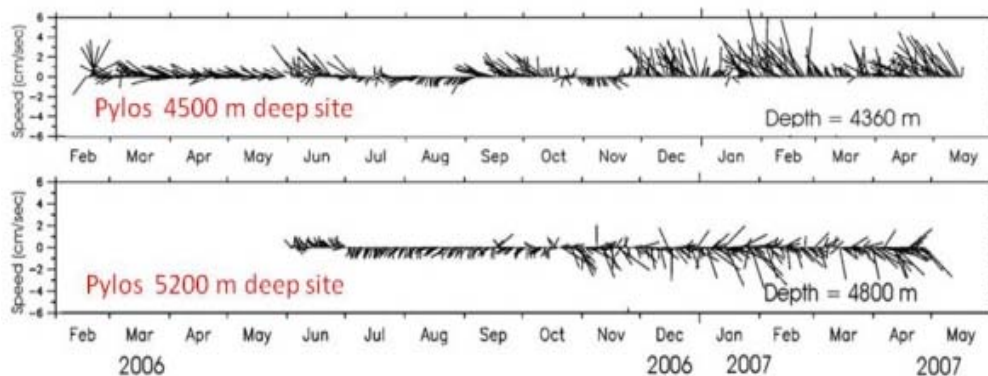
Figure 6-11: Sea water current measurements in the Pylos area. Measurements have been taken every 8 hours, north is towards the top.

late winter and spring were recorded at the Capo Passero site [**99**], and the Toulon site [**75**] showed the highest mass flux values during the autumn and early winter period (see Figure 6-12).
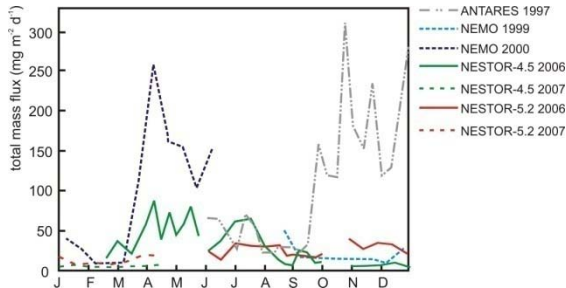
Figure 6-12: Downward total mass fluxes from the three areas.

6.4 Ongoing Measurements

The following are examples of instruments that will be used to provide additional useful information.

Figure 6-13: LIMS glass housing and mechanics.

Sedimentation Measuring System

A systematic research on sedimentation on optical modules is being carried out in the Pylos site. A dedicated apparatus named LIMS [**106**] (Light Intensity Measuring System) has been developed.

The resulting data will be analysed to study the correlation of the surface transparency of optical modules with underwater currents.

Mechanically, LIMS consists of a glass sphere, 50 cm in diameter, inside a steel construction (Figure 6-13). The electronics, several light sensors in designated positions and a power pack are located inside the sphere. Two LED light sources are located outside the glass sphere.

Radioactivity Probe

Direct information on the ^{40}K concentration may help in understanding temporal variations of the optical background. The activity of ^{40}K in the Mediterranean Sea is generally assumed to be 13 Bq/l.

A measurement of the actual activity, if different from the expected one, can help to explain variations of the background light.

Figure 6-14: Probe for ^{40}K monitoring.

For this reason a probe capable of measuring the spectrum of γ-rays from radioactive decays in deep-sea water has been developed. The sensor, which uses a NaI(Tl) crystal, can be used to measure the concentration of the various radio-nuclides occurring in sea water. The instrument was completed in October 2007 (Figure 6-14).

Biofouling

A solid structure in a pellagic environment such as a neutrino telescope will be subject to biofilm formation (biofouling). Biofilms are aggregates of bacteria encased in a structured polysaccharide matrix that they synthesize. The resulting film can lead to degradation of the transparency of the surface of the optical modules, and in the case of the
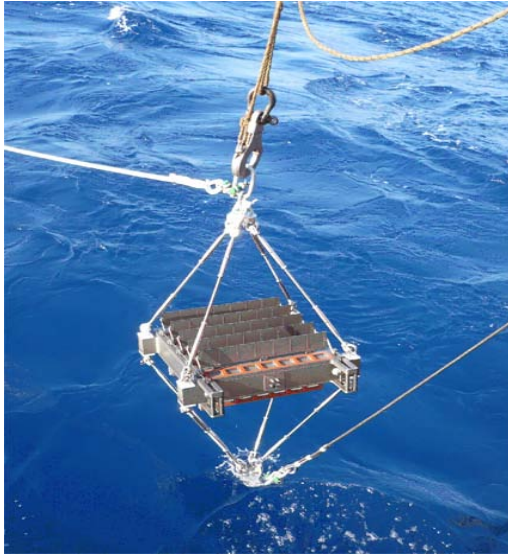
Figure 6-15: Biofouling measurement device during deployment.

Three sites suitable for installation of the neutrino telescope have been identified in the Mediterranean Sea. Extensive measurements of environmental properties, such as water transparency and background light conditions, have been performed at these sites. These activities are continuing in the framework of the KM3NeT project and will provide input for the site decision process.

presence of bioluminescent bacteria in the film to additional optical noise.

The formation of biofilms has been studied. The ongoing research at the Pylos location is concentrating on the metabolic activity of bioluminescent bacteria in the water column, and on the influence of various materials on the settlement of bacteria colonies and biofouling. A new instrument has been developed by the Kiel group in cooperation with GKSS Research Centre Geesthacht and is shown in Figure 6-15. It provides surfaces for bacterial growth and has a protective mechanism that prevents wash-off during retrieval. Such devices have been deployed at various depths from 1500 m to 4500 m, carrying sample surfaces of aluminium, titanium, glass, limestone and shale in two orientations (facing up and sideways). The biological film has been studied with scanning electron microscopy for samples exposed for 155 days in 2007. Further deployments will be performed in April 2008.

7 TECHNICAL IMPLEMENTATION

The technical implementation of the KM3NeT neutrino telescope, the optical module system, the mechanical structures connecting these elements in vertical assemblies, the seafloor infrastructure connecting the vertical structures to the shore, the readout system and the shore infrastructure will be reviewed. Deployment strategies will be discussed and the calibration needs of the neutrino telescope summarised. Finally, the implementation of associated science nodes is addressed.

7.1 OPTICAL MODULES

This section first describes the solutions adopted in the pilot projects. After identification of the potential areas where a significant improvement in the sensor performance can be obtained, some proposed technical solutions are presented.

7.1.1 Pilot Project Solutions

The three pilot projects have adopted a similar approach to their optical module. The photon sensor is housed in a glass sphere which is resistant to high hydrostatic pressures, is transparent to photons in the wavelength range 350-500 nm and is equipped with watertight and pressure-resistant connectors. All pilot projects chose spheres with a diameter of 42 cm.

The photon sensors selected by the three projects are large-area hemispherical photomultipliers with a bi-alkali sensitive area greater than 500 cm^2. The photon sensors have a quantum-efficiency of around 20% at 420 nm, a single photoelectron resolution of around 30%, good linearity, a transit time spread of approximately 3 ns (FWHM) and a dark count rate of less than 10 kHz with a threshold set at 30% of the most probable pulse-height corresponding to single photon signals (spe).

The photomultipliers are coupled to the glass sphere with optically transparent gel. This gel has very good light transmission properties and a refractive index close to that of the sea water, the glass sphere and the photomultiplier's glass window. It is also sufficiently elastic to absorb shocks

and vibrations during transport and deployment, as well as the deformation of the glass sphere under pressure.

The terrestrial magnetic field affects the trajectories of the electrons in the photomultiplier, especially between the photocathode and the first dynode. This effect, which can cause deterioration of performance, has been reduced by shielding the photomultiplier tube with a wire cage made of μ-metal, a nickel-iron alloy with very high magnetic permeability. The shape and the size of this cage have been designed to minimise shadowing effects on the photocathode (2%). A schematic drawing of the ANTARES solution [73] is given in Figure 7-1.

In all the pilot project experiments an external container is used to house the electronics that provides the charge integration of the signal and the communications with the shore. In addition it contains control electronics for the setting of high voltage and thresholds.
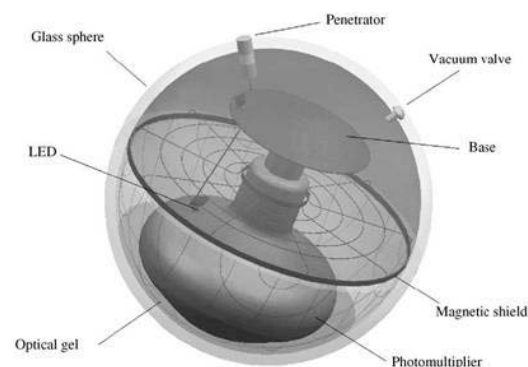
Figure 7-1: Schematic view of the standard optical module and its components.

7.1.2 Proposed Concepts

The design discussed in the previous section has proved to work effectively in the three pilot projects; however, thanks to recent technological developments, new solutions could be pursued in order to meet the following objectives:

- reduction of background due to bioluminescence and ^{40}K decay by excellent separation of single hits from multiple hits;

- ease of manufacturing and deployment;
- increased cost effectiveness.

Some designs take the approach that the pilot project optical modules are the correct solution but eliminate the external electronics housing, by placing the electronics inside the glass pressure vessel together with the photomultiplier tube. In the following other possible solutions are illustrated, starting with the approach that is most similar to the pilot project modules.

Direction-Sensitive Optical Module

It is possible to add the information of the direction of the detected Cherenkov light by replacing the standard hemispherical photomultiplier with a segmented one together with a mirror system. The check of geometrical compatibility between the reconstructed trajectory and the direction of the detected light allows for reduction of the background and therefore leads to improvement of the muon trajectory reconstruction, particularly for events with a small numbers of hits. The working principle is summarised in Figure 7-2 where it is shown how the mirrors focus the plane wave onto a single sector of the segmented photomultiplier.

Prototypes of 10 inch photomultipliers with 4-fold segmented anode have been recently manufactured. The realisation of the direction-sensitive
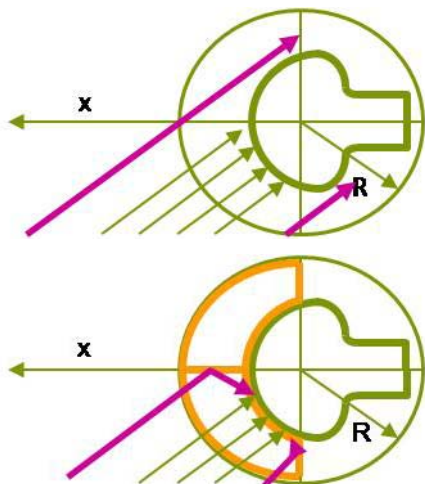
Figure 7-2: Behaviour of the standard optical module: the Cherenkov light illuminates the whole photocathode surface (top). The mirrors concentrate the light on a single sector of the photocathode surface (bottom).

optical module requires the re-arrangement of the components inside the glass sphere in order to accommodate the mirror system as shown in Figure 7-3. In addition it is necessary to provide a HV supply capable of powering the four dynode chains. The readout electronics is required to retain the information of the active sector of the photocathode. This can be achieved in one of the following ways:

- the phototube can be treated as four independent smaller photomultipliers;
- the four anode signals can be separately discriminated to identify the active sector(s) and added together to provide a single linear output.
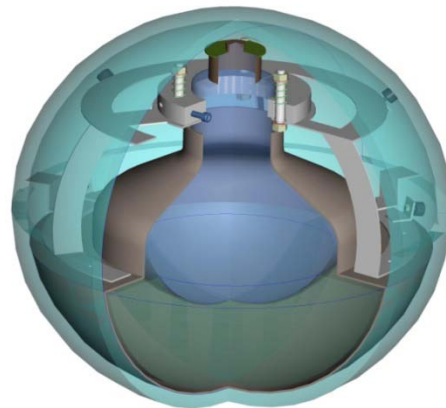
Figure 7-3: Schematic view of the direction-sensitive optical module and its components.

The direction in which the optical module is pointing must be continuously monitored.

Several Large Photomultipliers

One solution under evaluation is to fit more than one hemispherical photomultiplier into a glass sphere, if necessary with a diameter larger than the standard 42 cm. In particular a sphere with a diameter of 64 cm could contain three 10 inch photomultipliers of the type used in ANTARES. For connection purposes the two glass hemispheres can be suspended with a metallic ring which can also serve as part of a heat sink for internal electronics.

Many Small Photomultipliers

A cost effective way of maximising photocathode area inside an optical module might be through the use of many small 3 inch or 3.5 inch phototubes. The installation of up to 30 such tubes is envisaged. This approach gives several advantages which can be summarised as follows:

- The photocathode surface of 30 3 inch photomultipliers is 15% larger than the effective photocathode surface of three 10 inch photomultipliers.

- Based on the surface relations, a sea background of 5 to 10 kHz can be expected in a 3 inch photomultiplier. The reduced background per photomultiplier decreases its total integrated charge over the detector lifetime, resulting in a more stable gain as the photomultiplier ages.

- These photomultipliers are insensitive to the Earth's magnetic field and do not require μ-metal shielding.

- The candidate photomultiplier tube is available with enhanced quantum efficiency (30% at 400nm). Recent developments have shown that an efficiency of up to 55% is feasible for similar cost. This high quantum efficiency is combined with almost perfect electron collection, increasing the viewing range substantially.

- The segmentation of the detection area in the OM will aid in distinguishing single-photon from multi-photon hits. The Cherenkov light signal from a traversing muon produces light from a single direction with a significant probability of more than one photon arriving simultaneously. With the multi-photomultiplier OM two-photon hits can be unambiguously recognised if the two photons hit separate tubes which should occur in 85% of all cases. In addition adjacent tubes can be selected to increase signal to noise since signal comes from a single direction, whereas background is randomly distributed. This yields a low background rate of about 120 Hz per OM.

- High efficiency for downward-going muons reduces their misidentification. It also increases the sensitivity to Bremsstrahlung showers, which can potentially improve energy reconstruction.

- The reliability of the optical module is high, since failure of a single photomultiplier will minimally degrade the performance of the OM. Failure rates of small photomultipliers have been determined to be less than 10^{-4} per year.

Having increased the number of phototubes by a factor of 30 or more it is clear that great care must be taken to manage the readout system such that this increase does not result in a very expensive system. Two possible systems have been designed based upon measurement of time-over-threshold for each phototube, giving a logarithmic representation of amplitude (see Section 7.2.1). While time-over-threshold is imprecise at low pulse heights, small numbers of photoelectrons can be interpreted from the number of hit photomultipliers.

A maximum of 40 3 inch photomultipliers can be fitted inside a 42 cm sphere [107]. In a prototype (Figure 7-4) the photomultipliers are suspended in Styrofoam to allow for the compression of the sphere under high pressure. The present phototubes being tested have a flat entrance window. This is coupled to the inside of the glass sphere with a RTV-silicon "contact lens" (maximum thickness of 5mm). The contact lens simplifies the assembly procedure. A photomultiplier tube with a glass window matching the curvature of the sphere is being investigated, which would be connected to the glass using optical adhesive.

The dense packing constrains the space available for power supply and readout. A customised 100mW active base, providing high-voltage generation and integrated readout, has been developed (Figure 7-5). Suitably placed heat sinks and natural convection are sufficient to restrict temperature rises to 12°C above the ambient sea water.

Figure 7-4: 20 3-inch photomultipliers in their Styrofoam support.

Figure 7-5: The HV supply attached to each of the photomultiplier tubes. The cables are mainly for testing purposes.

The selection of the photomultiplier type will be based on the optimal size from simulation and measurements of:

- dark noise (< 1 kHz or <20% ^{40}K noise);
- timing properties (< 1 ns (σ) transit time spread);
- peak-to-valley ratio (> 3.2);
- cathode homogeneity (better than 5%).

The numbers in brackets indicate the values achieved with the Photonis XP53X2 photomultiplier.

A promising candidate might be a convex 3.5 inch tube equipped with a new high quantum efficiency photocathode (see Section 7.1.3). Simulations have to be performed to find the optimal layout of the tubes. From limitations imposed by sedimentation, blinding and the provision of penetrators for cable connection, the coverage will probably extend up

to 45° from the vertical. The choice of configuration will be governed by the best physics performance, taking into account the cost of the system, the power dissipation in the sphere and manageability of the manufacturing process.

The layout must be optimised to ensure the required full neutrino acceptance to 10° above the horizon.

X-HPD–based Optical Module

KM3NeT is investigating optical modules based on hybrid photon detectors (X-HPD) using a large-area spherical photocathode. High-energy photoelectrons from this cathode bombard a scintillating crystal target viewed by a small photomultiplier or equivalent. These devices promise larger solid angle coverage than conventional 'hemispheric' photomultipliers and greater electrostatic collection efficiency for photoelectrons, without the need for μ-metal screening against the Earth's magnetic field. These devices also have multi-photon capability in the same device, coupled with an effective gain in quantum efficiency.

The X-HPD concept was first proposed by Flyckt and Van Aller [108,109] for the Dumand project [110]. Philips produced around 30 examples of 38 cm spherical format (Philips XP2600, also called the Smart-tube). The tubes fitted inside standard 42 cm pressure spheres. Development stopped with the cancellation of Dumand in 1993.

The X-HPD idea was not lost, however. Several Smart-tubes had been installed in the Lake Baikal underwater neutrino telescope, and development was continued by the Baikal collaboration, culminating in the 'Quasar 370' X-HPD [111] (Figure 7-6), of which around 200 have been operated in the Baikal experiment since 1996.

The X-HPD concept was recently re-evaluated for the proposed 'CERN to Golfo di Taranto' neutrino oscillation experiment [112]. Prototype tubes in a new spherical geometry were developed by CERN and Photonis [113].

Although the experiment was not approved for funding, co-development of improved geometry X-HPD has continued under a joint agreement be-
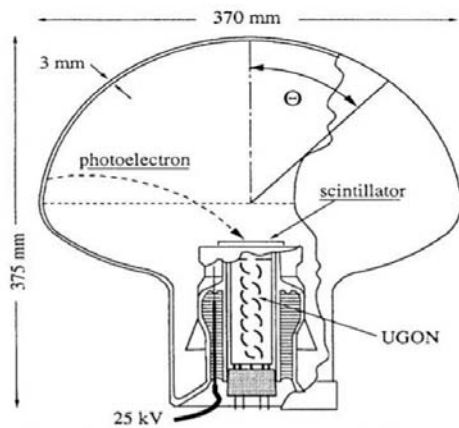
Figure 7-6: The Baikal Quasar 370 X-HPD tube, with a scintillator read out by a small photomultiplier.

Figure 7-7: Multi-photon separation in a Baikal Quasar 370 X-HPD tube.

tween CERN and Photonis and also within the context of the IN2P3-Photonis ´Groupement d'Interêt Scientifique´.

In these hybrid devices a photon is converted to an electron in a photocathode as in a normal photomultiplier tube. The produced photoelectron is accelerated not to the first of several multiplying dynodes, as in a photomultiplier, but to a crystal scintillator located at the centre of the device. The accelerating voltage of 25 to 30 kV is much higher than in a conventional photomultiplier. The crystal produces scintillation light of which 20-50 photons are detected by a small conventional phototube. Figure 7-6 shows a schematic drawing of such a device, the Baikal Quasar 370. The advantage of the large photon amplification provided by the scintillating crystal is seen in Figure 7-7, where the pulse height distribution shows well separated peaks due to single and multiple initial photons. Due to the relatively radial motion of the accelerated electrons the spread in path length and therefore the transit time spread is small at around 2 ns (RMS).

Full Spherical-Geometry X-HPD

Although the Philips X2600 and the Quasar 370 were the first X-HPDs, neither of them fully exploited the potential of a spherical envelope, through their use of disk-geometry scintillators.

Considerable improvements in performance are possible with a truly spherical geometry. Figure 7-8

shows such a device [113]. The 8 inch spherical dome has a bi-alkali photocathode. A 20-25 kV electric potential accelerates photoelectrons to an aluminium-coated cylindrical (12 mm diameter, 18 mm tall) scintillator situated at the exact geometrical centre of the dome. A future scintillator may be a less expensive phosphor-coated glass structure.

The concentric spherical geometry assures radial trajectories for the drifting photoelectrons, improving the transit time resolution, and giving almost 100% photoelectron detection efficiency over polar angles to 120° (conventional 'hemispherical' photomultipliers cover 55° at best). The spherical photocathode also gives an improvement in effective quantum efficiency, since double interactions with the photocathode are possible. The quantum efficiency measured at Photonis in a previous prototype reached 50% in the region where double interaction takes place [113]. Average quantum efficiencies greater than 33% are possible with a standard bi-alkali photocathode.

The spherical format X-HPD will be developed further in the CERN-Photonis collaboration and under the IN2P3-Photonis agreement. Target dates for the production of prototypes are indicated below:

2008: fabrication and test of prototype 20 cm tubes with metal anode;

Figure 7-8: Spherical geometry X-HPD prototype, with an 8 inch diameter (CERN-Photonis collaboration).

2009: fabrication and test of prototype 20 cm X-HPD tubes with crystal anodes in different scintillator types;

2010: fabrication and test of a prototype 38 cm X-HPD with best crystal anode.

7.1.3 Super Photocathode

Classical photocathodes are limited in quantum efficiency to around 25%. Both Hamamatsu and Photonis have recently developed new ´super´ photocathodes with quantum efficiencies in the range of 35-50% (Figure 7-9 and Figure 7-10). Presently 3 inch phototubes with these super photocathodes have been successfully manufactured. Such an increase in quantum efficiency would greatly enhance the detection capabilities of the optical modules.

7.2 Information Technology

This section discusses concepts in acquisition, processing, distribution and storage of data of the KM3NeT deep-sea infrastructure. The main purpose of the readout system is the conversion of the analogue outputs of the photomultipliers into formatted data for off-line analysis. The deep-sea infrastructure will also contain a large number of instruments for various scientific research activities. The operation of these instruments will be incorporated in the general readout system of the infrastructure.
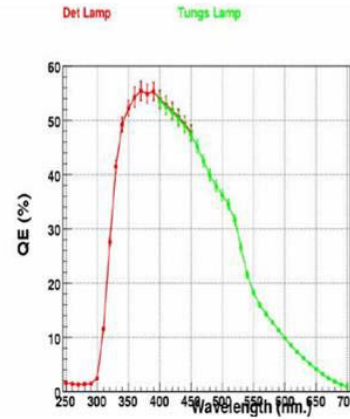
Figure 7-9: Measured photocathode quantum efficiency for the Photonis special bi-alkali photocathode.
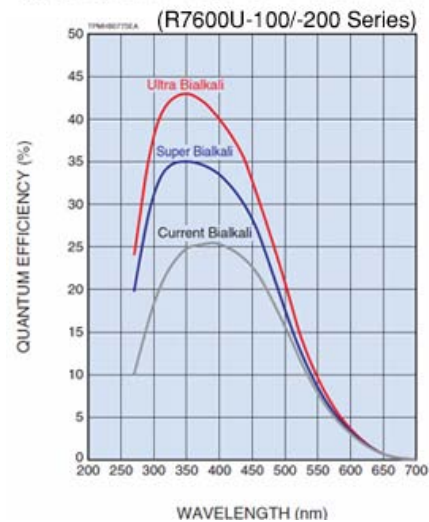
Figure 7-10: Measured photocathode quantum efficiency for the Hamamatsu Ultra and Super bi-alkali cathodes.

The preferred solution for the readout system for KM3NeT is one where all (digitised) data are sent to shore, where they are processed in real-time.

For a total effective photocathode area of $50 \, \mathrm{m^2}$ and 8 Bytes per recorded photon, a bandwidth up to about 0.1 Tb/s is required. This data rate to shore can be accommodated on a reasonable number of optical fibres using standard telecommunication protocols utilising either coarse or dense wavelength division multiplexing.

The total data rate exceeds that of any data storage capacity by several orders of magnitude. Hence, the raw data have to be filtered. The rare

neutrino (muon) signals can be discriminated from the random background utilising the time-position correlations produced by the traversing particle. The main challenge is this real-time filtering of the neutrino signal from the continuous random background. The effective volume of the neutrino telescope is to a high degree determined by the performance of the data filter, where the effective volume is defined as the volume of sea water in which a (muon) neutrino interaction with certain energy yields a detectable signal. To first approximation, a detectable signal is defined by a minimal number of time-position correlated photomultiplier hits (a hit is defined as a signal above a certain threshold, typically 0.3 spe). This is referred to as a "trigger". The trigger algorithm efficiency is typically defined with respect to the number of events that produce a minimum number of detected Cherenkov photons anywhere in the detector. The trigger should be optimised in terms of purity and efficiency.

For the trigger a relative time resolution of about 5 ns and a relative position resolution of about 2 m are required which are well above the final timing and positioning resolutions presented in Chapter 4. The timing is usually done by means of a designated clock system. The required timing accuracy should be achieved throughout a very large volume. Since the detector is subject to varying sea currents, the positions of the photomultipliers must be monitored continuously.

The overall readout system includes the submarine infrastructure, a shore station and various computing centres around Europe, together with external systems such as the gamma-ray burst coordination network (GCN). The architecture of the sub-marine infrastructure is mainly constrained by the seabed, the distance to the shore station and the depth of the site. The electrical power provided to the deep-sea installation is foreseen to be 50 kW at maximum. Assuming 10,000 optical modules, this corresponds to 5 W per optical module. The optical power budget depends on the length of the main cable and the number of branches. A shortage of optical power can be compensated by telecom-standard optical amplifiers (EDFA).

The shore station houses the main power supply, the data processing facility and a control room. The total data rate from the submarine infrastructure should be reduced by a factor 10000 to less than 10 Mb/s, to be able to transfer the data to the various computing centres in real-time and to store them on a permanent medium. Therefore, a high-bandwidth link of typically 100 Mb/s to the various European computing centres is required. Remote operation of the infrastructure is foreseen.

A high level of reliability of the deep-sea infrastructure is mandatory because of the high cost of off-shore repair and maintenance operations. Tools to enhance reliability are:

- reduction of the number of active components;
- large design margins;
- robust network topologies.

7.2.1 DAQ Model

The model for the data acquisition (DAQ) is based on a state machine. The possible states and the foreseen transitions are shown in Figure 8-12. The processes in the DAQ system can be considered as a set of concurrent state machines. The state transitions are caused by events that are generated by a human operator through the main user interface. The state machine logic and the control mechanism should be implemented using a generic framework that ensures the synchronisation of all DAQ components. A possible way to implement a state machine in software is based on the CHSM programming language.
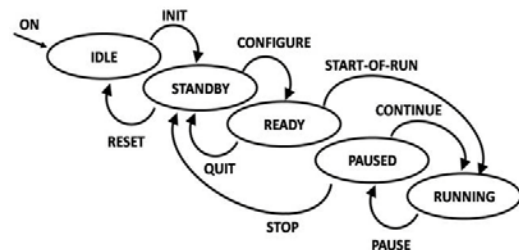
Figure 7-11: States and transitions of the DAQ system.

Photomultiplier Readout

The analogue signals produced by each photomultiplier have to be encoded by the front-end electronics in a way suitable for transmission to shore and subsequent processing. The encoding is aimed at extracting the relevant information from the analogue signal. The output of the front-end consists of "raw data" from which the relevant information can be extracted. A time stamping operation, which is described later, is necessary and can either be implemented after the transmission of data to shore, "on-shore", or "off-shore" in the front-end electronics. It is envisaged to implement the front-end electronics inside the optical module.

Front-End Implementation

Various options are possible for the implementation of the front-end electronics:

- analogue transmission;
- continuous sampling;
- self triggering.

The analogue transmission could be considered the ideal scenario, however for large distance to shore the original signal would deteriorate too severely and so this option will not be pursued.

The other options have in common that the analogue signal is converted to digital data. Continuous sampling is the option that aims at extracting as much information as possible from the analogue pulse. In general, this option requires the largest bandwidth. The required bandwidth is determined by the sampling frequency (typically 200 MHz) and the dynamic range of the analogue to digital converter (typically 8 bits) used to convert the instantaneous pulse height to a digital value. The data can be reduced by applying a zero-skipping mechanism. The traditional solution is based on a self-triggering system (e.g. a threshold crossing) in which the signal is time stamped using a time-to-digital converter (TDC) and the total charge is measured by an analogue-to-digital converter (ADC). The typical threshold is 0.3 spe.

A possible implementation of this concept could be an application specific integrated circuit (ASIC) as in the ANTARES experiment. The main functions that should be integrated in the design of this new device are pulse shape discrimination, timing, integration of the charge of the signals and analogue to digital conversion.

An alternative implementation could consist of using commercial ADCs and field programmable gate arrays (FPGA). Most of these incorporate data buffering for the efficient transfer of data.

The continuous sampling of a time-over-threshold signal is also under consideration because the design will require a small number of off-shore electronic components, thus minimising power consumption and maximising reliability. In this scheme, the leading and trailing edge of the signal above a certain threshold are time stamped. More information can be obtained by applying the same scheme at different threshold levels. This gives the same information as the continuous sampling solution.

Detection Unit Backbone and Data Transmission

The large distance to shore forces the use of single-mode optical fibres. The conversion of the electrical signals to optical signals can be implemented at different locations inside the detection unit. A possible solution is to convert the electrical signals immediately making each optical module an end-node in the fibre optic network. Wavelength multiplexing would be used to limit the number of fibres within a detection unit. In this, a purely optical network with star topology is made, based on passive optical multiplexers. An alternative solution could be based on a different star network consisting of an active switch with connections to the optical modules implemented as a copper link or fibre link physical layer.

Two data transmission schemes seem to be possible: (i) a synchronous protocol, which embeds clock signal and data transmission in the same stream, and (ii) an asynchronous protocol, which requires a separate clock distribution mechanism. In both cases, a clock signal that originates from an on-shore master clock is sent to the off-shore

front-end electronics. The front-end modules can then be synchronised. An alternative solution consists of transmitting the data to shore while retaining the time information. In that case, the time stamping can be done on shore.

For the on-shore trigger, the data need to be corrected for the phase offsets between the slave clocks of the different front-ends. Therefore, the synchronous protocol should have either a fixed (and known) latency or provide a way to measure the propagation delay of the on-shore to off-shore path. For the opposite direction, no requirements are necessary if the time stamping is implemented off-shore. However, to determine the propagation delay, the roundtrip time has to be measured somehow. The asynchronous protocol relies on a dedicated clock system which should be capable of calibrating the time offsets between modules.

A mixed solution between the two protocols could also be adopted, which remaps the asynchronous protocol onto a synchronous carrier in which clock and data are embedded. Again, the implementation should have a deterministic latency or provide a way to measure the propagation delay.

An alternative to the star network is based on so-called add-and-drop modules. Each storey adds (and drops, in the opposite direction) its payload to a backbone, which reaches all or a subset of the storeys in the detection unit.

Optical Network

The submarine optical network which connects the detection units to the main electro-optical cable should allow for a progressive enlargement of the apparatus through successive deployments of detection units. Such an assumption implies the use of submarine electro-optical connectors, at least up to the detection unit. The schematic view of the network is shown Figure 7-12.

Passive optical technology based on DWDM can be extensively applied to multiplex more wavelengths onto the same fibre and to avoid single point failures. The location where the conversion between optical domain and electrical domain takes place is subject to cost minimisation and system reliability.

If required, optical amplifiers could be used, both on- and off-shore, to provide sufficient optical power budget to reach the deep-sea infrastructure with an acceptable bit-error rate for the overall link.
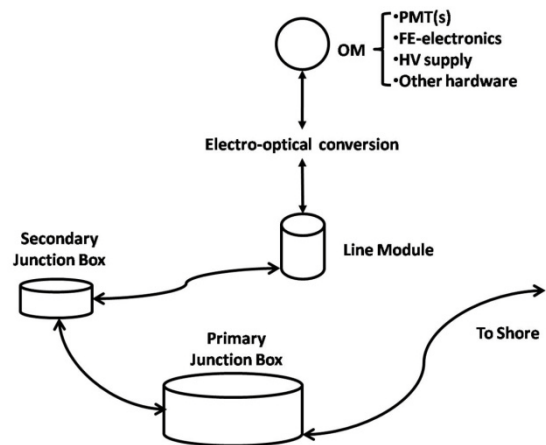
Figure 7-12: Schematic view of the data network.

Clock System

The main purpose of the clock system is to make the determination of the (arrival) time of a photon possible with the required accuracy regardless of the position of the photomultiplier in the detector. A possible solution is based on a master clock that provides a common clock signal to many slave clocks. The (relative) time offsets of the slave clocks can be determined by measuring the propagation delays of a designated calibration signal. This signal is distributed through the same clock system and returned by the slave clocks. These delays are measured on shore. The same clock system can be used to reset various time counters in the system at regular intervals. This provides a coarse but common time stamping of all signals. The master clock is linked to GPS to provide an absolute time. The accuracy of the absolute time is usually better than 1 μs.

The envisaged timing accuracy and the required bandwidths are compatible in the sense that the two systems could in principle be integrated, reducing the complexity and cost of the overall system. The integration of the two systems can be implemented in two different ways, namely in

software or hardware. The software implementation is based on a designated protocol. The hardware implementation requires a signal transmission system that retains time information at the required level of 1ns. Recent developments in fibre-optic technology have made the latter possible. As a result, most of the hardware can be moved to shore, maximising reliability and maintainability, while minimising cost.

Auxiliary and Calibration Instruments

There will be instruments to monitor the deep-sea environment and to calibrate the detector. For example, for the time calibration, optical beacons can be configured such that light flashes are produced at regular intervals. Given the number of optical beacons and the statistics required for the calibration, a flash frequency of 1 kHz should be sustained. The taking of these data will be organised in designated calibration runs. Because the detector is subject to varying sea currents, the positions of the photomultipliers must be monitored continuously while taking physics data. Depending on the chosen solution for the readout system of the photomultipliers, either the same system will be used for configuration and readout of these instruments or a designated readout system will be used and integrated with the readout system of the associated-science nodes.

This system will be based on a standard Ethernet network (100 Mb/s). Some instruments have an Ethernet port which can be integrated directly into this network. Other instruments make use of a serial bus (e.g. MODBUS) and rely on a specific protocol (RS485 or RS232). For these instruments, a custom made interface should be developed that communicates between the global Ethernet network and the local serial bus. A designated application should run on this interface to establish the communication.

7.2.2 Main Hardware Objects

Global Network

The whole readout system can be considered as an aggregate of active nodes over a global network, with these nodes situated either off-shore or on-

shore (see Figure 7-13). Due to present and foreseeable future state of IT technologies, it is reasonable to assume that the global network will be based on Ethernet and IP (v4 or v6). This does not preclude the existence of local networks behind some of the global network nodes, based on field busses, serial links and such.

Front End and Time Stamping Elements

The frontier of the readout system with actual Optical Modules will be the front-end elements in charge of the digitisation of the photomultiplier signals. Each front-end element will:

- process a cluster of n photomultipliers, where $n \geq 1$;
- include or be linked, through some synchronous connection, to one time stamping element.

Time stamping elements will time stamp every photomultiplier signal using the Clock System.

Acquisition Nodes

Every front-end or time stamping element pair is uniquely associated with an acquisition node in charge of:

- the primary formatting of the digitised and time stamped data;
- the asynchronous transmission of the data over the global network to the computing farm.

The network connectivity of the acquisition node could be either 100 Mb/s or 1000 Mb/s, or more, Ethernet.

Computing Farm

The CPU and network intensive activities of time-slice building and trigger processing will be achieved on a scalable computing farm made of a variable number of computing nodes interconnected with the global network through a high-performance switch or a set of cascaded switches.
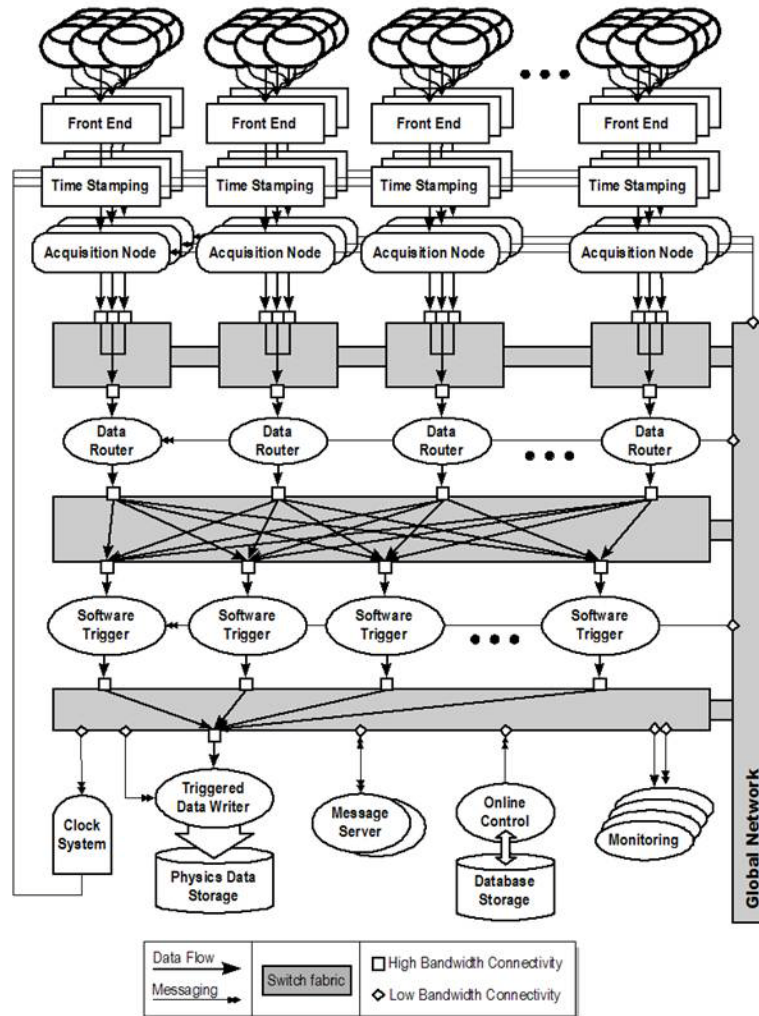
Figure 7-13: Schematic view of the overall DAQ architecture.

Storage Node

The data flow that is issued as the output of the trigger algorithm will be routed to a single node in charge of the physics data storage system. It will run the storing process.

Clock Control Node

One specialised node of the global network will be assigned to the control and operation of the clock system. This node will probably include specialised hardware such as GPS connectivity electronics. It will run the clock system process.

Readout Control Node

A unique standard node will be assigned to the overall control and operation of the whole KM3NeT detector. It will run the control and configuration process.

Monitoring Nodes

The monitoring nodes run the monitoring processes. Their number must be sufficient to accommodate the total computing power and display screens that are needed for all of them.

7.2.3 Main Core Processes

Acquisition Processes and Time-slice Builders

There is one acquisition process associated with every acquisition node. Whether this process is actually implemented in software or firmware is not determined, as it depends on architecture choices concerning the acquisition nodes. The major role of the acquisition process is to transfer the data in a proper binary format to their associated time-slice builders over the global network. Every

acquisition process is associated with a unique time-slice builder but there will probably be one time-slice builder for many acquisition processes: this cardinality is mainly determined by the ratio of the input bandwidth of the computing node on which the time-slice builder process is running and the output bandwidth of an acquisition node. It could be less than this ratio if the data processing capability of the time-slice builder is less than its input bandwidth.

Trigger Processes

Every time-slice builder routes the data it receives to a specific trigger process determined by the readout scheme (see further). Every trigger process is in charge of searching for possible physics events within the time-slice data it receives from time-slice builders. Whenever a candidate event is found by the trigger algorithm, the trigger process extracts all the data belonging to a configurable time window around the event and sends these to the data storing process for offline analysis. The time window can be different according to the event type: for instance, the time window around a typical neutrino event will be about 10 μs whereas a GRB event issued by a GRB alert will cover many minutes. As such a big time window can put an abnormal instantaneous stress on the global network and the data-storing process, the actual data transfer between trigger processes and data-storing processes might resort to caching.

Data Storing

The data-storing process is probably unique and produces the files containing the data that have passed the trigger. It unequivocally associates the data files to their corresponding run ID, the run ID being itself issued by the control and configuration process. The data files are produced using a persistence framework adapted to massive data storage, such as Root IO.

Clock System

The clock system process is unique and is in charge of:

- configuring the hardware and software components that implement the global clock distribution of the experiment;
- broadcasting the precise signal of every "Start of Run" through dedicated hardware;
- determining the precise time of the "Start of Run" signal in order to guarantee the reconstruction of the full-precision absolute time stamp of all stored data.

Control and Configuration

The control and configuration process is unique and fulfils the following functions:

- interaction between human operators and the system through GUI elements for command and status display;
- retrieval of predefined configurations and run conditions from the database;
- storing of run conditions and actual configuration in the database;
- production of run number and its unique association with run conditions and configurations;
- management of the distributed state machine in the experiment.

Monitoring

Monitoring processes display in real-time the human readable status of the detector subsystems. Contrary to most other processes, they are not controlled by the control and configuration process and function independently from the actual state in which the detector subsystems are. There are as many monitoring processes as are deemed necessary by the experts in charge of the development of the different subsystems.

Utility Processes

Some additional processes will be necessary, such as:

- a system control message server;
- a monitoring message server;
- a database server;
- a boot server.

7.2.4 Readout Scheme

Time-slice Building

All the data produced by the acquisition processes are time stamped. The trigger algorithms executed in any trigger process eventually need a global view of all signals produced by all detecting nodes within a time span of the order of 10 μs. All the data belonging to the time span must be concentrated within one trigger process. As a consequence, the routing of the data to specific trigger processes depends on their time-stamp.

At the moment when the data is routed, time stamp values are smeared by values of the order of the time needed for signals to propagate between detection nodes (microseconds). Consequently, the time window used to regroup the data belonging to the same time span within a single trigger process must be orders of magnitude greater than the smearing in order to reduce edge effects to negligible values. A time-slice is then defined as a time span of data to be routed to a particular trigger process running on a particular computing node of the computing farm and its duration will be specified at least in milliseconds if not in tens of milliseconds.

This scheme will ensure the scalability of the computing farm: any performance limitation in processing the incoming data flow will be extendable in principle, by adding computing nodes and network ports to the system.

Farm Management Policies

The default routing algorithm dispatches time-slices using a simple round-robin scheme. However, in order to take into account differences in CPU performance between computing nodes, one might implement dynamic policies, in which case a farm manager process will be needed.

Readout State Machine

The operation of the detector as a whole follows a state machine that must be followed by all subsystems. The control and configuration process ensures the synchronisation between the state machines of all subsystems. The transitions between states correspond to specific phases of detector operation:

- **on:** switching on or activating subsystems;
- **init:** extracting configuration and run conditions from database and dispatching these to all subsystems;
- **configure:** configuring all subsystems with dispatched configuration data; all subsystems are set to a state where they are sensitive to the precise "start" hardware signal;
- **start-of-run:** run ID is computed by the control and configuration process; hardware "start" signal is issued; acquisition nodes open the data flow over the global network.

7.2.5 Database Organisation Principles

Relational Database and Persistence Layer

It is foreseen to use a relational database for the management of hardware descriptions, configurations and run conditions and their association with stored physics data. Access to the database by any process must be done through a software persistence layer. The libraries implementing this persistence layer must therefore exist in all languages used for programmes that need to access the database, such as web access, GUIs and the control and configuration process.

Hardware Descriptions, Partitions, Logical Configurations

The database will include:

- the description of the hardware setup of the detector but also of all hardware setups of the different test benches run at different geographical sites;
- the description, for each hardware setup, of the associated logical configurations and run conditions; logical configurations ultimately specify the parameters used to initialise all hardware and software components within subsystems;

- logical configurations may include the description "partitions", i.e. subsets of the hardware setup to be actually used during specific runs.

The retrieval and storage of logical configurations should be done only by the control and configuration process which in turn broadcasts it to all subsystems. It is conceivable that monitoring processes access the database to retrieve hardware description and configuration for their own purposes.

Run Specification

The control and configuration process issues a unique ID for each run. This ID is a combination of a hardware description reference and a run number. It is stored in a unique row of a unique database table together with:

- the reference to every configuration used for the run;
- the precise GPS time of the run.

Permissions: Architect, Expert, Shifter, Scientist

Database access permissions should be different for different functions:

- an administrator has the right to create schemes, bases and users;
- an architect has the right to make structural modifications;
- an expert has the right to insert new configurations or hardware descriptions;
- a shifter has the right to insert new runs, referencing configurations and hardware descriptions already created by an expert;
- a scientist has the right only to read data from the database.

7.2.6 On-Shore Data Acquisition and Processing System

Overview and Requirements

The on-shore data processing system must handle all data arriving from the optical modules and the auxiliary instruments.

The key parameters for any DAQ system are the event rates and event sizes, and since these differ for optical modules and the various instruments, we propose two physically separate acquisition and processing systems on-shore for the optical modules and auxiliary instruments. The concepts described here apply to both.

The large number of Optical Modules (~10000) times the singles rate for each Optical Module (~100 kHz) times the number of bytes per Optical Module hit renders a strategy based on direct archival storage unfeasible.

Conceptual Structure Overview

It is envisaged that all data from the optical modules arriving on-shore will be stored in a buffer system to allow selection strategies (trigger algorithms) to examine the data of the whole telescope for a specific snapshot in time, or time slice. Triggering on a snapshot of the whole telescope on-shore is reasonable and, since the type of information is the same for each optical module, it permits the use of sophisticated triggering algorithms, which are adaptable to any actual detector geometry. In this scheme the actual processing of a continuous stream of time slices for the whole detector data requires about 1000 present day CPUs.
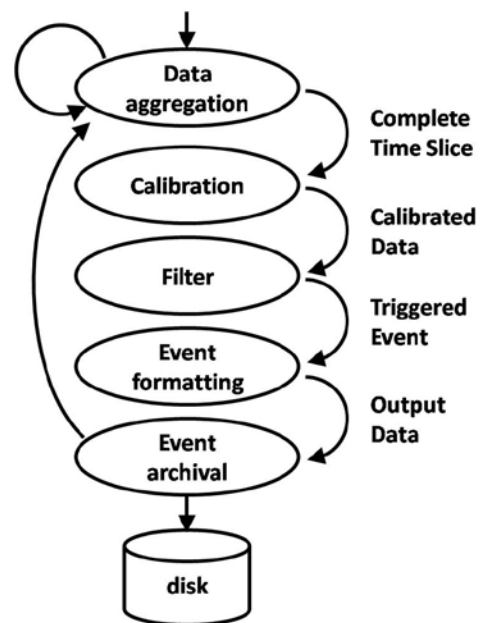
Figure 7-14: Functional block diagram of the trigger process.

The general concept entails the following tasks (illustrated in Figure 7-14):

- aggregation of time slices of all detector data on-shore;
- filtering of the data in the time slices to build events;
- archival and final storage of events.

Aggregation

The aggregation refers to the coalescence of a fixed number of consecutive time slices from each optical module into the buffer of a processing node on-shore. The next time slice will be assigned to the buffer of another processor node and so forth. This ensures continuous and dead-time-less read-out. Operationally, the allocation of time slices to processor nodes could be realised in a simple scheme, such as round-robin. We propose to maintain a degree of flexibility to allow for other allocation schemes, such as least-loaded, to make optimal use of buffering and processing resources. To first order the size of such a buffer depends on the number of Optical Modules and the amount of data making up a time slice. The length of the time slice can vary and is envisaged in the range 10-100 ms, and is related to the time it takes for a muon to traverse the detector.

Data Filtering

At the data filter stage, pattern recognition algorithms, based on space-time relationships acting on the snapshot of the data of the whole detector, must reduce the background rates by a factor of 10^4 to 10^5. The process involves calibration and using local and extended clusters in the detector, followed by event building.

Event Building

When the data pass the triggering criteria an event is built from all information from all optical modules in a time window around the hits causing the trigger. An event therefore contains:

- a list of clusters which made up the triggers (these are the events);

- a snapshot (optional) of the raw data of the whole detector in a pre-defined time window around the event.

7.2.7 Components Overview

Switch Fabric

On shore the switch fabric maps to the functional task of aggregation. The main purpose of the on-shore switch fabric is to route the data sent by the optical modules to the processing nodes. It must handle continuous data rates of about 100 Gb/s. An implementation for routing the data could be realised with IP addressing of the Ethernet protocol (level 2). The size of the switching fabric is then of the order of several hundred ports. The fabric does not need to be a monolithic component, but can be realised as a layered structure of switches which route the data to the buffers of processing nodes.

Data Filter Farm

The data filter farm maps to the functional task of data filtering. Since the data from the detector is organised as a series of snapshots of the whole detector, identical processing of each snapshot can be implemented on a farm of identical processing nodes. The processing power for performing the tasks of calibrating, triggering and event building can be realised with a farm of several hundred PCs, each with a processor speed of a few GHz.

The performance of the processor nodes and their data filter tasks are critical. To ensure prioritised task scheduling and deterministic task execution time lines, the nodes should run a real-time specific OS to make best use of the resources employed.

In an implementation scenario where server-like PCs are used as processor nodes, the buffer (RAM) keeping the data while processing it, can have a size of several GB, accommodating the data of a detector time slice. In fact it should be large enough to allow for contingency to queue several time slices of the whole detector for processing in the same processor node.

Local processor nodes will have a disk storage capacity sufficient to store the full raw data for about twenty minutes in case of special event triggers.

Archival Data Base

On the shore site temporary storage with a volume adequate for several weeks of data taking is envisaged. For permanent and final archiving, the data will be stored in European mass storage centres. It should be noted, that this concept applies equally to the event data, calibration data, and data from auxiliary instruments deployed for the associated sciences. A unified structured organisation of the data can be realised, employing a database system that handles the links and relationships between data. Controlled access to the database ensures prioritised read and write access for updating processes, user interfaces, GUIs, and analysis programmes.

Data Distribution

To provide rapid world-wide access of the data, it is planned to employ high bandwidth (1-10Gb/s) data link infrastructures (like the GRID) throughout Europe and distribute the data to any European computer centre in quasi real-time.

7.3 Mechanics

In this section the mechanical structure of the basic deployed detection unit will be described. First an analysis of the major substructures is presented and an attempt is made to identify critical areas of reliability, ease of manufacture and ease of transport and deployment. This must of course be combined with a cost optimisation. After identification of these issues, some proposed technical solutions are presented. The interfacing to the seabed infrastructure and to the readout is discussed in terms of identified boundary conditions for the design of both.

Many thousands of optical modules are likely to be required. These will be integrated into a few hundred detection units.

The principle constraints are construction time, costs and reliability.

Timescale and Construction

The timescale for production is driven by several considerations:

- the lifetime of the neutrino telescope will be a minimum of 10 years. This means the first detection unit must survive for the building time plus ten years;
- the procurement availability of some critical technologies could be as short as 5 years.

This indicates a building time of the full detector of around 4 years. Taking into account the numbers required for a cubic kilometre neutrino telescope this translates to a production rate of 5 to 10 optical modules per day. The deployment and connection of the detection units must proceed at a pace of 1 to 5 per month – uninterrupted for four years. Whereas the production of optical modules can be done at several different sites or outsourced to industry, the deployment seems to pose the tightest restriction on the timescale of the project. The mechanical structure of the detection units must therefore allow for rapid deployment: a ready-to-deploy concept. The fact that several construction and assembly sites may be used and that almost no handling at the quayside will be possible implies that the full detection unit must be easily transportable. This implies for instance that it must fit into standard 20 or 40 foot transport containers.

Cost

The cost analysis of the pilot projects shows that a relatively large fraction of the cost of the detection unit is represented by the cabling system and its connectivity. In order to attain a cost reduction lessons learnt from the pilot projects will be taken into account.

A cost reduction may also be obtained by simplifying the detection unit recovery system and by minimising the number of in situ deep-sea connection operations.

Titanium as construction material has become extremely expensive. Investigations into other materials have already started in some of the pilot projects, focusing on the use of marine aluminium structures and composite materials.

The number of electronics containers and their interconnections should be minimised. If power consumption is reduced, the placement of electronics inside the OMs becomes feasible.

Deployment operations represent a major cost for the time taken for the deployment of the each detection unit and for the mobilisation, demobilisation and transit time of the vessel. The deployment of a cubic kilometre scale detector will probably require a new approach Operations can be optimised and cost minimised if several detection units are loaded on board and deployed during a single sea operation.

Reliability
The pilot projects have so far proved to be reliable although some teething problems have occurred. ANTARES has operated one of its detection units for over two years, one for 18 months and a further eight for more than six months. No serious mechanical problems have occurred. Nevertheless there are areas where the risk of failure could be reduced even further. Any penetration through the wall of pressure housings that must resist the underwater pressure represents a potential point of failure. Minimising the number of penetrations should thus enhance reliability. The effect on the detector as a whole, in case of a water intrusion, should be confined. Risk analysis is a high-priority task for any mechanical design.

7.3.1 Detection Unit Concepts

Extended Tower Structure
This design is based on a structure developed within the NESTOR project but has 6 arms with a length of 50 to 60 m. A pair of OMs is placed at the end of each arm and a pair is also placed in the centre of the star. Eight to twelve of these storeys are suspended vertically with 50 to 60 m spacing. Optionally more pairs of OMs can be placed along the arms. Storeys are deployed one at a time and connected to form a tower. Power and readout connections to the OMs are made via the centre of the storey, either with or without intermediate electronics, to a central vertical cable which transfers the data to a junction box at the foot of the

tower. Each tower is connected to a central junction box, probably through a deep-sea mateable connector. Signal transfer is by fibre-optics.

The extension of the NESTOR concept to arm lengths of about 50 m is being investigated (NESTOR used 8 or 16 m lengths). The deployment concept then requires arms, which are modular to simplify transport, to be joined easily on or in the vicinity of a surface deployment platform. This technique has been applied, using various profile designs for the modular arms, and has been found to be a viable solution.

Key concepts: Rigid horizontal and flexible vertical structure; separation of mechanical support and data and power transport; all connections are dry mateable, connectors or penetrators, except a single connection to a central junction box that will be deep-sea mateable.

Requirements: Large structural elements; large vessel; some "extra-vehicular" activity during deployment;

Compact Tower Structure
This design uses relatively compact transportable horizontal structures (length ≤ 12 m) similar to those developed in the NEMO project. Optical modules are attached to the rigid structure. After production the full detection unit, which is transported and deployed in a compact state, is unfurled on the seabed using the inherent buoyancy. Connection between rigid storeys is by ropes. Cabling for power and data transport is separated from the mechanical support.

Key concepts: Rigid horizontal and flexible vertical structure; separation of mechanical support and data and power transport; all connections are dry mateable, penetrators or connectors, except a single connection to a central junction box that will be deep-sea mateable; compact deployment with unfurling on the seabed; modular design adjustable to the required number of storeys.

Requirements: Structural elements; continuous position measurement**.**

String Structure

Storeys are very compact without specific electronics containers. The full structure is placed in a ready-to-deploy container. The footprint of the container should be of the order of 10 m^2 in order to facilitate handling on the vessel. For transport the container must be narrower than 2.4 m. The full detector unit is "rolled up" inside the container. At deployment it can be winched to the seabed or left to freefall, after which it is positioned with a submarine. The unit is unfolded on the seabed by raising the container while leaving the anchor on the seabed. Buoyancy of the storeys must be sufficient. Electro/optical/mechanical cable must be very flexible to allow for easy unfurling.

Key concepts: Compact horizontal structures containing few optical modules; size dictated by transport and handling; compact deployment with unfolding on the seabed; possible integration of mechanical and data and power transfer functions; completely modular.

Requirements: thin flexible cable; continuous position measurement; a single wet-mateable connector per string.

Cable Based Concept

Only a single optical module with very large total photo-cathode area is installed per storey. The mechanical function of the cable is separated from the electro-optical one. An equipressure oil-filled cable system (hose) is foreseen. Breakouts of fibre optic and electrical connections are in equipressure. Each breakout is terminated by a connector matching the corresponding optical module. The sphere is connected to the cable via a minimal structure. The mechanical part of the cable structure is continuous and contains two strands. Deployment is foreseen similar to string structure concept.

Key concepts: Single optical module per storey; compact deployment with unfolding on the seabed; completely flexible; equipressure breakout; equipressure fibre optic and electrical cable; easy integration through use of connectors; all electron-

ics in the optical module; separation of mechanical and electro-optical functions.

Requirements: thin flexible cable; continuous position measurement; a single wet mateable connector per string;

Concepts for Cable and Deployment

A possible solution for the cable in some of these concepts is to take the same electro-optical-mechanical cable as ANTARES, and make an equipressure breakout. Then the deployment could be ANTARES like (storey by storey from the surface).

Alternatively an oil filled hose with electro-optical links inside and reinforcing fibres outside can be used. Here also an ANTARES type deployment is possible.

7.3.2 Discussion

Four separate solutions for the mechanical structure have been discussed. Each of these designs has parts which are universal. For instance the need for modularisation makes all designs follow the connector to optical module, breakout from electro-optical cable and single wet-mateable connector design. Differences occur in the implementation: is the mechanical structure rigid, semi-rigid or flexible — how many optical modules are implemented per storey and per detection unit — is the electro-optical cable separated from the mechanical one — is the breakout in equipressure or not.

In Table 7-1 we summarise the key features of the different designs and explore to what extent the other designs are compatible, incompatible or provide an alternative.

In general the concepts are certainly to a large extent compatible. Some of the subsystems are interchangeable.

Clearly, all designs emphasise the following:

- minimise wet-mateable connections;
- easy integration through connectors;
- transportability;

Concept	1	2	3	4
Number OMs per detection unit	144	64	60	20(x3) 1)
Rigid tower				
Compact tower				
Flexible cable				
Connector at OM				
Atmospheric breakout				
Equipressure breakout				
Fibre optic readout				
Full unit transportable	2)			
Multi-photomultiplier Optical Module				
Single photomultiplier Optical Module				
Multi unit deployment	3)			

	Default solution
	Compatible solution
	Provides an alternative
	Is not compatible

1) The multi-photomultiplier option gives at least three times the cathode area of a single 10 inch photomultiplier.
2) The large structures are not compatible with no-intervention transportation, modular arms are required and assembly at surface is required.
3) The large tower is the equivalent of several cable or compact tower detector units.

Table 7-1: Compatibility of the key parts of concepts. Concept 1 is the extended tower, concept 2 is the compact tower, concept 3 is the string structure and concept 4 is the cable-based concept.

- transport and deployment of several units in a single sea operation.

The following R&D on mechanics is planned:

- verification of the cable concepts;
- hydrodynamic behaviour of the detection unit;
- accuracy and reliability of free-fall deployment of compact structures;
- seabed transportation of folded detection unit;
- electro-optical dry mateable connectors.

7.4 Deep-Sea and Shore Infrastructures

7.4.1 Deep-Sea Power and Data Network

The neutrino telescope will consist of around 10000 optical modules with a total power consumption of about 50 kW. The estimated bandwidth for the full data transport system is of the order of 100 Gb/s. For the associated sciences infrastructure the equivalent numbers are less well defined but estimated to be less than 10 kW and 100 Mb/s. The seafloor network will consist of a main electro-optical cable running from the shore to a main junction box in the deep sea and of a network of secondary junction boxes linked by electro-optical cables and connecting to the telescope detection units and the associated sciences nodes. The final design of the network is still under development and may incorporate redundancy to mitigate single point failures.

Cable Power Transmission Concepts

For undersea observatories, both AC and DC power systems are viable and have their particular advantages and disadvantages. For instance an AC power system allows for the use of transformers and efficient high-voltage transmission. Power interruption is simpler in an AC system than in a DC system. Furthermore, DC systems have insulation problems that have no counterpart in AC systems; long-term high-voltage DC excitation can cause eventual breakdown of solid insulation. Although DC is conventionally used on long-haul undersea telecommunication cables, AC alternatives are considered. At conventional AC frequencies (50 Hz) the shunt capacitance requires inductive compensation.

For a qualified decision, the power system must be evaluated taking into account the cables, transformers, DC/DC converters, rectifiers, the required voltage stability and the level of short circuit capability. Each item is likely to impact significantly the total price of the power transmission network. This section focuses on cable considerations only.

Considering the power required and the distances, over which it must be delivered, the use of high

voltage is unavoidable. The maximum voltage that can be applied to a cable is limited by insulation breakdown. A maximum of 10 kV is typical for undersea telecommunication cables and is considered as an upper limit.

The current-carrying capability depends on the conductor heating and the voltage drop. The resistance of a typical telecommunication cable is about 1 Ω/km so that over the distances typical for KM3NeT the current is limited to a few tens of Amperes.

Power can be delivered in the following ways:

- three-phase AC (multi-conductor cable);
- DC with cable current return (multi-conductor cable);
- DC with current return through the sea (conventional single conductor telecommunications cable);
- AC mono-phase with current return through the sea (conventional single conductor telecommunications cable).

Main Electro-Optical Backbone Cable

The design requirements for an ocean observatory site-to-shore cable are compatible with the standard capabilities of telecommunications cables, for which a wide range of industry-approved standard connection boxes, couplings and penetrators exist, which can be readily adapted to interface with scientific equipment. The low failure rate among the large number of such components in service suggests mean times between failures of several thousand years.

As standard, a submarine telecommunications cable has to provide a service life of at least 25 years. It must be easy to deploy and repair at sea. The longevity of the installed cable depends on minimising the strain induced on the optical fibres. The cable structure, which houses the optical fibres and electrical conductors, must survive both the rigors of installation (torsion, tension due to self-weight and ship movement) and the seabed conditions (high ambient pressure, abrasion risk, unsupported span, etc.).

The cost of developing and qualifying a submarine telecommunications cable is high and is normally amortised over many thousands of kilometres of cable. However, these development costs are historic and therefore non-recurring.

The cost of a submarine cable repair at sea is substantial. However, since 1999, under the Mediterranean Cable Maintenance Agreement (MECMA-2004) cable ships, fully equipped with ROVs, are maintained on constant readiness at Catania and La Seyne-sur-Mer. These ships provide repair services for subsea cables owned by member organisations (about 40 as of 2008). The insurance character of this agreement offers members a repair capability for an affordable yearly contribution in proportion to the relevant cable length. Two of the pilot projects are members of MECMA. The five major cable manufacturing companies have formed the Universal Jointing Consortium [114] which offers qualified and proven jointing techniques for a wide range of cable types ("Universal Joint" and "Universal Quick Joint"). MECMA ships support universal jointing.

Virtually all reported submarine cable failures are due to accidents, notably from fishing activity and anchor falls in shallow water, although natural chafing, abrasion and earthquakes in the deep ocean also occur as shown on Figure 7-15. To avoid these risks, careful route planning is essential, and burial is used where circumstances require it.

Submarine cable armouring is selected to be compatible with the specific route; therefore the cable mechanical characteristics are an integral component of the overall system design. Submarine telecommunications cables can be equipped with virtually any fibre type and any reasonable number of fibres. At present all the major cable manufacturers deliver telecommunications cables with a number of fibres that does not routinely exceed 24. This is mainly due to the advent of Dense Wavelength Division Multiplexing (DWDM) technology and to the requirements of simplifying the cable mechanics.

The fibre types used for submarine transmission are optimised for minimum attenuation over the
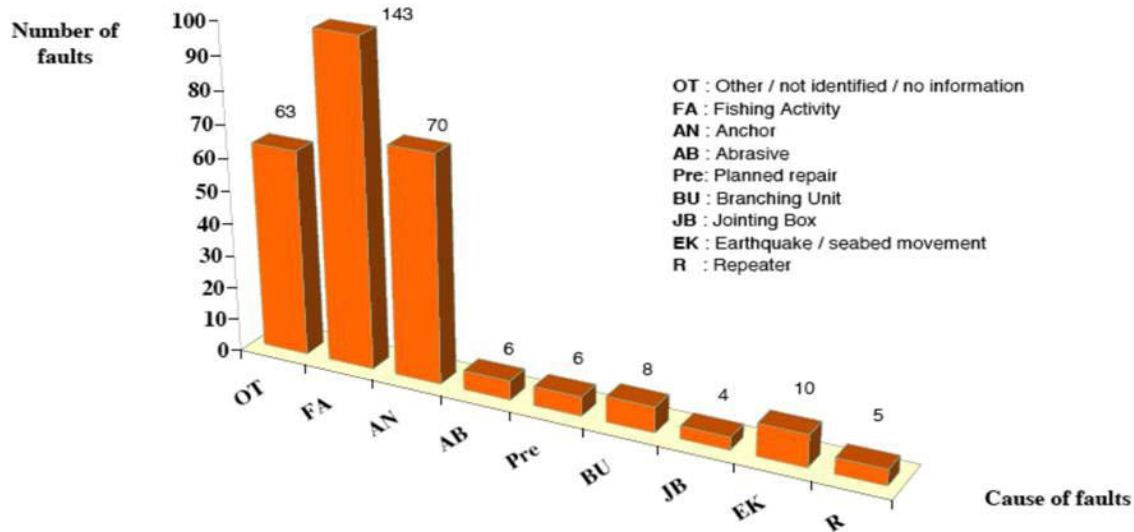
Figure 7-15: Causes of faults in deep-sea cables (source: MECMA).

full C-band (1530-1570 nm) with dispersion characteristics that depend on the application. The cable optical properties are an integral part of the optical communications system specification.

Electro-Optical Cables

Many types of submarine telecommunication cables are commercially available. The design varies depending on manufacturer, fibre count, power requirements, and the external protection. Figure 7-16 shows a range of mechanical configurations of telecommunications cables. The "double armour heavy" and "double armour light" cables are used in shallow water where the greatest level of protection is required. This is typically where the cable cannot be buried. The "single armour heavy" cables have a single layer of wires to protect the insulation, and are normally used to 1500 m water depth where full burial protection cannot be guaranteed. The "single armour light" cable has a single layer of smaller-diameter wires, and is normally used where a cable can be successfully protected by burial. This cable type is preferred for plough burial at installation depths of 2000 m or less. The "lightweight protected" cable incorporates a metallic tape to provide a certain degree of abrasion protection for the insulation. It can be deployed down to 7000 m and is often used in deep areas with high abrasion risk, such as slopes and high-

current environments. Finally, "lightweight" cable has a low weight per unit length and is used in deep water (deeper than 2500 m) installations where the seabed is flat and ambient currents are weak. The interface between a cable and the submerged infrastructure is complex. Not only must the connection provide load transfer through a mechanical discontinuity in the cable, but it must also maintain electrical insulation while supporting the safe connectivity of both optical fibres and electrical conductors. Any submerged component, such as a repeater, is connected to the cable through so-called extremity boxes, each effectively forming one half of a cable-to-cable joint.

Another cable type is the umbilical standard for data and power transfer from ship to instruments or devices placed temporarily on the seabed, such as ROVs.

7.4.2 Cable Design Examples

The design is likely to be driven by availability from telecommunications cable suppliers. In the following some presently available cable designs are discussed together with the different power options. These should be seen as examples of what is possible.

Figure 7-16: Different armouring on submarine cable.
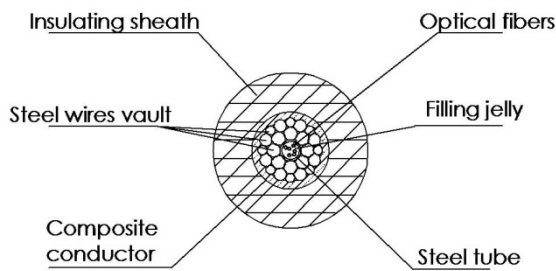
Figure 7-17: Example of monopolar sea cable.
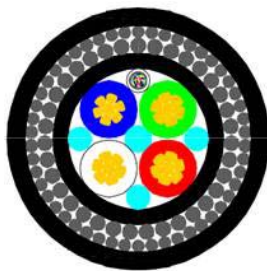
Figure 7-18: Bipolar cable, 4x35 mm^2.

Figure 7-19: Cable option for 3-Phase AC with 3x25 mm^2 conductors.

Monopolar Power Delivery

A monopolar system incorporates a current return via the sea water and will generally result in the smallest cable dimension and weight. Due to the extremely small resistance in the sea return this system has low power losses. Cables usable for this system are in fact the most commonly used in the telecommunications industry. To allow for the current return via the sea this system must incorporate sea electrodes both at the shore and in the deep sea. An example of such a cable, of the light weight design, is shown in Figure 7-17.

The most significant technical problem with a DC monopolar system is the danger of corrosion of neighbouring structures and installations. Due to electrochemical reactions on the sea-return electrodes chlorine gas is generated. If such a system is to be used these issues will have to be addressed.

Bipolar Power Delivery

In case of a bipolar system a return conductor is required. This can be achieved by incorporating a return conductor in a single cable or having a separate return cable. The choice will be driven by the relative cost. Figure 7-18 illustrates an example cable which contains four conductors where two are used for transmission and two for return.

	DC/AC bipolar 4x35 mm^2	DC/AC mono-polar	AC 3-phase 3x25 mm^2
Outer Diameter (mm)	55	17	50
Weight in air (kg/m)	6.6	0.5	5.7
Resistance Ω/km	0.8	1.4	0.8
Power loss (%)	20	10	20
Voltage drop (%)	16	9	16
Required supply voltage (kV)	6	6	6
Relative cost	4.0	1.0	3.0

Table 7-2: Approximate calculations of dimension, voltage drop along cable and losses for different power delivery systems. For AC systems a perfect compensation of the cable capacitance is assumed.

Three-Phase AC Power Delivery

In this system three conductors which share the current are required in the cable. An example of a cable usable for this system is shown in Figure 7-19. Such a system requires a balancing of the loads on each conductor. If this is not fully achieved extra power losses are incurred.

Summary

Table 7-2 summarises the main characteristics of the different options. The power loss and voltage drops are calculated for the maximum considered length of 100 km and 60 kW power requirement in the deep sea. For AC systems a perfect compensation of the cable capacitance is assumed. It should also be noted that any AC system will most likely require the use of a transformer which adds to the cost of the system but also enhances system stability.

Indications of the relative cost of the different cable solutions are also given in Table 7-2. In the case of the monopolar system the cost of the sea-return is included. Other important parameters that should be taken into consideration in a full cost evaluation are transportation, deployment and maintenance.

7.4.3 Shore Infrastructure

The shore infrastructures will comprise of a harbour with easy access and available warehousing facilities. In addition a shore station will house power supply equipment and computing amenities.

Harbour and Warehousing

For deployment and maintenance activities, access to a harbour is essential. Due to the large number of detection units and other scientific equipment arriving at the harbour for deployment, a warehouse will be required. The size of this warehouse is still to be specified. Because of the sensitivity of the detectors the temperature within the warehouse must be controlled.

Shore Station

The shore station which is naturally positioned at the cable landing site will house the power supply equipment for providing the power to the subsea infrastructure. It will also house the on-shore computing equipment for both the neutrino telescope and the associated sciences. This equipment will require a climate-controlled environment. The computing facilities will include a link to the European high-speed data network and up to about 1000 processing units.

The overall power requirement for shore station and underwater equipment is estimated to be less than 500 kW. A standard connection to the local power grid will suffice. For safety reasons the station and more notably the underwater equipment will require an uninterrupted power supply and surge and spike protection. The power system should incorporate a monitoring and control facility.

7.4.4 Renewable Energy Sources

Because of increasing awareness of the problems conventional energy production can cause through CO_2 and other harmful gas emission, an investigation has been performed into the possibility of providing the energy needs of the experiment

through either wind or photovoltaic local power generation. The Mediterranean basin is well suited to both kinds of energy generation.

The 500 kW of electricity 24 hours a day, 7 days a week required by the experiment translates into 4.4 GWh per year. The question is what level of investment would be necessary to provide these power needs from either wind or photovoltaic power generation.

Wind Power

The average wind speeds around the Mediterranean Sea are shown in Figure 7-20. It is clear that at the three candidate sites the wind conditions vary a little but are always good, being in the range of 7 to 10 m/s. The calculator provided by the Danish Wind Industry Association [**115**] is used to estimate the production capability. There is a choice of several wind turbine types. Data on the mean and distribution of wind speed is available from wind farms worldwide. This is important as the turbines have minimum wind speeds at which they start generating and typically increase power output, up to some maximum, with the third power of the wind speed. Four turbines rated at 600 kW or one at 2500 kW can provide the power requirements and are commercially available. The optimal choice depends on the exact wind characteristics at the placement site. The turbines themselves require an investment of around 2.5 M€, whereas the provision of infrastructure adds a further 1.5 to 2.5 M€. This last number could of course be minimised if the placement of the turbine for KM3NeT stimulates the local authorities to install a wind farm.

Solar or Photovoltaic Power

An alternative to wind is the generation of power using photovoltaic arrays. The Mediterranean coast gets typically 4 to 12 hours of sunshine per day. Most areas are in the neighbourhood of 4 hours in January and around 12 in August. The average is 8 hours a day.

A solar panel of 1 m^2 will produce 110 W of power when in full sun and angled correctly (110 Wp or
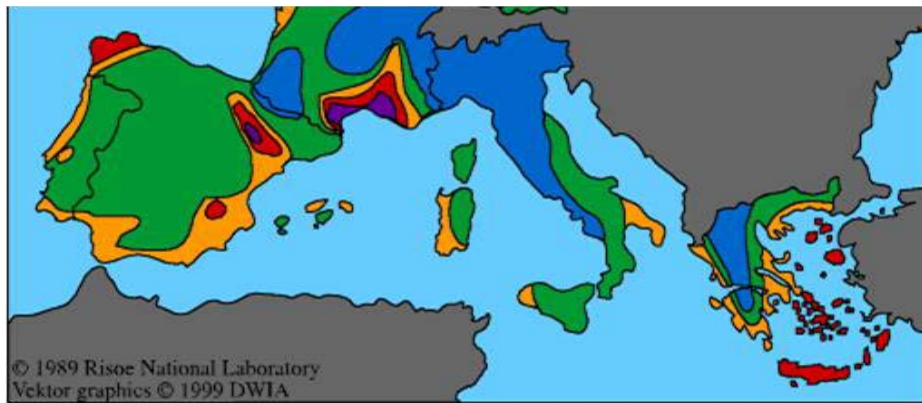
	Open sea		Hills and ridges	
	m/s	W/m^2	m/s	W/m^2
	>9.0	>800	>11.5	>1800
	8.0-9.0	700	10.0-11.5	1500
	7.0-8.0	500	8.5-10.0	1000
	5.5-7.0	300	7.0-8.5	500
	<5.5	<200	<7.0	<400

Figure 7-20: The wind map of the Mediterranean.

Watt peak). For the 8 hours a day one can assume an average of 100 W/m^2, i.e. 1 m^2 of photovoltaic cells produces 290 kWh per year. To produce the required 4.4 GWh 15000 m^2 are needed. A field of about 100 x 500 m^2 could house this, providing a power production capacity of 1.7 MWp. A preliminary estimate of the total cost for the project is about 10 M€ [116].

Maintenance costs for both systems are in the order of 10 k€ per year.

It seems to be perfectly feasible to make the KM3NeT detector energy-neutral by either photovoltaic or wind power. Systems to provide the amount of power needed are available almost off the shelf. Costs are not outrageous being less than 5% of the cost of the detector. Lifetimes of these systems are 20 years. Reducing power consumption makes this even more viable. The expected increase of the computing power in the next five years could well help in this respect.

7.5 DEPLOYMENT

The building and operation of a large scale neutrino telescope in deep water will require the deployment of structures to accurate positions on the sea bottom. In addition it may be required to recover elements of the detector for modification or repair. For these operations both surface vessels such as ships or specialised platforms as well as submersible vehicles are needed.

Experience gained from the pilot projects has shown that regular access to the same vessel and crew offers substantial advantages. Furthermore, availability of the vessel at a port near the neutrino telescope site is an asset.

Indispensible equipment for a deployment vessel includes:

- a GPS-referenced dynamic positioning system, allowing the vessel to maintain station with a precision of a few metres in sea states up to the level at which deployment can safely proceed;
- acoustic navigation equipment needed for precise placement of deployed objects;

- deck-to-sea transfer cranes and a deep-sea winch with adequate capacity and spool speeds allowing for placement of objects on the seabed at depths beyond 2500 m.

7.5.1 Ships

Many vessels suitable for deployment exist around the world, in particular for the off-shore oil and telecommunication industries. Such ships can either be chartered on a short-term basis (ships of opportunity) or on a long-term basis for the duration of the project, or even be purchased.

Figure 7-21 illustrates a typical deployment ship suitable for use in coastal waters; the open deck area is 30 m in length. Deployment is made over the fantail, with the derrick aft carrying the deck-to-sea transfer cranes and the pulley for the deep-sea winch cable.

7.5.2 Platforms

The use of ships, however well equipped, may not be the best solution for precise deployment or recovery operations. Dedicated platform vessels can provide easy access to the sea surface e.g. through a central well with crane coverage. It can minimise the rocking, pitching and rolling motion.

The Delta-Berenike Platform

The above considerations have motivated the development by the NESTOR Institute of a deployment platform, the Delta-Berenike (DB), which is a central-well, ballasted platform (see Figure 7-22).
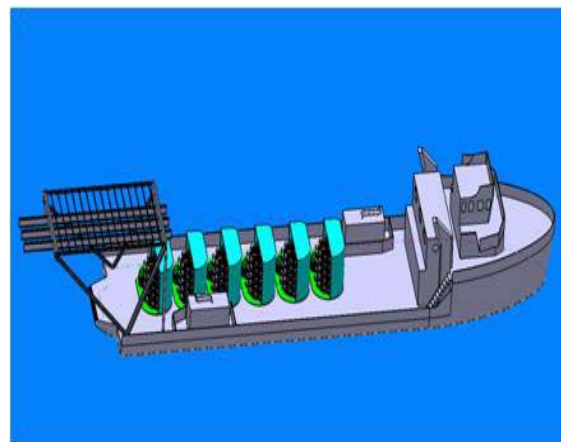
Figure 7-21: Schematic of a possible deployment ship, carrying detection units ready for deployment.

The platform is being upgraded at Elefsis Shipyards and delivery is expected by mid-2008.

She is an isosceles triangle 51 m on the sides and 44 m at the base. Her weight is 275 tonnes, which corresponds to 415 tonnes gross. The lower side of the deck of the triangle-shaped structure will be about 2 meters above the sea surface with three 6 m diameter cylinders each located at an apex of the triangle providing the required flotation. Each cylinder will house a 322 BHP motor coupled to a 360° steerable water jet. Using the combined power and thrust direction of these engines, the DB can sail the required course, or hold position on the open sea.

A system which can be successfully used in the open sea at a sea state of 4 Beaufort[4] is required in order to deploy large structures of complex geometry. Studies have shown that the hydrodynamic behaviour of DB is adequate up to this sea state and she can keep position. If the weather conditions worsen the operation will be suspended.

The dynamic positioning of the platform will be achieved by using three Global Positioning System (GPS) receivers which provide real-time information concerning the platform's location. A controller will use as input the GPS derived location, the desired location and weather conditions (e.g. sea currents and wind velocity) to control the direction and the power of the steerable water jet propulsion engines. The accuracy of the system for positioning is expected to be 2 m to 5 m.

Among other ancillary equipment this vessel is equipped with a bridge crane which has an 18 m long beam supported by two pairs of load-bearing columns and a height of approximately 9 m. An automatic heave compensation system is achieved by mounting the main pulley on a movable wagon.
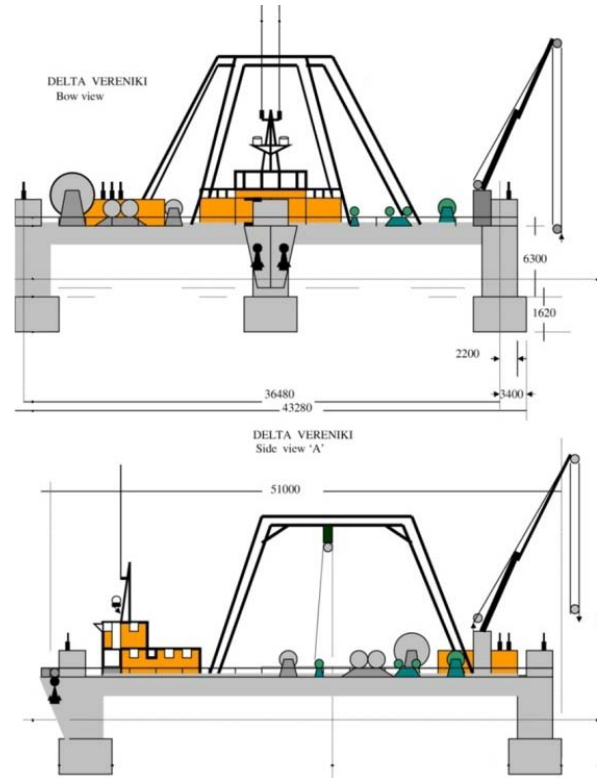
Figure 7-22: Schematic of the Delta-Berenike platform. Bow view (upper), and side view (lower).

The use of DB has been studied for the deployment of extended tower detection units (see Section 7.3). The arms of a hexagonal floor, which are already equipped with OMs, are brought floating to the DB and are attached onto the central unit. When all arms are installed, interconnecting ropes are attached to increase rigidity and the whole structure is lowered in the sea to an appropriate depth before assembling the next floor above it. After the completion of the required number of floors, the whole tower will be deployed to its position on the seabed.

The DB has a surface area of about 1000 m^2 which can be extended with outriggers. This surface can be used to carry a surface array for calibration purposes as described in Section 7.6.

---

[4] A sea state at the upper end of 4 on the Beaufort scale is characterised by winds up to 30 km/h with small waves (up to 1 m) and fairly frequent white horses.
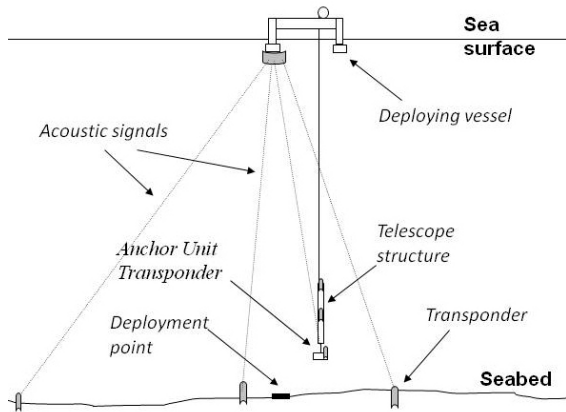
Figure 7-23: Components of the sea bottom positioning system.

7.5.3 Sea Bottom Positioning

To achieve accurate positioning of detection units during deployment, a Long Baseline Acoustic Navigation System (LBNS) will be used to monitor the position of the anchor and guide it to a predetermined position on the seabed. The LBNS is composed of several transponders deployed and positioned on the seabed, on the anchor of the detection unit and on the surface vessel (see Figure 7-23).

7.5.4 Deep-Sea Submersibles

For the construction of a deep-sea neutrino telescope, underwater robotic devices will be necessary for installation, maintenance and survey. These devices are either remotely operated underwater vehicles (ROVs) or autonomous underwater vehicles (AUVs). Some systems fall in a category between the two and are known as hybrids.

Continuous R&D activities on new systems and tools for deep sea operations are driven in particular by the expansion of the oil and gas industry to deeper underwater locations.

The submersibles should have manipulators, each with at least 5 degrees of freedom in order to perform the main deep-sea operations. It must be possible to replace the manipulators and the end-effectors in order to customise the equipment for the planned sea operations. In order to manipulate deep-sea mateable connectors they must be able

to exert a push force of about 400 N and bollard pull of about 200 N.

For specific operations the submersibles must be equipped with additional tools such as knives, cable cutters and a water jet for cleaning of surfaces and connectors.

Figure 7-24: Micro Class ROV.

Figure 7-25: General Class ROV.

Figure 7-26: Work Class ROV.

Remotely Operated Underwater Vehicles

A ROV is an underwater robot operated from the sea surface. A tether, or umbilical, carries power and operator control signals to the vehicle and sensor data in the opposite direction. Small systems are usually deployed from a vessel whereas in larger systems a sub-sea garage and tether management system are often included. Generally they can move freely in all three dimensions although some bottom crawlers also exist. Due to the diverse tasks required, ROVs can vary in size and complexity. Small vehicles can be fitted with only a TV camera whereas the largest systems can have several dexterous manipulators, video cameras and mechanical tools. For this reason ROVs are denoted, in order of size, as either Mini (or even Micro), General, or Working class. Examples of existing devices are shown in Figure 7-24 to Figure 7-26.

Some of the possible tasks of ROVs in the KM3NeT project are:

- connection of detection units to the seafloor infrastructure;
- instrument placement and retrieval;
- support for maintenance operations;

	Number of Models	Maximum Depth (m)	Maximum Load (kg)
Micro	7	300	5
Mini	20	1500	20
General	1	6000	500
	1	4000	
	41	2000	
Work Class	2	5000	4500
	1	4000	
	1	3500	
	11	3000	
Trenching ROV	1	3500	38000
	2	3000	
	8	2500	

Table 7-3: ROVs on the market.

- *in situ* experimentation;
- ecological studies and observations;
- sampling and light coring;
- surveys of environmental parameters.

A summary of presently available ROVs is given in Table 7-3.

Another class of ROV systems is represented by MODUS (Figure 7-27) which is a cabled system designed for deployment and recovery of GEOSTAR-class observatories. It can deploy and recover payloads up to 30 kN in a controlled and accurate fashion.

Autonomous Underwater Vehicles

Autonomous Underwater Vehicles (AUVs) (Figure 7-28) are free-swimming, untethered, unmanned submersibles.

Present applications include

- subsea inspection (pipelines and cables);
- oceanographic sampling and environmental monitoring;
- iceberg profiling and under-ice surveys;
- mine detection;
- diver support;
- wreck searches;
- underwater photography.

The AUV industry is presently emerging from the R&D and prototyping phase. Over the past decade, nearly 200 AUVs have been built and about 20 programmes are presently active in scientific and military applications.

The typical period of autonomous operation of commercial AUVs is continuously improving and is at present about 50 hours. Further improvements will allow for higher speeds, additional sensors and higher-intensity lighting for underwater photography. For more complex and longer operations the limitations in power are likely to prevail for the near future.

Figure 7-27: MODUS.
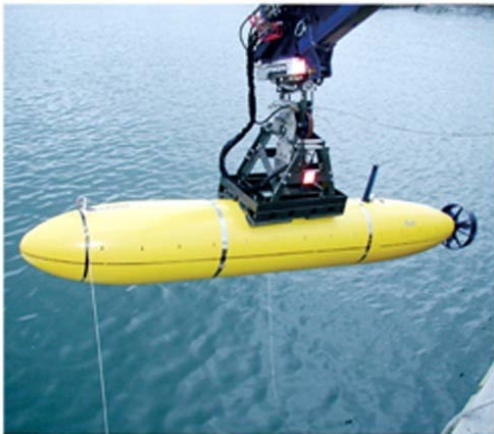
Figure 7-28: Autonomous Underwater Vehicle System.

Hybrid AUV and ROV Systems

In some cases a hybrid AUV/ROV system could provide a convenient solution. Here, an autonomous module, transporting a standard ROV and tether management system, would be launched from the host vessel. It would be programmed to make its way to the site where it would plug into a permanently cabled docking station to pick up power and communications. The ROV performs its task under operator control while the AUV recharges its batteries in order to transport the ROV

at the end of operations. Such systems are under study.

7.6 CALIBRATION

The events are reconstructed from the arrival time of the Cherenkov photons at the photon sensors, knowing the sensor positions. The quality of the reconstructed track direction thus depends on the timing and position accuracies. The reconstruction of the particle energy in addition requires the measurement of light amplitudes. Consequently, the detector needs a calibration system for the time and amplitude information of detected photons and for the position of the photon sensors. Further, to observe celestial objects, a precise absolute pointing calibration is needed. An absolute timing calibration is required to correlate the neutrino events with observations from other instruments.

7.6.1 The Timing Calibration Systems

Relative Timing

There are two contributions to the relative uncertainties in the timing of the photon detection system. The first is the transit time spread in the photomultiplier tubes and the second comes from variations in the delays within the electronics systems. The relative timing calibration systems under study determine these contributions both separately and combined.

Electronics calibration: In Section 7.2, a number of data acquisition and transmission paradigms are presented, in all of which provision is made for calibration pulses to be sent from shore to the photon sensors in order for the delays in the electronics system to be determined to better than 1 ns.

Transit time calibration: The need for monitoring the transit time spread of the photon sensors depends on the photon sensor technology finally chosen. If dedicated transit time monitoring is required, illumination of the photocathode at the level of a few photoelectrons is desirable. This can be achieved via an LED pulser (mounted close to

the photomultiplier tube), or via a fibre illuminated with a laser or LED outside of the optical module.

Full system calibration: In the pilot projects the required timing accuracy has been achieved by using systems that produce short duration light pulses. This basic timing calibration concept remains the same; for KM3NeT the following three different implementation options are being studied:

- LED beacons. Commercial LEDs can be pulsed with a typical rise time of 1.5 ns to 2.0 ns. This technique is applied in ANTARES using optical beacons with many LEDs. Recent investigations have focussed on alternative pulsing circuits using high Q factor laser switches and on high-gain operational amplifiers and the identification and operation of commercial LEDs capable of emitting ten times the intensity of those used in ANTARES without compromising the timing features of the light pulse.
- Laser beacons. Lasers are capable of producing very short light flashes; for example, those used in ANTARES have a FWHM less than 800 ps. A number of technologies exist including solid state lasers and laser diodes. In order to distribute the light from a laser flash to many optical modules it is preferable to inject the light into a diffuser.
- Optical pulsers and fibres. A third approach exists in which the light from optical pulsers is injected into a fibre optic network and directed towards the Optical Module. It is required to know the path length accurately. This approach based on LED pulsers has been implemented in the NEMO project. Another such system based on lasers is used in the IceCube detector. The lasers to be used in such a system for KM3NeT would have specifications similar to those discussed above.

Pre-deployment calibration: A great deal of important information can be acquired from dark room tests carried out prior to deployment. It is expected that a number of pre-deployment tests will take place in order to establish initial timing cali-

bration constants. This will require calibration test benches to be built at the sites where final construction and assembly will take place.

Absolute Timing

Studies indicate that time-stamping at millisecond accuracy is sufficient for relating KM3NeT observation with those of other instruments. This is easily achievable with commercially available GPS units. No additional research and development is foreseen in this area.

7.6.2 The Relative Position Calibration Systems

Since all the proposed mechanical structures have flexible parts, water current will move these structures and displace the optical modules by up to several meters. In order to be able to reconstruct the tracks properly, the position of the photon sensors must be known with a precision of around 40 cm. Therefore, the measurement of the optical modules' positions is necessary. Two possible positioning systems are considered: an acoustic and tilt-meter/compasses system, and an acoustic/optical system.

Acoustic and Tilt-Meter/Compass System

The detection unit shape is reconstructed using measured positions, tilts and orientations of specific points along the unit, taking into account the weight and drag coefficients of all elements. This kind of system has been successfully used in the ANTARES and NEMO pilot projects. The numbers of required hydrophones, tilt-meters and compasses depend strongly on the mechanical structure chosen.

The required input is provided by two independent systems: an acoustic system giving the 3D position of hydrophones placed along the detection unit and a set of tilt-meter/compass sensors giving the local tilt angles of each storey with respect to the horizontal plane (pitch and roll) as well as its orientation with respect to the Earth magnetic north (heading).

The acoustic positioning method: It is based on the measurement of the travel times of acoustic pulses

between emitters fixed on the seafloor and receiving hydrophones placed along the detection unit. The 3D position of each hydrophone is then obtained by triangulation. The uncertainty in the depth coordinate of the emitter position can be overcome by relative depth measurements during connection operations.

The ANTARES and NEMO detectors use systems based on this concept. With the ANTARES acoustic positioning system an accuracy on the spatial positions of the hydrophones better than 5 cm has been achieved.

Tilt-meter/compass system: Complementary to the acoustic positioning system, tilt-meters and compasses can be used for the shape reconstruction of the detection units as well as for measuring the Optical Modules' orientations. Ideally, a tilt-meter and compass should be installed on each storey. However, some studies are underway to investigate reconstruction accuracy using less tilt-meters and compasses. Again this aspect depends strongly on the final mechanical structure used.

Additional measurements: To apply the method proposed, it is necessary to know the sound velocity in the water which can be measured using conductivity-temperature-depth sensors or dedicated sound velocity meters.

It is also useful to monitor the sea current along the full height of the detection units with acoustic Doppler current profilers.

The Acoustic/Optical Positioning System
The alternative method to determine the position of the optical modules is to use LED beacons which produce short light pulses. From the arrival time of the light pulses from several LED beacons the position of an optical module can be determined. The position of the LED beacons is determined by acoustic triangulation using hydrophones mounted at the LED beacons and fixed transponders at the seabed similar to the system explained above. From preliminary simulation studies, a resolution of the Optical Modules' positions of 25 cm seems realistic. The advantage of such a system is in the reduction of the number of calibration units; however, such a system may interfere with the neutrino detector operation and this is currently under study.

7.6.3 Absolute Orientation System
There are three methods, which could provide such calibration.

Acoustics Method
The position determination of the detector is based on the precise measurement of the geographical coordinates and the depth of the anchors of the detection units. The coordinates of several fiducial points separated by long distances give the absolute azimuth of the detector. A set of depth measurements of anchors determine the tilt of the detector.

Measurement of the depth: The anchor of each detection unit will carry a pressure sensor to measure its depth. In addition these depth measurements can be verified using a ROV equipped with an accurate pressure sensor. The temperature and salinity profile of the water at the site is needed for high precision. After tide and atmospheric pressure corrections, the relative depth of all the transducers can be determined with an accuracy of 10 cm. With a lever arm of the order of a kilometre, this corresponds to an accuracy of the absolute tilt angles of the detector of around 0.01 degrees.

Measurement of the geographical coordinates: These measurements are performed using an acoustics method to relate the undersea coordinates to the surface coordinates. A surface boat, equipped with an acoustic transducer, above the detector field determines simultaneously its own position with a GPS/Galileo receiver and the distance to a given deep-sea transducer by sound transit time. A kilometre lever arm and a position accuracy of 20 cm yield an absolute azimuth accuracy of around 0.02 degrees.

A combination of these measurements gives an absolute pointing accuracy of the neutrino telescope of better than 0.03 degrees. Reliable pointing calibration is essential for neutrino astronomy

and so it is important to verify it with independent methods.

Sea Surface Detector

A surface detector array floating above the neutrino telescope can be used for pointing calibration of the deep-sea detector. The method employs cosmic-ray induced atmospheric showers that contain muons of sufficient energy, $E > 2\,\text{TeV}$, to reach the undersea detector.

The implementation under investigation is based on the HELYCON design [117]. The HELYCON detector module is a scintillation counter of $1\ \text{m}^2$ active area with a read-out system based on a high-precision time to digital converter chip. The calibration capabilities of three autonomous detector arrays on floating platforms were quantified by a Monte Carlo study. The platforms were assumed to float 4000 m above the neutrino telescope, at distances of 150 m from each other, positioned around the vertical symmetry axis of the telescope. Each platform contains 16 detector modules, covering an area of about $360\ \text{m}^2$. Every single floating detector array is operated independently from the others.

Simulated air showers were analysed to reconstruct the direction of the axis of the shower with the surface array and the direction of contained muons with the neutrino telescope. These directions were compared on an event-by-event basis to evaluate the average difference between these two angles. It is found that this calibration system will achieve a pointing accuracy of 0.05° within ten days of operation.

The absolute position of the underwater telescope can be also measured using the surface detector. The technique is based on measuring the distance, on an event by event basis, between the impact points of the reconstructed muon track and the shower axis. This method can be used to measure the absolute position of the neutrino telescope with an accuracy of better than a metre within a ten day data taking period.

Moon Shadow

Another check of the absolute orientation of the neutrino telescope can be performed by looking at the "Moon shadow" in reconstructed downward-going muons. Since the Moon absorbs cosmic rays, a deficit of atmospheric muons from the direction of the Moon disk (angular radius 0.26°) is expected. Such a technique has been applied successfully in several underground experiments [118,119].

Simulations indicate that a 3σ effect can be detected in about two months of data-taking with a cubic kilometre detector. It is estimated that such measurements can be used as a cross-check of the absolute orientation of the apparatus, down to the level of a fraction of a degree.

7.6.4 Amplitude Calibration

A measurement of the amplitude of the photomultiplier signals is essential for event selection and reconstruction. Consequently a calibration of the photomultiplier response is required.

For low amplitude pulses, the ^{40}K decays provide signals facilitating permanent monitoring of the response of the photomultipliers at the single photoelectron level. Since the response of a photomultiplier is linear for low amplitudes, an additional measurement of the pedestals suffices to convert a measured charge into a number of photoelectrons.

7.7 IMPLEMENTATION OF ASSOCIATED-SCIENCE NODES

This section is only concerned with describing the implementation and infrastructure in terms of sea-floor power and data connections, not with the details of instrumentation. It provides specifications for:

- node requirements;
- physical node implementation;
- data extraction, management and distribution.

Associated-Science Node Architecture

The underwater architecture for the KM3NeT network will consist of a sub-sea cable connecting the observatory to the shore station and a series of

nodes and branches connected to the cable via junction boxes as shown in Figure 7-29.

Each junction is capable of supporting a series of instruments and modules via wet-mateable connectors. Depending on the complexity of the node and the instrumentation required this could be achieved by daisy chaining junction boxes or further subdividing the architecture with a set of secondary junction boxes as shown in Figure 7-30.
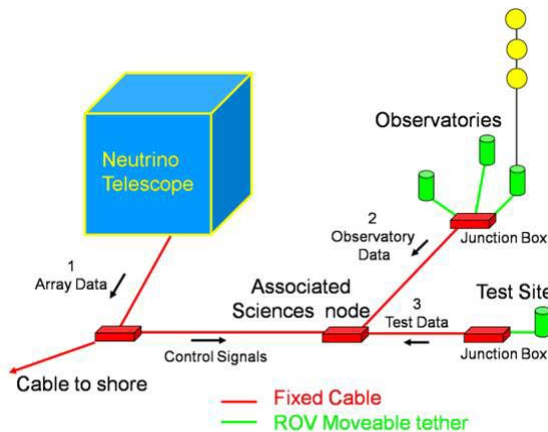
Figure 7-29: Basic node architecture for the associated sciences.

The data links between the shore station and the primary junction boxes are via optical fibre. The links between the primary junction box and the secondary junction boxes are envisaged as either optical or copper Ethernet cable and those between the secondary junction boxes and the instruments are either by copper Ethernet cable or an asynchronous serial link such as RS422, RS485 or RS232. This choice is open and corresponds to
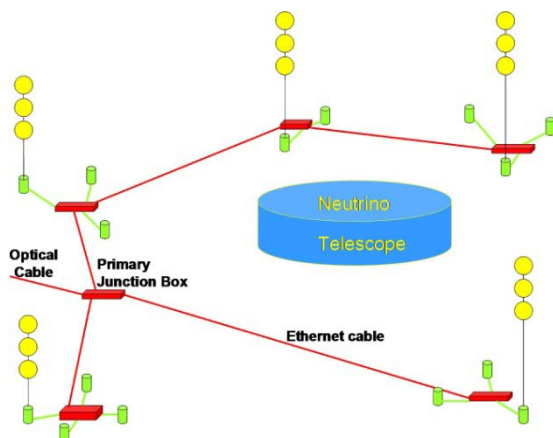
Figure 7-30: Associated-science node with secondary junction boxes and daisy chains.

most of the modular designs employed in oceanography.

The voltage currently envisaged for the network is up to 10 kV DC to the primary junction box. Power converters are then used to supply 400 V DC to the secondary junction boxes.

Typically a secondary junction box will have connections to one or two mooring strings. There should be spare connections so that if any are damaged this does not invalidate the node; typically 6 in use at once, maybe 12 to 16 in total.

As the observatory develops it is envisaged to have branches connected to further junction boxes or have extension cables with a range of up to 100 km (see Figure 7-31). These will require fibre optics for the readout and high voltage for the supply of power. Due to these limitations most instruments will be within a radius of 1 km from the junction box.
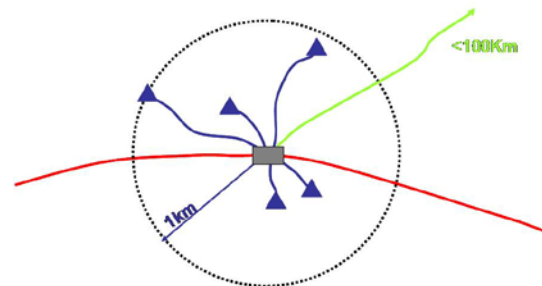
Figure 7-31: Associated-science node footprint.

Unlike the neutrino telescope, the associated-science infrastructure will be continually evolving and as such needs to be designed so that adding components can be achieved in a simple and cost effective manner.

Node Requirements

The network infrastructure will provide bi-directional communications, as well as power and timing signals to underwater instruments located on or near the node. Continuous operation is required.

Interfaces are to be designed such that an instrument may be placed in service simply by connect-

ing its wet-mateable connector to the interface and enabling power. The network design will not preclude the definition and provision of other interface or connector types. Where possible a single connector per interface shall be the preferred option.

Each system shall be designed and located on the observatory allowing for easy access by all types of ROV or AUV. Provision shall be made to isolate pins on wet-mateable connectors where failure to do so could cause additional damage in the event of a connector flooding.

All underwater housings that are not at ambient pressure must during the design life prevent or mitigate harmful effects caused by seal bypass or intrusion of sea water or gasses present in seawater. All equipment shall be qualified for the required external working pressure and temperature range.

Power Requirements

The primary purpose of the power delivery system is to enable the operation of sub-sea scientific instrumentation. The power system shall provide a means of setting controllable limits to power delivery to any underwater interface and shall support multiple levels of power delivery limits. Power levels shall be monitored across all underwater node interfaces and the system shall be capable of maintaining a constant and stable supply to all instruments. On detection of problems the system shall be capable of isolating the output to any underwater instrument.

The associated sciences infrastructure will comprise several instruments such as seismometers, pressure sensors, fluorescence detectors, CO_2 and O_2 sensors, conductivity, current and temperature meters. Acoustic modules, still and video cameras are also foreseen. These will potentially have differing power requirements. For flexibility the associated-science node junction box should be designed to configure power delivery to the different outputs.

The observatory is to be serviced on a six or twelve monthly basis during its life time. This will enable instruments to be replaced or upgraded, new instruments to be added and new branches to be created. Servicing should not affect the power supply to any of the remaining branches or junction boxes.

Communications Requirements

The bandwidth required by the associated-science infrastructure will be driven by the image and sonar data. In the case of high definition video this will consist of data streamed at a rate of approximately 25 Mb/s. Table 7-4 gives an example of the type of power and data rates required by the most demanding instruments. The communication system shall provide a means of raising the priority of a particular underwater interface. To make maximum use of the bandwidth the low level data could be stored and forwarded on a regular basis. Where necessary the communication system shall provide a means of disconnecting or disabling communication to any underwater interface, should problems be encountered. It shall ensure that a fault on any communication interface shall have no impact on any other interface. A failure on a single communications channel should not affect any of the other channels.

The end-of-life bit-error rate for the worst-case underwater to shore interface link shall be better than 10^{-10}. The end-of-life optical link performance margin shall be sufficient to ensure that all performance requirements can be met. The throughput should be at least 90% of theoretical maximum and the end-of-life throughput should be no less than 90% of the beginning-of-life throughput. It may be necessary to provide data buffering in order to reach this specification.

The communication subsystem and timing requirements are well below those of the neutrino telescope. Time stamping to 1 ms will be sufficient.

Configuration Requirements

The observatory may require a configuration capability to permit dedicated rapid sampling of specific instruments when abnormal events are detected. The infrastructure will possibly include a junction

box dedicated to testing and validating new and novel equipment.

On system restart the network infrastructure should automatically isolate faulted cable segments. System monitoring and control is performed remotely. The system should incorporate the possibility of individual remote dead-start and where necessary it should be possible to isolate subsystems until the time when deep-sea maintenance is available. Where possible this shall apply to all instrumentation and software packages.

Reliability Requirements

The reliability of the observatory will depend primarily on the reliability of the cable and junction boxes. Chosen manufacturers will be required to provide mean-time-between-failure figures and transmission error rates. The amount of redundancy built into the observatory will be driven by costs and data continuity requirements.

As the science community becomes more experienced with operating the deep-sea observatory and the observatory evolves over time, the issue of redundancy may need to be revisited.

Reliability criteria for network infrastructure and instrumentation shall be defined during the technical design phase of the project.

Measurement Frequencies

The data rates and acquisition frequencies shall be determined for both nominal and abnormal situations. The rules governing the collection rates shall be defined and agreed so that the procedures for re-configuring the observatory during exceptional events are known.

Sensor and Node Certification

Each sensor or node to be included shall conform to the certification standards for deepsea observatories as specified by the ESONET network of excellence. This shall ensure that observatory sensors are standard, allowing for the ability to share and compare data throughout the European community and where possible on a more global scale.

A test bed facility representing the associated-science infrastructure shall be provided where sensors can be certified as part of a servicing and installation procedure. The certification will be re-

Instrument	model	power (W)	future dev factor for power	voltage (V)	sampling frequency (Hz)	bandwidth (Mb/s)	future dev factor for bandwidth	Data format	number per mooring	On line ratio
Fish Finding sonar** (transceiver unit & transducer)	EK-60	75	50%	12 110 220	1	2	100%	Ethernet	1	100%
ADCP	RDI 300 RDI 75	1 2	20% 20%	24/48 24/48	1.0 0.1	0.01 0.001	100%	RS-232	2*	100%
HD-video camera light (HID)	Sony DSP&L	10 100	20% 0%	12 12-120	- -	20 -	50% -	Ethernet -	1 2	100% 100%

*) at least 3 moorings   **) current depth rating 1500 m

Table 7-4: Energy consumption and bandwidth of possible associated-science node instruments.

quired for all sensors prior to shipping and installation. This shall be part of the Observatory Quality Management System (QMS) which is part of the ESONET remit. It would make sense to implement the system recommended by the Network of Excellence.

Data Processing Requirements

Observatory data will be available from instruments within the associated-science nodes and the neutrino telescope. In addition to the data collected from the standard package the following data may be recorded by the neutrino telescope and would be of use to the associated-science community:

- photomultiplier counting rates;
- turbidity;
- array structure movements;
- temperature changes;
- current flow;
- sound velocity.

Data can be held centrally in one database or distributed and held in separate databases with one dedicated to the neutrino telescope and the other to the associated-science observatory. Data may also be held as raw data or processed data. If raw data is to be stored then additional processing information such as calibration data must also be maintained for each instrument. Other EU projects such as ESONET are currently addressing this issue in terms of standardisation and input from them would be valuable to ensure commonality with other EU deep-sea observatories.

The full raw data stream will be stored on shore and an open software system will be implemented for the processing, distribution and specialised storage.

Safety Requirements

From experience gained during testing on the ANTARES extension for associated sciences, it is important to define a safety allowing for reduced cost of sub-sea intervention whilst minimising the risk of collisions during such interventions.

A safety distance between the neutrino array and the associated-science nodes has to be defined and agreed between the astroparticle physics and the associated-science communities. The position of an associated-science node relative to the array, as shown in Figure 7-32, will need to take into account this safety distance and the optimum position for the best scientific results.
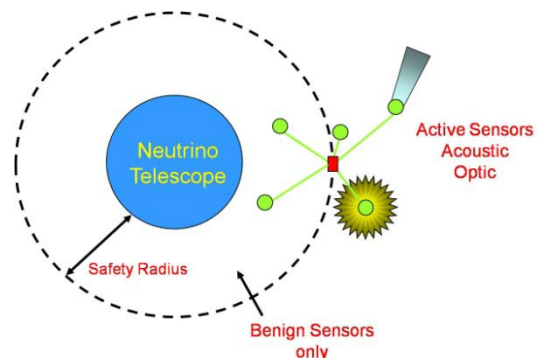
Figure 7-32: Safety radius.

Options for technical implementation of the KM3NeT infrastructure have been investigated. Various designs of units of light detection, optical modules, are under study. Varying numbers and sizes of photomultiplier tubes are fitted inside pressure resistant glass housings, which also contain the necessary electronics components. The optical module data will be multiplexed using passive optical or active electronic systems. The resulting data stream is transported from the detector to shore using optical fibres. The mechanics of the detection units follow the main ideas developed for the pilot projects, with some adaptations to ease transport and deployment being investigated.

Power supply for the infrastructure requires of the order of 50 kW to be transported to the deep-sea structures over up to 100 km. Various options for the power system and the main cable have been studied. The cable choice is likely to be dictated by the standards of the telecommunications industry. This may restrict the number of communication fibres and the maximum power load.

At the landfall of the cable a shore station is required, where power and computing facilities for the data handling will be housed. Furthermore, KM3NeT will require easy access to a harbour with adequate warehousing capabilities.

Deployment of the telescope will necessitate the use of deployment ships or platforms. Submersibles are required for underwater connections of equipment.

Small-scale local generation of power via wind or photovoltaic systems is considered and is viable for a modest investment.

The neutrino telescope relies on detailed information on the position of the light detectors and on the accuracy with which arrival times of signals can be determined. To ensure the validity of this information, calibration systems have been developed in the pilot projects. These systems will be updated for the KM3NeT telescope configuration.

The associated sciences comprising marine biology, oceanography, climatology, geophysics and geotechnics will use the infrastructure for connecting a host of instruments for long-term monitoring. These experiments will form part of wider global environmental monitoring systems.

8   NEUTRINO TELESCOPE DEVELOPMENT PLAN

The concepts described in this document are to a large extent based on the experience built up in the pilot projects, which have spent many years progressing from the conceptual stage to the full production, deployment and finally physics data collection phase. A great deal has been learned from these pilot projects that were by conception conservatively designed. Many of the challenges and pitfalls of working in the deep sea have only been recognised after extensive prototype testing. It is clear from the success of most notably the ANTARES project in reaching the full data taking stage that the pilot projects have ascended the steep learning curve.

8.1   DEVELOPMENT STAGES

Design Verification

Experience has taught that the design should be driven by a risk analysis of the full detector system. For KM3NeT the lifetime of the experiment is required to be at least 10 years from full completion, without major maintenance. This fact alone dictates a re-evaluation of the risk factors. In addition, the size of the detector and the available budget force a redesign of many key components of the detector in order to reduce cost. The options being considered have been discussed in Chapter 7. To allow for a precise risk analysis of the different designs, the figures of merit for individual components and the designs as a whole must be determined. First and foremost the physics performance of the designs must be verified with simulations. If the performance passes the requirements, an assessment of the full system must take place in order to verify the technical feasibility. The outcome of this assessment is a report summarising the technical capabilities of the design. It should also specify input parameters for the risk analysis, such as mean times between failure for all components, identification of possible single point failures, redundancies, power consumption and data bandwidth figures. These figures must be backed up by data either from industry, obtained from the pilot

projects or from small-scale prototyping. In any case the figures must be verified to accurately reflect the envisaged use. Each design will then be subjected to the risk analysis. The anticipated failure rates must be low enough to ensure that more than 90% of optical modules remain operational during a period of 10 years, without major maintenance.

In the area of data transport the design should be verified either by industry standard simulation techniques or by physical prototyping. Here the emphasis will be on matching bandwidth and data throughput to the requirements of the detector and the users.

Component Qualification

The optical modules, electronics and readout system must first be completely qualified in laboratory tests. Initially functional tests must be made, followed by qualification tests which take into account the environment the system will encounter during construction, installation and operation in the sea. An essential aspect of the environmental qualification will be pressure tests for all relevant parts of the system in hyperbaric chambers. Shock and g-load tests must be performed on all relevant components prior to transportation and deployment.

Extensive sea trials are a vital part of the development of the neutrino telescope. Initially, purely mechanical elements will be deployed to test the deployment systems. Later tests involving cables will be required to complement the tests in hyperbaric chambers; only tests in the sea allow for long-term trials, in which the systems must be operated over extended periods. It is likely that the early stages of the sea trial development programme will be carried out with autonomous lines recording data using battery-powered systems.

Prototyping

The full system has to be verified to be compliant with the requirements specified by the design, in

particular power consumption, avoidance of single point failures, and redundancy of the sub-sea infrastructure.

To achieve this, prototyping and qualification testing of the full detection unit will be pursued.

Concepts for Manufacturing

KM3NeT has a number of diverse parts. Most prominently, there are the neutrino telescope detection units, of which several hundred must be manufactured. At the intermediate scale there are calibration units for the neutrino telescope that require tens of units to be built. In addition a significant amount of manufacturing will be required for the seafloor infrastructure and to a lesser extent for the shore and surface infrastructure.

The major manufacturing task will therefore be concentrated on the neutrino telescope detection units. The sheer numbers to be produced preclude many of the procedures used in the pilot projects. These were labour intensive and the assembly work was performed in the science institutes.

In the concepts for the detection unit, the modularity of the design has been stressed. This will allow for substantial parts to be outsourced to industry, while still keeping the overall integration and system testing in house. In pursuing the avenue of industrial manufacturing it has been recognised that the testing procedures must be geared to the industrial environment. Tolerances must be defined at a level to ensure successful manufacture, while controlling costs. Maintaining the quality of the design remains the key issue for the manufacturing concept.

8.2 Development of Risk Analysis in KM3NeT

The objective of risk analysis is to identify and mitigate potential risks. This can be achieved by answering three questions:

- What can go wrong?
- How probable it is?
- What are the consequences?

Two major phases can be distinguished in risk analysis: qualitative analysis and quantitative analysis.

Qualitative analysis involves the understanding of the system functional operation, the role and contribution of each and every subsystem within the overall system. It also involves the identification of possible hazards or threats (e.g. single point failure, network bottlenecks) to the operability of the system and the inherent capabilities of the system to mitigate risks (e.g. redundancy).

Quantitative analysis involves the calculation of the probability with which each hazard or threat is expected to occur. This is done on the basis of quantifying the relevant risk data for each component in the system.

Qualitative Analysis Methodology

The qualitative risk analysis answers the first and third questions of a risk analysis mentioned above and can be decomposed into a number of steps:

- description of the system in terms of components and processes;
- analysis of failure conditions in terms of functionality, reliability and availability;
- identification and classification of risks;
- creation of a logical model;
- decision on quality of design:
  - negative: Implies redesign of either full system or a component and reapplication of the quality assurance process;
  - positive: Generate risk model for final design.

The output of this analysis is a logical model of the system incorporating the functional interdependences of the various components of the system and the combination of failures and/or actions that can lead to system failures of varying degrees of severity.

Quantitative Analysis

The quantitative analysis for the KM3NeT project will follow a bottom-up approach. In this approach reliability of components is assumed to be known or assessed through accelerated testing, and the
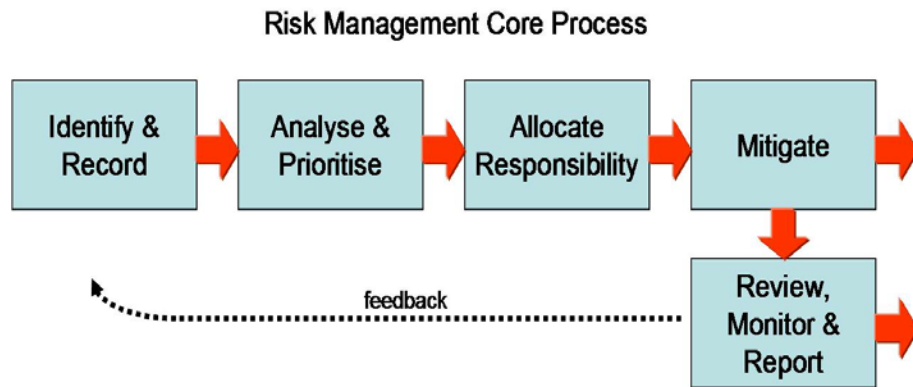
Figure 8-1: Risk management process.

component quantitative performance measures are combined to derive the overall system quantification.

Component Reliability Requirements

Component reliability data can be obtained in several ways:

- *Historical data:* Many organisations maintain internal databases of failure information on the devices or systems that they produce, which can be used to calculate failure rates for those devices or systems. For new devices or systems, the historical data for similar devices or systems can serve as a useful estimate;

- *Government and commercial failure rate data:* Handbooks of failure rate data for various components are available from government and commercial sources. Several failure rate data sources are available commercially that focus on commercial components, including some non-electronic components;

- *Testing:* The most accurate source of data is to test samples of the actual devices or systems in order to generate failure data. By using this approach it might be possible to obtain data for an initial analysis more rapidly.

Risk Management Implementation

The KM3NeT project will have some significant risks during its lifetime that must be addressed and mitigated. They can be classified into a number of major risk categories, covering:

- technical: design, test, construction, integration, and operation;

- commercial: costs, manufacturing, tendering, and scheduling;

- management and resources, both human and material;

- external pressure: political, media, public, economic.

The risk management will be performed by an independent panel, charged with this task only. The risk management process is illustrated in Figure 8-1. A simple but powerful approach to risk analysis involves assessing risks along two key dimensions:

- probability of the risk occurring;

- impact, i.e. the severity of the consequences when the risk occurs.

Each of these two dimensions is classified as High, Medium or Low. Risks are then charted according to their classification on a 3 by 3 matrix (Table 8-1). A score for a risk is determined by its position in this table. This gives a measure of priority – the higher the score, the higher the priority. All risks with a risk score greater than 3 require mitigation plans or action to be taken to reduce the score to 3 or below.

The consequences of the mitigating actions on the science performance must be assessed. If all options fail the criterion, then the project management must accept the risk and its consequences explicitly.

A further consideration in assessing risk priorities is the point in the project lifecycle where the risk is encountered. Risks that occur much later in the

Probability of risk occurring	Impact if risk occurs		
	Low	Me-dium	High
High	3	6	9
Medium	2	4	6
Low	1	2	3

Table 8-1: Risk assessment matrix.

lifecycle should not deflect already allocated resources that are being applied to resolving already existing problems. However, care is needed to make sure that any immediate actions to mitigate long-term risks are not ignored.

A comprehensive project risk register will be used for the recording and reporting of risk and information. In outline, the information held is:

- unique risk identifier;
- risk type / classification;
- risk ownership;
- date raised;
- risk title and description;
- risk probability score / category;
- risk impact score / category;
- risk score;
- risk mitigation action type and description;
- risk mitigation action status;
- risk probability score / category after mitigation;
- risk impact score / category after mitigation.

To assist with setting an appropriate priority to risks according to the current position in the project lifetime, a list of the 'Top 10' risks is used to manage the mitigation actions. This list is regularly reviewed and updated.

Responsibility for each risk is assigned to the most appropriate risk owner for resolution. Options for mitigation of risks are:

- preventative measures;
- reduction measures to reduce the probability or impact of the risk;
- fallback and containment measures (including contingency planning and implementation);

- risk sharing with associated parties;
- choice of an alternative design.

Risk reviews are used to evaluate the following:

- identification of new risks with risk factor above 3;
- assessment of mitigation actions on existing risks;
- reranking of the risks on the top 10 list;
- reidentifying risk owners.
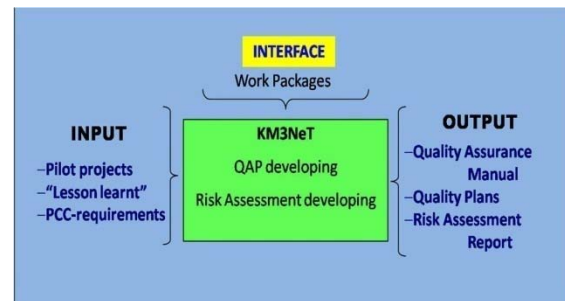
Figure 8-2: Quality assurance process.

8.3 QUALITY ASSURANCE FOR KM3NET

In order to ensure efficient resource management and a high-quality and reliable installation, a quality assurance system will be implemented. Figure 8-2 shows the interactions between the various representatives within the KM3NeT consortium.

Quality Assurance is pursued through an assessment of:

- needs and the expectations of the project and of the users;
- policies and the objectives of the organisation;
- processes and responsibilities needed to achieve the objectives for the quality required
- resource management;
- tools to be used to detect and prevent non-conformities;
- reviews of the Quality Management system (QMS).
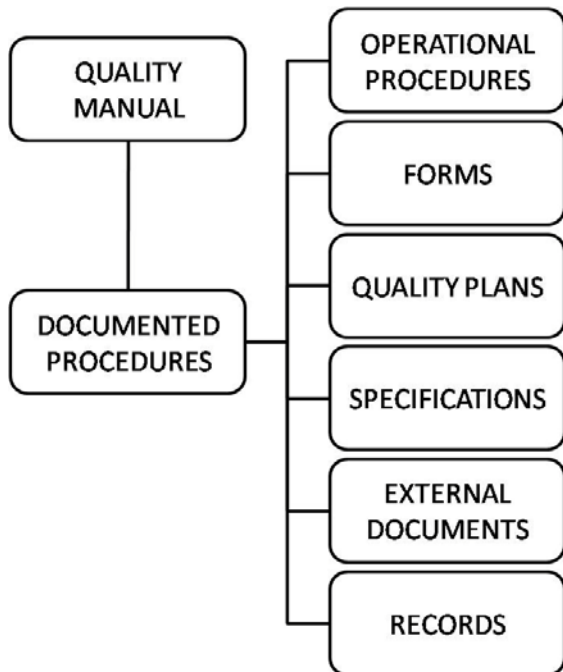
Figure 8-3: Configuration and documentation management.

A functional analysis identifies the required performance criteria. They are defined as requirements that feed into the technical specifications for the overall system and individual components and processes.

The KM3NeT quality assurance procedure will be developed with reference to an existing standard, such as ISO9000, and adapted to the needs of the project. It should be developed in a modular fashion so that the implementation is clear and manageable by the collaboration.

Quality Assurance Implementation

The role of the management in the QMS is to allow the quality objectives to be met by making available the necessary resources, and by taking decisions related to the quality policy.

A document management system will be established to control and provide traceability of all technical documentation. This is especially important in the areas of interfacing and configuration. It also provides a means of auditing the entire system.

Products will be traced through all stages of production and supply providing information on history, status and location of the products.

This applies to:

- raw materials;
- processes;
- non conformities;
- communications between supplier, customer or end user;
- product identification using unique labels;
- change of design requests.

There are plans within ESONET to establish registers for sensors, testing facilities, scientific needs and interfaces. Where appropriate such tools will be investigated and possibly adopted.

Initial trials of the KM3NeT QMS should be used during some of the prototyping phases to gain experience in the implementation and feedback from users.

The QMS should comply with national and European norms, standards and laws related to the health, safety and environment regulations.

In order to enable decision making on the various concepts for the neutrino telescope, a risk analysis must be performed. Laboratory qualification tests, including tests in hyperbaric chambers, are necessary to provide input data to this process. Later, larger-scale prototypes will allow for integrated system tests. Deployment in the deep sea will be part of longer-term testing. Before the start of manufacturing, a quality management system must be in place. Outsourcing of the production of major parts of the infrastructure is being considered.

9 PROJECT IMPLEMENTATION

9.1 TIMELINES AND DECISION PATHS

The anticipated time lines are indicated in Figure 9-1. The design study work following the completion of the present document will concentrate on the production of a technical design report. For this report, decisions on the implementations of the different components of the neutrino telescope must be taken. A full costing of the solutions will be produced, and the cost dependence on the site will be identified. The production, transport and deployment costs will be included. The labour force required for each of these phases must be determined and the cost of the labour calculated and included in the overall cost. A full risk analysis of the design options will take place and for this the quality management system and risk analysis procedure must be in place. The decision process will be based on the risk analysis and the cost issues and will culminate in a single design for the full detector. It is anticipated that this design will then be subjected to review by external experts. The technical design report will include a full characterisation of the three candidate sites and its publication is anticipated for the end of 2009.

The KM3NeT preparatory phase started in March 2008 and will continue until March 2011. In this phase a small-scale engineering model of the de-tection unit and the seafloor infrastructure will be produced and subjected to verification trials including deep sea deployment. The final selection of the KM3NeT site will be pursued in the framework of the preparatory phase and will likely involve decisions at the political level.

After completion of the preparatory phase the construction phase will start with final prototyping and qualification tests. Once funding has been established, tendering processes will be initiated and assembly sites will be put into operation. Data taking will commence once the first detection unit has been deployed.

9.2 OPERATIONAL ISSUES

Management of KM3NeT

A joint operations management of the marine science infrastructure and the neutrino telescope will be set up. This body will be responsible for coordinating deployment, maintenance and emergency situations and shall be available for consultation at any time during the life time of the project. It will also coordinate data sharing between the neutrino telescope and the associated sciences projects. In addition the neutrino telescope and the associated sciences infrastructure will each have their individual management structure to deal with "local issues".
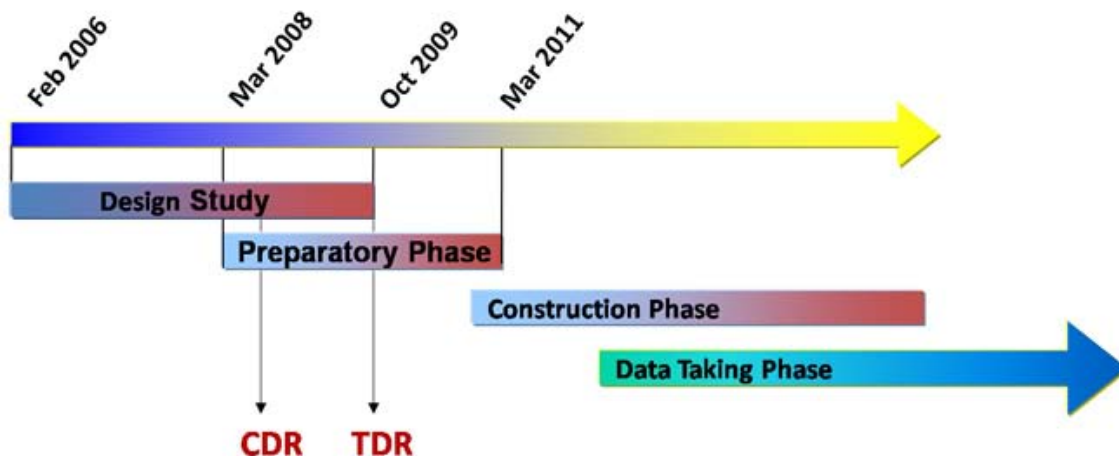
Figure 9-1: Anticipated timeline.

Neutrino Telescope Operations

The telescope will be run via a control centre situated either in the shore station or at one of a limited number of remote centres and shall be operated by a small group of operators on a 24 hour, seven day a week basis. Technicians should be based locally for maintenance operations and emergency situations. The system will provide continuous monitoring of the status of all major components such as optical cable, junction boxes, detection units, power supply, data links and local environmental variables.

An alert system will be implemented such that operators will be alerted when out-of-boundary conditions are detected by the system. Procedures need to be defined in advance of system installation, especially for emergency situations.

Marine Science Observatory Operations

The associated science communities have understood and accept the principle of priority to neutrino telescope operation and that under no circumstances, except those agreed in advance, the associated science infrastructure operation should disturb that of the neutrino telescope.

Three categories of observatory operation are recognised:

- operational and civil protection, i.e.
  - earthquakes;
  - tsunamis;
  - oceanography - GOOS (global ocean observing system) contribution;
- ocean & geosciences research;
- engineering trials.

In the first category, a high standard of reliability and real-time availability is required; significant down-time is unacceptable. In the following category a certain amount of service interruption is acceptable but continuity is a priority albeit at low data rates; data buffering will be required. In the last category performance and availability is negotiable.

For this reason, the associated science user community will have a coordinating body. Its operational staff will be tailored according to the size and complexity of the associated-science nodes. This could be managed according to the rules and methods established in ESONET NoE (concept of Regional Legal Entity).

The management team will ensure efficient integration between the KM3NeT associated science communities, environmental agencies and organisations at the regional, national and international level including ESONET, EMSO, GOOS and ORFEUS, thus maximising dissemination and use of data.

At least one person must be responsible for associated science operations at the management level. This will guarantee that if any conflicts arise between experiments on these associated-science nodes due to unforeseen power reductions, data communication restrictions or sensor failures, these issues will be dealt with swiftly and the nodes reconfigured according to predefined and accepted procedures.

Installation, Configuration, Maintenance and Decommissioning

The deployment of the neutrino telescope shall be performed in several stages. The backbone of the full cable infrastructure and the shore station must be the first to be implemented and tested. This will be followed by a number of years of installation of detection units with their associated seafloor cabling. Each detection unit will be integrated with the shore station and commissioned. Once each unit has been commissioned data taking from this unit will commence.

For each phase of the installation and commissioning a standard set of procedures shall be defined to verify the connection both for power and data transmission, while the connection operation is proceeding. Commissioning is completed by a series of predefined tests that closely represent real operation.

Procedures shall also be identified for performing and recording, in a database, any configuration changes to the array including reasons for change

and accountability. Those needing to be made aware of these changes must be identifiable.

Unlike for the associated-science nodes it is not anticipated to perform major maintenance operations on a regular basis. The system will be designed with sufficient redundancy to allow for a certain number of optical module failures. Unforeseen large-scale failures should be repaired on an ad hoc basis. The possibility of reconfiguration in this instance should ensure that units can be disabled from the array without unduly impacting on normal operations.

Procedures should also address the integration of the associated-science nodes with the rest of the system to ensure the smooth transition to the operational phase.

Once the observatory is operational, all future configuration, maintenance, servicing and upgrades of the associated sciences node(s) shall be handled through agreed procedures by the combined management team. Procedures shall be reviewed on a regular basis to maintain and improve efficiency and to ensure the smooth operation of the associated-science nodes and the neutrino telescope at all times.

KM3NeT is planned to be a long-term installation, but the design will ensure that, in the final decommissioning, all components can be removed from the seabed within an acceptable time interval; the resources for such an operation will be included in the overall financial and personnel planning.

Data Management and Access

The neutrino telescope data acquisition system transports all data to the filtering processing farm on shore in real-time. The output data from the filtering must be archived and distributed to the users around Europe and beyond. Data processing, filtering and reconstruction may take place, online, at the shore station, whereas further reconstruction and data analysis may occur remotely. One option to implement the required computing resources could be a "data centre" similar to those used by astronomical observatories.

Data shall be archived using a relational data base and therefore be easily accessible. Data access shall be controlled via user groups and access rights. KM3NeT may need to employ a dedicated data manager with responsibilities for managing user access, maintaining the outreach programmes and replying to general queries.

These questions, as well as the implementation of user-specific operational issues, will be investigated in the preparatory phase.

The associated-science data management system (DMAS with reference to the NEPTUNE concept) will allow access:

- to generic sensor data by a large community for model assimilation and warning for civil protection;
- to specific experiment data by their principle investigators;
- to images and associated data by the public at large;
- to test data by engineering teams.

The data management system will be modular to allow for the implementation of the data processing, data quality checking and multidisciplinary cross checking software.

Procedures shall be designed to permit free data interchange between the astroparticle physics and the associated-science community in KM3NeT.

Public Relations and Outreach Programme Management

It is important that the observatory results are made available in a simple and visual manner to the citizens of the European Community and beyond. In order to achieve this, activities of the KM3NeT observatory will be publicised on a regular basis and links to outreach programmes made available at all the institutes involved in the project.

All KM3NeT results will be posted on the KM3NeT web site. The site will be split in two sections, one for the layperson and a more advanced one for scientists.

An aim of the layman's site is to get young people interested in all aspects of KM3NeT science and allow the general public to understand how funds are being used to enhance scientific and technical knowledge. The advanced site will aim at generating scientific and technological knowledge among European scientists.

Where possible, real-time data shall be displayed on the website, with access for the general public. Cross links to and from the astroparticle physics community should also be implemented. The exact model and rules of data dissemination to the science community will be assessed in the preparatory phase.

Users and Stakeholders

It is envisaged that access to the system and its data will be granted to:

- scientists from member institutes;
- external scientists from within the EU;
- scientific institutions external to the EU;
- EU government departments and organisations;
- non-governmental organisations.

Different levels of secure access are envisaged as shown in Figure 9-2. Some data will only be accessible within a small community of participants. Operational data on earthquakes and tsunamis for civil protection is to be streamed directly to national agencies. Political, Legal and Strategic Aspects

Political Processes

The KM3NeT effort is closely linked to relevant
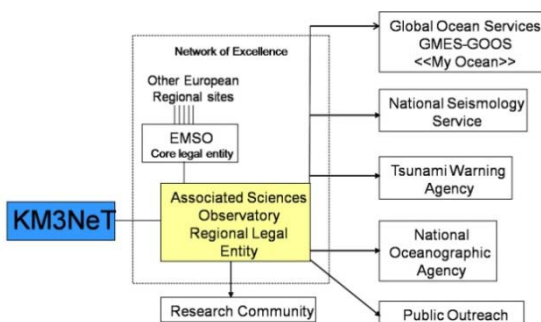
Figure 9-2: Users and stakeholders of the KM3NeT associated-science infrastructure.

ongoing processes at the European level:

- *The European Strategy Forum on Research Infrastructures (ESFRI):* This is a panel with governmental and funding agency representatives assessing the future needs and priorities of European research infrastructures. In 2006 ESFRI published the *Roadmap of European Research Infrastructures* [**120**]*,* which lists KM3NeT as one of 35 major research infrastructures that were identified to be of significant interest to Europe.

- *The Astroparticle Physics European Coordination (ApPEC):* This committee was formed to foster European coordination in this new dynamically developing field. Through its expert panel, the Peer Review Committee, ApPEC has produced a *Roadmap for Astroparticle Physics in Europe* [**121**], which contains a strong recommendation for the realisation of KM3NeT.

- *The ASPERA ERANET project:* This project, funded in FP6, was initiated by ApPEC and has been active since mid-2006. It will transform the ApPEC Roadmap into a resource profile of astroparticle physics in Europe over the next decade; the KM3NeT project is included in this process at a high priority level.

In establishing these links, the KM3NeT design study has been highly useful and instrumental, in providing both the required resources and in forming a platform for promoting the project.

The KM3NeT Preparatory Phase Project

From the start of the design study a dedicated work package has explored the resources required to prepare for construction of the KM3NeT infrastructure.

In FP7 a new EU funding instrument "Preparatory Phase Projects" is available to research infrastructures on the ESFRI Roadmap. A corresponding project for KM3NeT has been proposed and endorsed; it has started in March 2008. The major objectives are:

- *Political convergence:* The objective is to ensure a formal, coordinated approach at a high

political level, providing all necessary background information and administrative support for a continuous consultation process between national authorities. This overcomes the traditional problems encountered by nationally instigated initiatives for Pan-European research facilities. In the past these have been severely hampered and delayed by the lack of adequate models for collaboration for both the construction and operation phases. The outcome of this coordination will provide a basis for decision making at the European level.

- *Legal, governance, financial engineering and site issues:* The legal form and governance model will be worked out and the access rights to sites will be negotiated. Taking into account the temporal funding profiles in Europe, a financial plan for the construction of the infrastructure will be generated. Finally a business plan for the operational phase will be drafted. These activities will also provide the necessary input for the political process that will be required to reconcile national and regional political and financial priorities with the scientific and technological considerations. These may have a bearing on the key decision concerning the site selection for the KM3NeT infrastructure.

- *Strategic issues and international networking:* The implications of specific funding profiles, a possibly distributed infrastructure or extendibility will be assessed in terms of operational, technological and time-scale issues. Furthermore, possibilities of additional resources from countries not currently involved in KM3NeT will be explored and fostered.

- *Preparation for production and operation:* A substantial part of the preparatory phase project is dedicated towards the detailed preparation of the production and installation process. Moreover, the operation of the KM3NeT infrastructure, including observatory aspects, data handling and dissemination issues, will be covered.

Funding Prospects

The estimated budget for KM3NeT lies in the range 220-250 M€, with a projected spending profile peaking in the period 2011-2014. In order to maximise the physics potential, it is intended to construct a telescope with the largest possible effective volume (sensitivity), within this budgetary constraint. Indications are that a sensitivity exceeding that of all existing neutrino telescopes by a substantial factor, as required by the physics objectives, can be reached.

Present Funding Situation

In the past year there have been the following important developments concerning the funding for KM3NeT:

- *Greece:* In a letter dated October 22, 2007, the Greek Secretary General for Research and Technology (Ministry of Development) informed Commissioner Potocnik of the Greek *"…Government's decision to host the Cubic Kilometre Neutrino Telescope (KM3NeT), a European Research Infrastructure on the ESFRI Roadmap, and fund it from 2009 on with 20% of the total cost with a ceiling of 50 Million Euro if it were located in Pylos."*

- *Italy:* A letter of support sent by the President of the regional government of Sicily to the Italian Minister of University and Research, mentions an investment of 30 M€ from regional funds. *"..Inoltre, per le motivazioni che finora Le ho esposto, se la candidatura della Sicilia dovesse andare a buon fine, la nostra regione si impegna a concorrere alla sua realizzazione con un contributo fino a trenta milioni di euro."*

- *Netherlands:* Request for 8.8 M€ submitted by Nikhef, through FOM, to the National Funding Agency (NWO); a decision is expected by mid-2008**.**

The funding commitments and requests listed above cover about 40% of the projected cost for the implementation phase of KM3NeT.

Nevertheless these positive developments are subject to the cautionary remarks of the next paragraph concerning ERDF funding.

FP7 and European Regional Development Funds

The European Commission proposal for FP7 originally anticipated a contribution of up to 20% to the construction cost for new European Research Infrastructures. However, in December 2006, the final Council Decision for FP7 reduced the budget for the "Capacities" section of FP7 from 7486 M€ to 4097 M€. As a result the FP7 contribution to the construction phase of new research infrastructures is no longer present. This development has serious implications, especially in terms of the European Commission's role in facilitating a coherent, coordinated, overall perspective concerning the infrastructures on the ESFRI Roadmap.

The need for coordination of funding instruments is particularly acute in view of the fact that funding through the European Regional Development Funds (ERDF) will be subject to regional constraints. Furthermore, the time profile of ERDF funding for different regions will have to be closely coordinated. Such coordination will be supported by the work done in the preparatory phase.

The European Research Area and the Role of the EC in Implementing the ESFRI Roadmap

The EC Green Paper "The European Research Area: New Perspectives" [**122**] states, "…*on the basis of the results of the consultation and debate, the Commission intends to propose initiatives in 2008*". The corresponding consultation process has started. It is therefore important and urgent for the KM3NeT community to respond to this Green Paper through the appropriate channels (funding agencies, research ministries).

The research infrastructures on the ESFRI Roadmap cover a wide range of scientific and technological disciplines from social sciences to astroparticle physics and from life sciences to information technologies. Decisions related to the hosting of these research infrastructures involve a complex set of

scientific, technological, financial, legal and political considerations that can only be addressed at the European level. The EC is uniquely positioned to act as facilitator for the processes and deliberations that will lead to the implementation of the Roadmap projects. It is clear that the effectiveness of this facilitation role will be greatly enhanced if part of the implementation cost were to be provided through EU funds. It is important for the KM3NeT community to stimulate an EU involvement by providing a solid and well documented case.

Associated-Science Infrastructure Legal and Financial Issues

The legal (ownership, liability, environmental impact) and financial issues that require to be addressed as part of the KM3NeT associated-science infrastructure are very similar to those addressed by the ESONIM (ESONET implementation model) project. The ESONIM project final report may be used as a guide for European deep sea observatory developments, under ESONET, EMSO and KM3NeT.

The KM3NeT design study process has brought together a strong science and engineering community preparing all elements necessary for the successful design, construction, management and operation of a deep sea infrastructure consisting of a neutrino telescope and associated science platforms.

GLOSSARY

ADC	Analogue-to-digital converter
ADCP	Acoustic Doppler current profiler
AGN	Active galactic nucleus
AMANDA	Antarctic muon and neutrino detector array (neutrino telescope at the South Pole)
ANTARES	Astronomy with a neutrino telescope and abyss environmental research (neutrino telescope in the Mediterranean Sea)
ApPEC	Astroparticle physics European coordination
ASIC	Application specific integrated circuits
AUV	Autonomous underwater vehicle
CDM	Cold dark matter
CERN	Centre européenne pour la recherche nucléaire (particle physics laboratory)
CPU	Central processing unit
CTD	Conductivity-temperature-depth probe
CU	Crab unit (unit of flux for photons)
DEOS	Dynamics of Earth and ocean systems (deep-sea observatory network)
DAQ	Data acquisition
DB	Delta-Berenike
DMAS	Data management and archiving system
DMS	Data management system
DUMAND	Deep underwater muon and neutrino detector (neutrino telescope near Hawaii)

EBL	Extra-galactic background light
EDFA	Erbium doped fibre amplifier
EGRET	Energetic gamma-ray experiment telescope (satellite-borne)
EMSO	European multidisciplinary sea-floor observatories (deep-sea observatory network)
ERDF	European regional development funds
ESFRI	European strategy forum on research infrastructures
ESONET	European seafloor observatory network of excellence
ESONIM	ESONET implementation model
EU	European Union
eV	Electron Volt
FPGA	Field-programmable gate array
FWHM	Full width at half maximum
GCN	Gamma-ray burst coordination network
GMES	Global monitoring for environment and security (monitoring network)
GOOS	Global ocean observing system
GPS	Global positioning system
GRB	Gamma-ray burst
GUI	Graphical user interface
GUT	Grand unified theories
GZK	Greisen-Zatsepin-Kuzmin cut-off
H.E.S.S.	High energy stereoscopic system (TeV gamma-ray telescope)
IR	Infrared

LAERTIS	Laboratory in the abyss of Europe with real time data transfer to shore for interdisciplinary studies
LBNS	Long baseline acoustic navigation system
LED	Light-emitting diode
LIMS	Light intensity measuring system
MACRO	Monopole, astrophysics and cosmic ray observatory
MARS	Monterey accelerated research system (cabled observatory project)
MECMA	Mediterranean cable maintenance agreement
NEMO	Neutrino Mediterranean observatory (neutrino telescope in the Mediterranean Sea)
NEPTUNE	North east pacific time-integrated undersea networked experiments
NESTOR	Neutrino extended submarine telescope
OM	Optical module
ORFEUS	Observatories and research facilities for European seismology
pc	Parsec (astronomical unit of length)
PC	Personal computer
pe	photo-electron
PWN	Pulsar wind nebulae
QMS	Quality management system
RAM	Random access memory
RMS	Root mean square (deviation)
ROV	Remotely operated vehicle
RTV	Room temperature vulcanisation
SN	Supernova
SNR	Supernova remnant

spe	Single photon equivalent signal in a photomultiplier
SUSY	Supersymmetry
TDC	Time-to-digital converter
TDR	Technical design report
VHE	Very high energy
WIMP	Weakly interacting massive particle
X-HPD	Crystal scintillator hybrid photon detectors

BIBLIOGRAPHY

[1] R.M. Bionta et al. (IMB collaboration), *Phys.Rev.Lett.*, 58(1987)1494.

[2] K.S. Hirata et al. (Kamiokande collaboration), *Phys.Rev.Lett.*, 58(1987)1490.

[3] M. Ambrosio et al. (MACRO collaboration), *Phys.Lett.*, B434 (1998)451.

[4] M. A. Markov, in *Proc. Int. Conf. on High Energy Physics*, Rochester, U.S.A., 1960, 183.

[5] P. Bosetti et al. (DUMAND collaboration), Harvard HDC-2-88, 1988.

[6] E. Andrés et al. (AMANDA Collaboration), *Nature*, 410(2001)441.

[7] I.A. Belolaptiko et al. (Baikal Colaboration), *Astroparticle Physics*, 7 (1997)263.

[8] J.A. Aguilar et al. (ANTARES Collaboration), *Astroparticle Physics*, 26(2006)314.

[9] P. Piattelli (NEMO collaboration), *Nucl.Phys.Proc.Suppl.*, 143(2005)359.

[10] G. Aggouras et al. (NESTOR collaboration), *Astroparticle Physics*, 23(2005)377.

[11] S. L. Glashow, *Phys.Rev.*, 118(1960)316.

[12] M. Crouch, in *Proc. 20th Int. Cosmic Ray Conf.*, Moscow, 1987, 6-165.

[13] Y. M. Andreev, V. I. Gurentzov, and I. M. Kogai, in *Proc. 20th Int. Cosmic Ray Conf.*, Moscow, 1987, 6-200.

[14] M. Aglietta et al. (LVD Collaboration), *Astroparticle Physics*, 3 (1995)311.

[15] Ch. Berger et al. (Frejus Collaboration), *Phys. Rev.*, D40(1989)2163.

[16] C. Waltham et al. (SNO Collaboration), in *Proc. 27th Int. Cosmic Ray Conf.*, Hamburg, 2001, 991.

[17] J. Abraham et al. (Pierre Auger Collaboration), *Science*, 318:5852(2007)938.

[18] F. Zwicky, *Phys.Rev.*, 55(1939)726.

[19] E. Waxman, *Phys.Scripta*, T121(2005)147.

[20] R. Mukherjee et al., *Astrophys. J.*, 490(1997)116.

[21] F. Aharonian et al. (H.E.S.S collaboration), *Astron. Astrophys.*, 448(2006)143.

[22] F. Aharonian et al. (H.E.S.S. collaboration), *Nature*, 440(2006)1018.

[23] R. White, in *Proceedings of 30th Int. Cosmic Ray Conf.*, Merida,Mexico, 2007.

[24] W. Benbow et al. (H.E.S.S. collaboration), in *Proceedings 30th Int. Cosmic Ray Conf.*, Merida,Mexico, 2007.

[25] S. Gabici and F. A. Aharonian, *Astrophys. J. Lett.*, 665(2007)L131.

[26] F. Halzen, *Astrophys. Space Sci.*, (2007).

[27] M. L. Costantini and F. Vissani, *Astroparticle Physics*, 23(2005)447.

[28] A. Kappes, J. Hinton, C. Stegmann, and F. Aharonian, *Astrophys. J.*, 665(2007)870.

[29] F. A. Aharonian, A. M. Atoyan, and T. Kifune, *MNRAS*, 291(1997)162.

[30] J. Albert et al. (MAGIC collaboration), *Science*, 312(2006)1771.

[31] S. Aiello et al. (NEMO Collaboration), *Astroparticle Physics*, 28(2007)1.

[32] D. Band et al., *Astrophys. J.*, 413(1993)281.

[33] E. Waxman, *Astrophys. J.*, 452(1995)L1.

[34] S. Razzaque, P. Meszaros, and E. Waxman, *Mod. Phys. Lett.*, A20(2005)2351.

[35] J. Ahrens et al. (IceCube collaboration), *Astroparticle Physics*, 20(2004)507.

[36] J. De Dios Zornoza, PhD. Thesis, Universitat de Valéncia, Valéncia, Spain, 2005.

[37] E. Bernardini et al. (IceCube collaboration), *Nucl. Instrum. Meth.*, A567(2006)418.

[38] E. Waxman and J. N. Bahcall, *Phys. Rev.*, D59(1999)023002.

[39] S. Kuch, PhD Thesis, University of Erlangen, Erlangen, Germany, 2007.

[40] E. V. Derishev, F. A. Aharonian, and V. V. Kocharovsky, *Phys. Rev.*, D68(2003)043003.

[41] L. A. Anchordoqui, D. Hooper, S. Sarkar, and A. M. Taylor, *Astroparticle Physics*, 29(2008)1.

[42] V. S. Berezinskii, S. V. Bulanov, V. A. Dogiel, V. L. Ginzburg, and V. S. Ptuskin, *Astrophysics of cosmic rays*. Amsterdam , Netherlands: North Holland, 1990.

[43] R. Atkins et al. (MILAGRO collaboration), *Phys. Rev. Lett.*, 95(2005)251103.

[44] A.A. Abdo et al. (MILAGRO collaboration), *Astrophys. J. Lett.*, 658(2007)L35.

[45] E. Komatsu et al. (WMAP collaboration), *Astrophysical Journal Supplement Series*,

Astroparticle Physics, 23(2005)131.

[94] Riccobene, et al., *Astroparticle Physics*, 27(2007)1.

[95] A. Capone et al., *Nucl. Instr. Meth.*, A487(2002)423.

[96] E.G. Anassontzis et al. (NESTOR collaboration), *Nucl. Instrum. and Meth.*, A349(1994)242.

[97] P. J. Henning, Ed., *Bioluminescence in action*. London, U.K.: Academic Press, 1998.

[98] E. A. Widder, I. M. Latz, and J. F. Case, *Biol. Bull.*, 165(1983)791.

[99] M. Ambriola et al. (NEMO collaboration), *http://nemoweb.lns.infn.it/sites/SiteReport/NEMO-Site-Report.pdf*.

[100] Gillibrand et al., *Marine Ecology Progress Series*, 341(2007)37.

[101] I.G. Priede et al., *submitted to Deep Sea Reseach, part I*.

[102] M. Naumann-Godó, *Nucl. Phys.*, B (Proc. Suppl.) 172(2007)36.

[103] E.G. Anassontzis et al., *Nuclear Physics*, B (Proc. Suppl.) 151(2006)279.

[104] L. Ursella, NEMO Internal Note http://nemoweb.lns.infn.it/sites/SiteReport/NEMO_Annex4-Report-Currents.pdf, 2002.

[105] T.A. Demidova et al., in *Proc. 2nd NESTOR Int. Workshop* , 1992, 284.

[106] E.G. Anassontzis et al. (NESTOR collaboration), NESTOR NOTE.160.2007, 2007.

[107] D. Adams, *Hitchhikers guide to the galaxy*. New York, U.S.A.: Ballantine Books, 1995; ISBN 0-345-39182-9.

[108] G. van Aller et al., *Helvetia Physica Acta*, 59(1986)1119.

[109] P. Bosetti, *http://www.phys.hawaii.edu/~dumand/dumand_3_93.pdf*.

[110] A. Roberts et al. (DUMAND collaboration), in *Proc. Internat. Neutrino Conf., Aachen, Germany*, 1976, 688.

[111] R. Bagduev et al., *Nucl. Instr. Meth.*, A420(1999)138.

[112] A.E. Ball et al., *Eur.Phys.J.*, C49(2007)1117.

[113] A. Braem, C. Joram, J. Seguinot, P. Lavoute, and L. Pierre, *Nucl.Instrum.Meth.*, A570(2007)467.

[114] Universal Jointing Consortium, *http://www.ujconsortium.com*.

[115] Danish Wind Industry Association, *http://www.windpower.org/en/tour/wres/pow/index.htm*.

[116] International Energy Agency, *for instance http://www.iea-pvps/cases/nld_01.htm*.

[117] A. G. Tsirigotis, in *Proc. of 20th European Cosmic Ray Symposium*, Lisbon, Portugal, 2006.

[118] Ambrosio, M. et al. (MACRO collaboration), *Astroparticle Physics*, 20 (2003)145.

[119] E.W. Grashorn et al. (MINOS collaboration), in *Proc. of the 30th Int.l Cosmic Ray Conf.*, Merida, Mexico, 2007.

[120] ESFRI, Office for Official Publications of the European Communities ISBN 92-79-02694-1, 2006.

[121] ApPEC, "Roadmap for Astroparticle Physics in Europe," *http://www.aspera-eu.org/images/stories/files/Roadmap.pdf*.

[122] European Commission, COM(2007)161.